

The HST Key Project on the Extragalactic Distance Scale

XII. The Discovery of Cepheids and a New Distance to NGC 2541¹

Laura Ferrarese^{2,3}, Fabio Bresolin^{4,5}, Robert C. Kennicutt, Jr.⁴, Abhijit Saha⁶, Peter B. Stetson⁷, Wendy L. Freedman⁸, Jeremy R. Mould⁹, Holland C. Ford¹⁰, John A. Graham¹¹, John G. Hoessel & Mingsheng Han¹², John Huchra¹³, Shaun M. Hughes¹⁴, Garth D. Illingworth¹⁵, Barry F. Madore¹⁶, Randy Phelps⁸, Shoko Sakai⁶ & N.A. Silbermann¹⁶

ABSTRACT

We report the detection of Cepheids and a new distance to the spiral galaxy NGC 2541, based on data obtained with the Wide Field and Planetary Camera 2 on board the Hubble Space Telescope (HST). The observations are part of the HST Key Project on the Extragalactic Distance Scale, which aims to provide a measurement of the Hubble constant H_0 with 10% accuracy. A total of 13 epochs are obtained using the F555W filter (transformed to Johnson V), and five epochs using the F814W filter (transformed to Cousins I). Photometric reduction of the data is performed using two independent packages, DoPHOT and DAOPHOT II/ALLFRAME, which give

¹Based on observations with the NASA/ESA *Hubble Space Telescope*, obtained at the Space Telescope Science Institute, which is operated by AURA, Inc. under NASA Contract NO. NAS5-26555.

²Hubble Fellow

³California Institute of Technology, Pasadena CA 91125, USA

⁴Steward Observatory, University of Arizona, Tucson AZ 85721, USA

⁵European Southern Observatory, Garching, Germany

⁶Kitt Peak National Observatory, NOAO, Tucson AZ 85726, USA

⁷Dominion Astrophysical Observatory, Victoria, British Columbia V8X 4M6, Canada

⁸Carnegie Observatories, Pasadena CA 91101, USA

⁹Mount Stromlo and Siding Spring Observatories, Institute of Advanced Studies, ANU, ACT 2611, Australia

¹⁰Johns Hopkins University and Space Telescope Science Institute, Baltimore MD 21218, USA

¹¹Department of Terrestrial Magnetism, Carnegie Institutions of Washington, Washington DC 20015, USA

¹²University of Wisconsin, Madison WI 53706, USA

¹³Harvard Smithsonian Center for Astrophysics, Cambridge MA 02138 USA

¹⁴Royal Greenwich Observatory, Cambridge CB3 OHA, UK

¹⁵Lick Observatory, University of California, Santa Cruz CA 95064 USA

¹⁶NASA/IPAC Extragalactic Database and California Institute of Technology, Pasadena CA 91125, USA

very good agreement in the measured magnitudes. A total of 34 bona fide Cepheids, with periods ranging from 12 to over 60 days, are identified based on both sets of photometry. By fitting V and I period-luminosity relations, V and I distance moduli are derived assuming a Large Magellanic Cloud distance modulus and mean color excess of $\mu_{LMC} = 18.50 \pm 0.10$ mag and $E(B-V) = 0.10$ mag respectively. Assuming $A(V)/E(V-I) = 2.45$, we obtain a true distance modulus to NGC 2541 of $\mu_0 = 30.47 \pm 0.11$ (random) ± 0.12 (systematic) mag ($= 12.4 \pm 0.6$ (random) ± 0.7 (systematic) Mpc), and a total (Galactic plus internal) mean color excess $E(B-V) = 0.08 \pm 0.05$ (internal error) mag.

Subject headings: galaxies: individual (NGC2541) - galaxies: distances - stars: Cepheids

1. Introduction

This paper presents, analyzes and discusses Hubble Space Telescope (HST) V and I observations of the SaS6 (RC3, de Vaucouleurs et al. 1991) galaxy NGC 2541. These were obtained over a 47 day interval for the purpose of discovering and measuring Cepheid variables, and then using their period-luminosity (PL) relation to determine a Cepheid distance to their host system.

The observations are part of the HST Key Project on the Extragalactic Distance Scale (Freedman et al. 1994a, 1994b, 1994c; Kennicutt, Freedman and Mould 1995). Cepheid distances measured for the 18 Key Project galaxies, all within a redshift of approximately 1500 km s^{-1} , will provide an accurate absolute calibration for a number of secondary distance indicators, such as the Tully-Fisher relation, the planetary nebula luminosity function, the surface brightness fluctuation method, the expanding photosphere method, the globular cluster luminosity function and the type Ia supernova standard candle. The ultimate goal of the Key Project is to employ the above-mentioned distance indicators to determine the Hubble constant, H_0 , to within 10% accuracy.

NGC 2541, with an inclination of 58° (Bottinelli et al. 1985b), was selected as part of the Key Project because of its potential as a Tully-Fisher calibrator. Its proximity (~ 8 Mpc, Bottinelli et al. 1986) makes it a relatively easy target for the detection and measurement of Cepheid variables using HST; in addition, the galaxy has the same metallicity as the LMC (which we use as calibrator for the zero points of the Cepheid PL relation), therefore the derivation of its Cepheid distance bypasses any complications associated with a dependence of the PL relation on metal abundance (Kennicutt et al. 1998).

The galaxy (RA = $08^{\text{h}}14^{\text{m}}40^{\text{s}}$, Dec = $+49^\circ03'44''$ at equinox 2000) belongs to the NCC 2841 group (de Vaucouleurs 1975), which occupies a $15^\circ \times 7^\circ$ region of the sky near the border of

Ursa Major and Lynx. Besides the loose triplet formed by NGC 2541, NGC 2500 and NGC 2552, the group is comprised of four additional large spirals and, possibly, several dwarf systems. All of the members have low systemic velocities, in the range 420 to 750 km s⁻¹; in particular, the 21 cm velocity for NGC 2541 is 556 ± 4 km s⁻¹ (RC3, de Vaucouleurs et al. 1991).

NGC 2541 is the 11th Key Project galaxy for which a distance has been determined; published results include M81 (Freedman et al. 1994a), M100 (Freedman et al. 1994c, Ferrarese et al. 1996), M101 (Kelson et al. 1996, 1997), NGC 925 (Silbermann et al. 1996), NGC 3351 (Graham et al. 1997), NGC 3621 (Rawson et al. 1997), NGC 7331 (Hughes et al. 1998), NGC 2090 (Phelps et al. 1998), NGC 1365 (Silbermann et al. 1998) and NGC 4414 (Turner et al. 1998).

These measurements further expand the existing database of Cepheid distances, measured by a number of collaborations both using HST (NGC 4603, Zepf et al. 1997; M96, Tanvir et al. 1995; NGC 4639, Saha et al. 1997; NGC 4536, Saha et al. 1996a; NGC 4496A, Saha et al. 1996b; IC 4182, Saha et al. 1994; NGC 5253, Saha et al. 1995) and ground based facilities (SMC and LMC, Welch et al. 1987; M31, Freedman and Madore 1990; M33, Freedman et al. 1991; IC 1613, Freedman 1988; NGC 6822, McAlary et al. 1983; IC10, Wilson et al. 1996; WLM, Madore and Freedman 1991; NGC3109, Capaccioli et al. 1992; as well as for more distant galaxies, including NGC 2403 and the M81 group, Freedman and Madore 1988; NGC 300, Freedman et al. 1992; Sextans A and Sextans B, Madore and Freedman 1991; Leo I, Hodge and Wright 1978; Leo A, Hoessel et al. 1994; Pegasus, Hoessel et al. 1990; M101, Alves & Cook 1995; and the Virgo galaxy NGC 4571, Pierce et al. 1994).

This paper is organized as follows: §2 describes the data and the preliminary reduction. §3 and §4 deal with the photometric reduction and the variable star search. The *V* and *I* PL relations and the apparent distance moduli are discussed in §5, while §6 deals with the extinction and the true distance modulus. Discussion and conclusions can be found in §7.

2. Observations and Data Reduction

NGC 2541 was first observed as part of the HST Key Project on December 28, 1994, when the Wide Field and Planetary Camera 2 (WFPC2, Biretta et al. 1994) was used to obtain two F555W (close to Johnson *V*) and two F814W (close to Cousin *I*) images, with the purpose of surveying the field and assessing the correctness of the exposure times. A 47 day long observing sequence, specifically designed for finding Cepheid variables, began almost one year later, on October 30, 1995, and comprised a total of 25 F555W images, divided amongst 12 epochs, and nine F814W images, divided amongst four epochs¹⁷. The time interval between subsequent epochs was chosen as to maximize the probability of detecting Cepheids with periods between 10 and 60 days, allowing at the same time for an optimum sampling of the light curves and reducing the possibility of aliasing (Freedman et al. 1994a). The observation log is given in Table 1. All observations, including the 1994 pre-visit, were carried out at the same telescope pointing (within 0''.5) and roll

angle, with the telescope guiding in fine lock (nominal pointing stability of about 3 mas).

Figure 1 shows the WFPC2 field of view superimposed on a V band image of NGC 2541 obtained at the FLWO 1.2-m telescope. Each of the three Wide Field Camera (WFC) chips has a scale of 0.10 arcsec/pixel and a field of view of 1.3×1.3 arcmin, while the Planetary Camera (PC) chip has a scale of 0.046 arcsec/pixel and a field of view of 36×36 arcsec. The gain and readout noise for each chip are about $7 \text{ e}^-/\text{DN}$ and 7 e^- respectively.

HST/WFPC2 data are routinely calibrated using a standard pipeline maintained by the Space Telescope Science Institute (STScI). The reduction steps (described in detail by Holtzman et al. 1995a) are performed in the following order: correction of small A/D errors; subtraction of a bias level for each chip; subtraction of a superbias frame; subtraction of a dark frame; correction for shutter shading effects and division by a flat field. We performed a few additional non-standard manipulations on our images: the vignetted edges of the CCD are blocked out; bad pixels and columns are also masked using the data quality files provided by the standard pipeline, and the images are multiplied by a pixel area map to correct for the WFPC2 geometric distortion. Finally, all images are multiplied by four and converted to integer format.

As for all other Key Project galaxies, no correction is made to account for the WFPC2 charge transfer efficiency (CTE) problem (Whitmore and Heyer 1997, Whitmore 1998). This consists in a loss of counts for point sources which has increased steadily from a few percent to over 20% during the past three years, in the least favourable case of faint stars at the top of the chip (high y values) and very low sky background. While this is a potentially serious problem for any photometry project, its magnitude is less severe for long exposures with high background such as ours. In the specific case of NGC 2541, which was observed in late 1995 when the problem was still contained, we derive an upper limit to CTE losses of 1.5% (0.016 mag) for stars located at the top of the chip (or 0.008 mag for stars at the center of the chip). This effect, even if systematic, is negligible when compared to other sources of errors in the photometry (see §6.1), and will therefore be ignored.

3. Photometric Reduction

Photometric analysis of the data was performed independently using DAOPHOT II and ALLFRAME (Stetson 1994), and a variant of DoPHOT especially formulated to deal with the peculiarities of HST data and PSFs (Schechter et al. 1993, Saha et al. 1994). As extensively discussed in Hill et al. (1998) and Ferrarese et al. (1998), DoPHOT and DAOPHOT II/ALLFRAME use radically different approaches to solve the complicated problem of measuring magnitudes of stellar objects in crowded fields, therefore comparison of the DoPHOT and ALLFRAME outputs provides a powerful tool for revealing systematic errors in the measured magnitudes that could easily go unnoticed if only one of the two programs was used.

¹⁷Multiple exposures were obtained at each epoch to facilitate identification and removal of cosmic rays.

Both DoPHOT and ALLFRAME rely on a master star list to identify objects in each frame. The list is created from a very deep image obtained by combining (and rejecting cosmic rays in the process, as described later) all of the frames. The master star list contains our best approximation to a complete list of stars expected in each frame. At this point, DoPHOT and ALLFRAME follow very different routes: while DoPHOT is run independently on each image, ALLFRAME simultaneously reduces all images, identifying as real only objects belonging to the master star list and appearing in a significant fraction of the frames. This makes ALLFRAME very robust in identifying cosmic ray (CR) events, while DoPHOT is more easily run on images from which CR have been already removed. Flagging CR hits is easily done since two images, taken one immediately after the other with the same (within 0.1 pixels) pointing, are available for each epoch. The two images can be combined and cosmic rays flagged by comparing the difference in values between pairs of corresponding pixels (after accounting for possible differences in the sky level due to changes in orbital position of the spacecraft between subsequent exposures) to a local sigma calculated from the combined effects of Poisson statistics and local noise. Pixels differing by more than four sigma are flagged as cosmic rays and replaced in the combined image by the lowest of the two input values. Because of the severe undersampling of the PC and, in particular, of the WFC PSF, particular care is taken in assuring that tips of bright stars are not erroneously identified as CR hits. In summary, DoPHOT is run on a total of 13 F555W and five F814W images, while ALLFRAME is run on the original 27 F555W and 11 F814W images.

Both DoPHOT and ALLFRAME compute ‘PSF magnitudes’ for each identified star. The DoPHOT PSF magnitudes are proportional to the height of the fitted PSFs. These differ from the integrated magnitudes (flux subtended by the PSF) by an amount (the ‘aperture correction’ term) which is constant for every given chip and epoch, but will change from epoch to epoch due to PSF variations depending on telescope focus, jitter, etc. DoPHOT aperture corrections are calculated as the mean difference between aperture magnitudes (integrated within 0''.22 for the PC and 0''.5 for the WFC) and PSF magnitudes for all bright, isolated stars with errors on the aperture magnitudes less than 0.05 mag and converging growth curves (i.e. aperture magnitudes must change by no more than 0.05 mag for one pixel increments between 5 and 8 pixels). In practice, in the uncrowded NGC 2541 field, the number of stars meeting the above-mentioned criteria varies between a few (F555W/WF4) and about 80 (F814W/WF2). The DoPHOT aperture corrections calculated for the 10/30/95 epoch are listed in Table 2; to insure a uniform photometric system, aperture corrections for each other epoch are calculated as the mean difference between the aperture corrected magnitudes for the 10/30/95 epoch and the PSF magnitudes for the epoch in question.

Finally, the DoPHOT magnitudes obtained by summing the aperture corrections (AC) to the PSF magnitudes (M_{PSF}) can be converted first to the Holtzman et al. (1995b) ‘ground system’ F555W and F814W magnitudes (m_g) and then to V and I magnitudes (M) using the zero points (ZP, normalized to a unit exposure time) and color corrections listed in Table 2 (see Hill et al. 1998 and Holtzman et al. 1995b for additional details), and scaling by the exposure time t .

appropriate for each frame:

$$M = m_{PSF} + AC + ZP + 2.5\log t + C2(V - I) + C3(V - I)^2 = m_g + C2(V - I) + C3(V - I)^2. \quad (1)$$

The zero points ZP , listed in Table 2, include the ‘long exposure’ corrections (0.05 mag in both V and I) described by Hill et al. (1998), and a $2.5 \times \log(4.0)$ correction since the images have been multiplied by four before being converted to integer format.

ALLFRAME aperture corrections were derived from 10–20 bright, isolated stars for each chip, each filter *and* each frame, as the mean difference between the ALLFRAME PSF magnitudes and the 0.5 arcsec aperture magnitudes. The latter were determined with a growth-curve analysis obtained with the program DAOGROW (Stetson 1990). Equation (1), with the coefficients listed in Table 2, also provides photometric calibration for the ALLFRAME magnitudes (see Hill et al. 1998 and Silbermann et al. 1997 for additional details). The ALLFRAME aperture corrections for the first and second exposures of the 10/30/95 epoch are listed in Table 2; because of focus/jitter changes, aperture corrections for other epochs can differ by a few hundredths mag.

3.1. Comparison of the DoPHOT and ALLFRAME Photometry

The comparison between the DoPHOT and ALLFRAME magnitudes is shown in Figure 2 for a set of bright isolated stars in each chip, whose positions and DoPHOT photometry are tabulated in Tables A6a–d of the Appendix. The figure plots the difference in magnitudes between the two sets of photometry as a function of the DoPHOT magnitudes, for F555W and F814W respectively (note that, since the color correction coefficients from Table 2 are the same for ALLFRAME and DoPHOT, differences in F555W magnitudes, or F814W magnitudes, correspond to differences in V , or I , magnitudes). The weighted means and errors of the DoPHOT–ALLFRAME offsets for the secondary standard stars are tabulated in Table 3. The agreement between the two sets of photometry is excellent and well within the uncertainties associated with the aperture corrections listed in Table 2 and with the photometric errors (DoPHOT or ALLFRAME photometric errors for a 24th F555W magnitude star are of the order of 0.03 mag). The mean DoPHOT–ALLFRAME offsets and errors derived for the Cepheid stars are tabulated in Table 4 and plotted in Figure 3, and will be discussed in the next section.

4. Variable Star Search

4.1. DoPHOT Selection Criteria for Variability

The search for variable stars was performed on the V band images, following the procedure described in Saha and Hoessel (1990), the main points of which are summarized below. We

required that a star be detected in at least 10 of the 13 frames to be checked for variability. We also excluded all stars in crowded regions by rejecting candidates with a companion contributing more than 50% of the total light within a two pixel radius. Each star meeting these requirements was first tested for variability using a χ^2 test. The reduced χ_r^2 is defined by

$$\chi_r^2 = \frac{1}{(n-1)} \sum_i^n \frac{(m_i - \bar{m})^2}{\sigma_i^2}, \quad (2)$$

where m_i and σ_i are the magnitude and rms error of a particular star as measured in the i -th epoch, \bar{m} is the magnitude of the star averaged over all epochs, and n is the number of epochs in which the star is detected. A star was always flagged as variable if $\chi_r^2 \geq 8$. Stars shown as variables at a 99% confidence level (as defined in Saha and Hoessel 1990) but with $\chi_r^2 < 8$ were checked for periodicity using a variant of the Lafler and Kinman (1965) method of phase dispersion minimization, in the period range between 3 and 100 days. Stars with $\Lambda \geq 3$ were flagged as variables, where Λ is as used in Saha and Hoessel (1990), following the definition by Lafler and Kinman (1965).

Several spurious variables are detected in this procedure, as a consequence of non-Gaussian sources of error (Saha and Hoessel 1990), various anomalies in the images (e.g. residual cosmic ray events), and crowding. Therefore each star selected on the basis of the χ_r^2 and the Λ tests was visually inspected by blinking several of the individual frames against each other. This allowed us to select from the original list a total of 56 variable stars. The best period for each variable was selected by phasing the data for all periods between 3 and 100 days in incremental steps of 0.01 days. Although in most cases the final period adopted corresponds to the minimum value of the phase dispersion, in a few cases an obvious improvement of the light curve was obtained for a slightly different period. Because of the careful sampling of the data, aliasing does not present a serious problem, and we were always able to determine a preferred period for all variables, except for those with period exceeding the length of our observing window. For these long period variables, the one-year previsit helps in narrowing the possible ranges of acceptable periods, but does not remove the degeneracy completely.

4.2. ALLFRAME Selection Criteria for Variability

A total of 45 variables are identified based on the ALLFRAME photometry, using two independent methods. The first method searches for stars with unusually high dispersion in the mean V magnitudes. The second method employs a variation of the correlated variability test by Welch & Stetson (1993). Suitable candidates were defined by having the ratio σ of the average absolute deviation from the mean to the mean error in excess of 1.3. Periods for the candidate variables are found using a phase-dispersion minimization routine as described by Stellingwerf (1978). The resulting light curves are checked by eye to verify the best period for each candidate.

4.3. Definition of the Final Cepheids Sample

To be included in our final list of ‘bona fide’ Cepheids, we require a star to be detected and meet the variability criteria for both ALLFRAME and DoPHOT. Cepheids have highly periodic and very distinctive light curves. In the period range we are interested in, they are characterized by a steep rise and slower (by over a factor two for the shorter period Cepheids) decline, and a narrow maximum and broader minimum. These asymmetries are less pronounced the longer the period (a relationship known as the Hertzsprung progression), but only the longest period Cepheids (100 days or more) have nearly symmetric light curves. The magnitude range spanned is of the order of one magnitude in V , increasing slowly with period. For these reasons, variables with sinusoidal light curves or small amplitude are to be regarded suspiciously and are not included in our final Cepheid sample.

Forty-four variables are in common between the DoPHOT and ALLFRAME lists; of these, 34 show convincing Cepheid-like light curves based on both sets of photometry. These stars are listed in Table 5, numbered in order of decreasing period (shown in Table 8, to be introduced later). The epoch-by-epoch DoPHOT photometry for each Cepheid is given in Table 6 for F555W and Table 7 for F814W; we do not tabulate the ALLFRAME photometry for any of the variable stars, this is however available on line through the HST Key Project Archives at <http://www.ipac.caltech.edu/H0kp>. A list of variables that were not included in the final Cepheid list, along with detailed reasons for the exclusion, is given in the Appendix.

The 34 newly discovered Cepheids and the additional variables are identified in each of the WFPC2 chips in Figures 4a-d. Finding charts for the Cepheids are given in Figures 5. These finding charts cover a 5×5 arcsec region and have the same orientation as the corresponding chips displayed in Figures 4a-d. The contrast and intensity level have been adjusted differently for each finding chart, therefore the relative brightness of the Cepheids cannot be inferred from them. The DoPHOT light curves for all Cepheids are shown in Figures 6. Finding charts and light curves for the remaining NGC 2541 variables are shown in the Appendix.

4.4. Mean Magnitudes

In line with all other papers in this series (e.g. Ferrarese et al. 1996), we calculate both intensity averaged m_{int} and phase weighted m_{ph} mean magnitudes for all Cepheids:

$$m_{int} = -2.5 \log_{10} \sum_{i=1}^n \frac{1}{n} 10^{-0.4 \times m_i}, \quad (3)$$

$$m_{ph} = -2.5 \log_{10} \sum_{i=1}^n 0.5(\phi_{i+1} - \phi_{i-1}) 10^{-0.4 \times m_i}, \quad (4)$$

where n is the total number of observations, and m_i and ϕ_i are the magnitude and phase of the i -th observation in order of increasing phase.

Differences between m_{int} and m_{ph} are more pronounced the less uniform the phase coverage of the data points. Typical absolute differences are of the order 0.01–0.02 magnitudes, but reach 0.1 magnitudes in a few cases of not very well sampled light curves (e.g. C4 and C20). The mean difference between DoPHOT phase weighted and intensity averaged magnitudes is -0.01 ± 0.05 for F555W and 0.00 ± 0.04 for F814W.

Because of the poor phase coverage of the F814W light curves, an additional correction to both intensity averaged and phase weighted magnitudes is needed, as described in Freedman et al. 1994a. Following the finding that a Cepheid V light curve can be mapped into its I light curve by simple scaling by a factor $\alpha = 0.51$ (Freedman 1988), this correction is equal to α times the difference between the mean F555W magnitude obtained using the complete (up to 13 points) data set and the F555W magnitude calculated using only the data points in common with the F814W observations (up to 5, minimum 2). The result (which needs to be calculated separately for intensity averaged and phase weighted magnitudes) is then summed to the mean F814W magnitudes, obtained by applying (3) and (4) to the complete set of F814W data points. Typical absolute values are about 0.01–0.02 magnitudes, but they range between -0.1 to 0.1 magnitudes, being more substantial for the less uniformly sampled F814W light curves.

The final list of Cepheids, their periods, F555W, F814W (corrected as described above), V and I intensity averaged and phase weighted mean magnitudes are listed in Table 8 for DoPHOT and Table 9 for ALLFRAME. The corrections adopted for the F814W magnitudes, calculated as described above, are shown in parenthesis.

The agreement in the periods determined independently from the DoPHOT and ALLFRAME photometry for the 34 Cepheids is excellent (see Tables 8 and 9), often within 2–3% or better. This is shown in Figure 7. As already noted, aliasing is a problem only for Cepheids with period longer than ~ 45 days. These variables are characterized by a wide trough in the Lasler-Kinman plot, with no wall at the long period end (the effect of the one year pre-visit is to resolve the trough in a series of narrow minima, but the degeneracy is not removed). Because the difference in the ALLFRAME and DoPHOT periods from Figure 7 is always contained within $\pm 10\%$, this can be considered as a rough upper limit on the period uncertainty, at least for Cepheids with periods less than 45 days.

The DoPHOT and ALLFRAME phase weighted mean magnitudes for the common Cepheids are compared in Figure 3, and the mean differences are tabulated in Table 4. Within the quoted errors, the WF chips are consistent with zero offset. The Cepheids in the PC field differ by five hundredths of a magnitude, or two to three times the quoted uncertainty in the mean. This difference is not significant when compared to errors in the photometry and aperture corrections (see §3 and §6.1).

Before proceeding to use our Cepheid sample to derive apparent and true distance moduli to

NGC 2541, it is wise to perform two further checks. The first is to make sure that the photometric errors for the Cepheids are similar, in the mean, to those of non-variable stars with comparable magnitude. One concern addressed with this point (to be discussed in more detail in Ferrarese et al. 1998, which will deal with the photometric recovery of artificial stars in crowded fields), is that some of the Cepheids might be part of (not necessarily physical) pairs which are not resolved by DoPHOT and/or ALLFRAME, so that their magnitudes are measured too bright. Photometric errors in this case would be higher than expected for an isolated star of similar magnitude. The DoPHOT photometric errors are shown in Figure 8 for the 10/30/95 epoch and WF2; these are representative of the errors for all other epochs, and since WF2 is the most crowded chip, they are upper limits to the errors measured in the other chips. The Cepheids, plotted as solid dots, lie on the main error ridge-line, with the exception of two outliers: C2 which is in a crowded region in WF3 (therefore a larger error is to be expected), and C8 which was measured with a large uncertainty in the 10/30/95 epoch, but normal (for its magnitude) uncertainty in all other epochs. The second test is to confirm that all variables listed as Cepheids lie within the instability strip in a color magnitude diagram (CMD). An I , $V - I$ CMD is shown in Figure 9; Cepheids are marked by the large filled circles, while all other stars are plotted as points. The Cepheids do in fact lie in a band between $0.4 \leq V - I \leq 1.4$, fully within the instability strip.

5. The Period-Luminosity Relation and the Apparent Distance Moduli to NGC 2541

We will first consider the apparent distance moduli derived from the DoPHOT photometry. In keeping with all other papers in this series, the V and I PL relations derived by Madore and Freedman (1991) for a sample of 32 Cepheids in the LMC, provide the zero points for calibration of the apparent V and I distance moduli to NGC 2541. Assuming an LMC true modulus and average line-of-sight reddening of 18.50 ± 0.10 and $E(B - V) = 0.10$ mag respectively, these PL relations give for the absolute magnitude M of Cepheids as a function of period P :

$$M_V = -2.76[\log_{10}(P) - 1.0] - 4.16 \quad (5)$$

and

$$M_I = -3.06[\log_{10}(P) - 1.0] - 4.87. \quad (6)$$

As in all other papers in this series, in fitting the NGC 2541 data, the slope of the PL relation (both in V and I) is fixed to the LMC values given in equations (5) and (6). This minimizes those biases due to incompleteness at short periods in the NGC 2541 sample, which would artificially produce a shallower PL slope. Because Cepheids C1 through C6 (Table 8) do not have well defined periods, they are not used in fitting the PL relation. Since our sample does not contain

Cepheids with period less than ≈ 8 days (the shortest period Cepheid, C34, has $P = 12$ days) we are confident that all of the Cepheids are oscillating in the fundamental mode, rather than in the first harmonic (Smith et al. 1992).

The fits to the NGC 2541 V and I PL relations are performed as described in Freedman et al. 1994a. Outliers falling more than three sigma away from the mean, in either the V or I PL plots, are excluded from the fit. The best fitting PL relations for the remaining 27 Cepheids, using phase weighted mean magnitudes are:

$$m_V = -2.76[\log_{10}(P) - 1.0] + (26.58 \pm 0.03) \quad (7)$$

and

$$m_I = -3.06[\log_{10}(P) - 1.0] + (25.76 \pm 0.04), \quad (8)$$

where the uncertainties are equal to the rms of the fit (0.18 mag in V and 0.23 mag in I) divided by the square root of the number of Cepheids constraining the fit (27). The best fitting PL relations are shown by the solid lines in Figure 10. The dashed lines, drawn at ± 0.54 mag for the V PL plot, and ± 0.36 mag for the I PL plot, reflect the finite width of the Cepheid instability strip, and thus the expected intrinsic scatter around the best fitting PL relation. The only 3σ outlier, C11, is marked by the open circle. Of all the Cepheids, C11 is the one with the least well defined light curve: this appears fairly symmetric in DoPHOT (but much less so in ALLFRAME), and the minimum might be flatter than expected. A posteriori, we conclude that C11 is likely contaminated by a companion.

The values given in equations (7) and (8), combined with the LMC calibrating PL relations (equations 5 and 6), give for the apparent distance moduli to NGC 2541:

$$\mu_V = (26.58 \pm 0.03) + 4.16 = 30.74 \pm 0.03 \quad (9)$$

and

$$\mu_I = (25.76 \pm 0.04) + 4.87 = 30.63 \pm 0.04. \quad (10)$$

A complete estimate of the errors on the apparent distance moduli will be derived in §6.1. As discussed in §4.4, the fact that all of the Cepheids have very well sampled light curves gives rise to only very small differences between phase weighted and intensity averaged magnitudes. As a consequence, the apparent distance moduli in equations (9) and (10) are reproduced (to within 0.01 mag in V and 0.001 mag in I) if intensity averaged magnitudes are used instead. A weighted fit to the PL relations, using the inverse of the χ^2 (Table 8) as a measure of the ‘goodness’ of

each Cepheid, also gives distance moduli well in agreement with equations (9) and (10) within the formal uncertainty of the fit.

A more serious source of concern is the fact that the faint end incompleteness intrinsic to the photometry and the finite width of the PL relation, will in general conspire to produce an *overall* shift of the PL relation towards brighter magnitudes (since the slope of the PL relation is kept fixed). Fake stars simulations of the NGC 2541 field, to be described elsewhere (Ferrarese et al. 1998), show that incompleteness effects are noticeable for $V > 26.5$ (about 50% of $V = 26.5$ mag stars are recovered). From Table 8, $V = 26.5$ mag corresponds to Cepheids with period of about 15–18 days. To be precise, because our sample of Cepheids includes only objects with high quality (small errors) photometry, a star needs, by definition, to be in a fairly uncrowded field to be selected as a Cepheid, therefore the Cepheid sample is *by construction* not as affected by faint end incompleteness biases (which are mainly produced by crowding) as the complete non-variable star sample, and we expect significantly more than 50% of $V = 26.5$ mag Cepheids to be detected. However, to be conservative, we fit PL relations to the subsample of 15 Cepheids with periods larger than 20 days (C7 to C21). The resulting distance moduli are 0.02 magnitudes larger, in both V and I , than the ones quoted in equations (9) and (10); this increase is not significant when compared to the formal internal errors in the fits (0.04 mag in V and 0.05 mag in I when the smaller sample is used). Therefore the concerns arisen by Ferrarese et al. (1996) for the M100 Cepheids (for which a 0.1 increase in the apparent distance moduli was observed when the period cutoff was moved from eight to 20 days) do not apply to the closer and less crowded NGC 2541 field. Therefore, we adopt the distance moduli given in (9) and (10) as our final values.

Using the phase weighted magnitudes derived from the ALLFRAME photometry (Table 9) and performing an unweighted fit gives distance moduli $\mu_V = 30.70 \pm 0.04$ and $\mu_I = 30.62 \pm 0.04$, in agreement with the DoPHOT distance moduli within the formal uncertainty of the fits.

6. The Extinction and the True Distance Modulus

The true distance modulus to NGC 2541, μ , is given by

$$\mu = \mu_V - A(V) = \mu_I - A(I) \quad (11)$$

where the V and I band absorption coefficients $A(V)$ and $A(I)$ obey the relation $A(V)/E(V - I) = 2.45$. This is consistent with the extinction laws by Cardelli, Clayton and Mathis (1989), Stanek (1996) and Dean, Warren and Cousins (1978), and assumes $R_V = A(V)/E(B - V) = 3.3$.

Given the apparent distance moduli determined in the previous section, we obtain from equation (11) $A(V) = 0.27 \pm 0.17$ (internal error) and therefore $E(B - V) = 0.08 \pm 0.05$ (internal error). The true distance modulus is therefore¹⁸

$$\mu = 30.47 \pm 0.11(\text{random}) \pm 0.12(\text{systematic}) \text{ mag}, \quad (12)$$

where the quoted errors will be discussed in §6.1. Using the distance moduli derived from the ALLFRAME photometry gives a true distance modulus to NGC 2541 of 30.50 mag, and a color excess $E(B-V) = 0.06$.

6.1. Error Budget

The error budget in the determination of the true distance modulus is given in Table 10. There are five main sources of uncertainty:

- i) errors in the calibrating LMC PL relations given in equations (5) and (6) (including errors in the LMC true distance modulus and in the zero points of the LMC V and I PL relations). Because this uncertainty affects all Key Project galaxies exactly the same way, it has a systematic nature.
- ii) errors in the adopted value of R_V for NGC 2541. This and all subsequent errors propagate randomly to the entire sample of Key Project galaxies.
- iii) errors intrinsic to the assumption that the LMC and NGC 2541 share the same metallicity and ratio of total to differential reddening R_V ;
- iv) errors in the photometric calibration of the NGC2541 data (photometric zero points and aperture corrections, see Table 2); and finally
- v) errors associated with fitting the PL relation to NGC 2541 (equations 7 and 8).

A detailed discussion on the errors associated with the LMC calibrating PL relations (point i) is given in Phelps et al. (1998) and summarized in Table 10, and amount to a 0.12 mag.

Varying R_V within an acceptable range (e.g. Cardelli, Clayton and Mathis 1989) produces negligible effects on the final distance modulus. We assumed $R_V = 3.3$ for both the LMC and NGC 2541 throughout our derivation of the true distance modulus; if $R_V = 3.0$ instead, then we obtain from equation (11) $A_V = 0.26$, and the distance modulus is underestimated by only 0.01 magnitudes.

Point iii) is more subtle. There are two concerns: the first is that metallicity differences between the calibrating LMC sample and the project galaxy (NGC 2541 in our case), can affect the absolute slope and zero point of the PL relations (Kochanek 1998). The second is that the ratio of total to differential reddening R_V might be different between the LMC and NGC 2541, in which case, as explained in Ferrarese et al. (1996), the true distance modulus to NGC 2541

¹⁸ As discussed in Ferrarese et al. 1996, this result is correct if R_V is the same for the LMC and NGC 2541. If this is not the case, the distance modulus to NGC 2541 will depend on the value of $A(V)$ for the LMC. This source of uncertainty is discussed in §6.1.

has an explicit dependence on the value of the visual absorption A_V to the LMC. The first point is of little consequence for NGC 2541: the recent work by Kennicutt et al. (1998) based on observations of Cepheids in two fields in the nearby spiral galaxy M101, points to a weak dependence of the inferred distance modulus μ on metal abundance: $\delta\mu/\delta[O/H] = -0.24 \pm 0.16$ mag dex $^{-1}$. Moreover, the measured oxygen abundance in the LMC and NGC 2541 are almost identical: [O/H] = -0.40 for the LMC (Kennicutt et al. 1998), and [O/H] = -0.42 ± 0.09 for NGC 2541 (Zaritsky, Kennicutt & Huchra 1994). This would lead to a overestimate of the distance to NGC 2541 of 0.005 ± 0.02 mag.

Differences in the value of R_V between the LMC and NGC 2541 can produce larger errors: from equation (8) of Ferrarese et al. (1996), assuming $R_V = 3.0$ for NGC 2541, $R_V = 3.3$ and $E(B-V) = 0.2$ for the LMC (foreground plus internal reddening, Bessell et al. 1991), would lead to a true distance modulus 0.03 mag smaller than quoted in equation (12).

Errors on the photometric calibration include errors in the aperture corrections (Table 2, we conservatively adopt the largest of the measured uncertainties, 0.011 mag in V and 0.014 mag in I), in the photometric zero points (± 0.02 mag, Hill et al. 1998) and in the long-vs-short exposure correction (± 0.02 mag, Hill et al. 1998). These errors, being uncorrelated, are added in quadrature to give a 0.03 mag random error in both V and I . When propagated to the true distance modulus, the errors $\epsilon(V)$ and $\epsilon(I)$ on the V and I magnitudes thus derived, are to be combined in quadrature (since they are uncorrelated), weighted by the term $R = A(V)/E(V-I)$, so that the corresponding error on the distance modulus is equal to $\sqrt{\epsilon(V)^2 \times (1-R)^2 + \epsilon(I)^2 \times R^2}$ (see equation 7 of Ferrarese et al. 1996 for further details).

Finally, errors in the V and I PL relations are equal to the rms scatter of the data points with respect to the fit, divided by the square root of the number of Cepheids contributing to the fit. Much of the scatter in the individual PL relations is highly correlated (as opposed to the errors in the individual data points which are largely uncorrelated), where that wavelength-correlated scatter is due to intrinsic color and differential reddening differences from star to star. Further discussion on this point can be found in Madore et al. (1998).

7. Discussion and Conclusions

The distance modulus to NGC 2541 was calculated by Bottinelli et al. (1984, 1985b, 1986) based on the B-band Tully Fisher relation (Bottinelli et al. 1983), the zero point of which was calibrated using the assumed distances to 12 nearby galaxies (de Vaucouleurs 1978a-d). Bottinelli et al. (1984) give a distance modulus of 29.41 ± 0.18 mag, later revised to 29.53 ± 0.26 mag (Bottinelli et al. 1985b) and 29.82 ± 0.19 mag (Bottinelli et al. 1986). An independent distance modulus of 29.50 ± 0.23 mag was derived by Bottinelli et al. (1995a) using the method of ‘sosie’ galaxies (‘sosies’ are defined as having the same morphological type, axis ratio and maximum rotational velocity as one of 14 calibrating galaxies, where the data are derived from the Bottinelli

et al. 1983 catalog of HI line data and the Second Reference Catalog of Bright Galaxies). Finally, de Vaucouleurs (1975) found a distance modulus of 29.53 ± 0.2 mag to the NGC 2841 group, to which NGC 2541 belongs, based on a variety of secondary distance indicators (HII regions, brightest stars, luminosity class).

All published distances to NGC 2541 are summarized in Table 11. While they are in very good agreement with each other, there is a significant disagreement with the Cepheid distance derived in this paper. However, we notice that the distance moduli given by Bottinelli et al. (1986) for NGC 2500 and NGC 2841, likely members of the same group, are 30.44 ± 0.91 mag and 30.54 ± 0.17 mag respectively, close to our value for NGC 2541. NGC 2541 forms a triplet with NGC 2500 and NGC 2552. Their peculiar velocity are 556 km s^{-1} , 516 km s^{-1} and 519 km s^{-1} respectively (RC3), suggesting in themselves association, and it seems unlikely that NGC 2541 is a foreground object as the Bottinelli et al. distance would have us believe.

An independent IR Tully–Fisher distance to NGC 2541 was kindly provided by Stephane Courteau (private communication). Based on the Willick et al. (1997) Tully–Fisher calibration, the distance modulus to NGC 2541 is 30.86 ± 0.3 mag. Using the inverse Tully–Fisher relation instead (Willick et al. 1997), a consistent result is obtained: 30.78 ± 0.3 mag. Within the quoted errors, these values are in agreement with the Cepheid distance modulus found in this paper, and strengthen the suspicion that the data used by Bottinelli et al. (1984, 1985b, 1986) are in error. Unfortunately, there are no early-type galaxies in the vicinity of NGC 2541 that can be used to derive an independent distance to the group using the surface brightness fluctuation or planetary nebulae luminosity function methods.

The following is a brief summary of the results presented in this paper. HST/WFPC2 images of the spiral galaxy NGC 2541, distributed over 13 V and five I epochs within a 47 day window, allowed the discovery of 34 Cepheid variables and 23 additional variable stars, none of which previously known. Photometry for all the stars in the field has been performed independently using a variant of the DoPHOT program (Schechter et al. 1993, Saha et al. 1994) and the DAOPHOT II/ALLFRAME package (Stetson 1994); very good agreement (within 0.05 mag) is found between the two sets of photometry. A subsample of 27 Cepheids with well defined periods between 12 and 47 days, was chosen to fit V and I PL relations and derive V and I apparent distance moduli by assuming a Large Magellanic Cloud distance modulus and mean color excess of $\mu_{LMC} = 18.50 \pm 0.10$ mag and $E(B - V) = 0.10$ mag respectively. Assuming $R_V = A(V)/E(B - V) = 3.3$, we derive $A(V)/E(V - I) = 2.45$ based on the extinction laws by Cardelli, Clayton and Mathis (1989), Stanek (1996) and Dean, Warren and Cousins (1978). This leads to a true distance modulus to NGC 2541 of $\mu_0 = 30.47 \pm 0.11$ (random) ± 0.12 (systematic) mag ($= 12.4 \pm 0.6$ (random) ± 0.7 (systematic) Mpc, and a total (Galactic plus internal) mean color excess $E(B - V) = 0.08 \pm 0.05$ (internal error) mag.

LF wishes to thank Dr Stephane Courteau for providing an IR Tully–Fisher distance to NGC 2541.

LF acknowledges support by NASA through Hubble Fellowship grant HF-01081.01-96A awarded by the Space Telescope Science Institute, which is operated by the Association of Universities for Research in Astronomy, Inc., for NASA under contract NAS 5-26555

The work presented in this paper is based on observations with the NASA/ESA Hubble Space Telescope, obtained by the Space Telescope Science Institute, which is operated by AURA, Inc. under NASA contract No. 5-26555. Support for this work was provided by NASA through grant GO-2227-87A from STScI.

A. Other Variable Stars in the NGC 2541 Field

The 23 stars that did not make the final Cepheid list for the reasons listed below, are reported in Table A1. Their epoch-by-epoch DoPHOT photometry is shown in Tables A2 and A3 (the ALLFRAME photometry is tabulated for V6, which was not measured by DoPHOT), and their periods and phase weighted and intensity averaged magnitudes are listed in Tables A4 and A5 for DoPHOT and ALLFRAME respectively. Figures 11 and 12 show 5×5 arcsec finding charts and light curves respectively.

Of the 45 variables identified from the ALLFRAME photometry, all but one (which was not measured by DoPHOT) are in common with the DoPHOT variable list. Five variables selected on the basis of the DoPHOT photometry did not show convincing evidence of variability from the ALLFRAME photometry. For all of them, the ALLFRAME internal errors are large compared to the magnitude range spanned, and therefore the stars fall significantly short of the ALLFRAME cutoff criterion for variability, i.e. $\sigma \ll 1.3$. Furthermore, the ALLFRAME Lafler-Kinman plots for these stars are extremely noisy and do not have a convincing minimum. Seven more DoPHOT variables were not found in the ALLFRAME master star list.

For ten of the 44 variables in common between DoPHOT and ALLFRAME that meet the selection criteria listed in §4.1 and §4.2, the quality of the light curves was not deemed good enough for the stars to be promoted to the ‘bona fide Cepheids’ rank, and used in fitting the PL relation. The notes to Table A4 list in more detail the reasons for excluding these variables from the Cepheids sample. These reasons include the fact that the light curve appears symmetric, the I light curve is not variable or is not measured, or the amplitude of the V light curve is small, possibly suggesting that the star is contaminated by a bright companion.

Note that a few of the variables which were not found in the ALLFRAME photometry do show convincing Cepheid-like light curves based on the DoPHOT photometry (in particular V9). The requirement that only variables measured as such by *both* DoPHOT and ALLFRAME be in the final Cepheid list protects us from uncertainties in the determination of the periods and small (≤ 0.1 mag) systematic errors in the photometry (larger errors have already been excluded based on the comparisons shown in Figure 2).

Fig. 1.— V band ground-based image of NGC 2541, obtained at the FLWO 1.2-m telescope. Superimposed is the HST/WFPC2 field of view; the PC is the smallest of the four chips, WF1, WF2 and WF3 follow counterclockwise.

Fig. 2.— Comparison between the DoPHOT and ALLFRAME F555W and F814W magnitudes for the secondary standards, whose positions and DoPHOT photometry are tabulated in Tables A6a-d.

Fig. 3.— Comparison between the DoPHOT and ALLFRAME F555W and F814W magnitudes for the Cepheids listed in Table 8.

Fig. 4.— Deep HST F555W images of NGC 2541 obtained by combining all F555W epochs. The 34 Cepheids and the additional 23 variables are identified in each of the WFPC2 chips by white circles and labeled following the convention adopted in Tables 8 and A1.

Fig. 5.— Finding charts for the Cepheids listed in Table 8. Each finding chart covers a 5×5 arcsec region and has the same orientation as the corresponding chips displayed in Figures 4a-d. The cross marks the position of the Cepheid. The contrast and intensity level have been adjusted differently for each finding chart, therefore the relative brightness of the Cepheids cannot be inferred from them.

Fig. 6.— DoPHOT light curves for all Cepheids listed in Table 8. Variables in the plots are labeled with their ID numbers; DoPHOT periods, F555W and F814W magnitudes (before applying the correction discussed in §4.4) are also reported. Solid and open squares are for F555W and F814W data points respectively.

Fig. 7.— Comparison of the DoPHOT and ALLFRAME periods for the 34 Cepheids found in the NGC 2541 field. The dashed lines correspond to a period difference of $\pm 10\%$.

Fig. 8.— DoPHOT photometric errors for the 10/30/95 epoch and WF2: the lower curve represents errors in the V magnitudes (scale to the left), while the upper curve shows errors in the I magnitudes (scale to the right). These errors are representative for all epochs, and since WF2 is the most crowded chip, they are upper limits to the errors measured in the other chips. The Cepheids are plotted as large solid dots.

Fig. 9.— Color magnitude diagram for all the stars in NGC 2541. Magnitudes are derived as the mean of the measured magnitudes over all available epochs. The Cepheids, shown by the large solid dots, are located within the boundaries of the instability strip

Fig. 10.— V and I PL relations for the sample of 34 Cepheids (see §5 for details). The best fitting PL relations are shown by the solid lines. The dashed lines, drawn at ± 0.54 mag for the V PL plot, and ± 0.36 mag for the I PL plot, reflect the finite width of the Cepheid instability strip, and thus the expected intrinsic scatter around the best fitting PL relation. The only 3σ outlier, C11, is marked by the open circle. Phase weighted DoPHOT magnitudes are used in the plots.

Fig. 11.— Finding charts for other variable stars in NGC 2541, which were not deemed of high enough quality to be included in the final Cepheid list (Table A1, see §4.3 for more details). Each finding chart covers a region 5×5 arcsec and is oriented as the chips in Figures 4a-d. In each panel, the cross marks the position of the Cepheid.

Fig. 12.— Light curves for the variable stars listed in Table A1. Variables in the plots are labeled with their ID numbers, periods, F555W and F814W magnitudes (before applying the correction discussed in §4.4). Solid and open squares are for F555W and F814W data points respectively.

REFERENCES

- Alves, D.R. & Cook, K.H. 1995, AJ, 110, 192
Bottinelli, L., Gouguenheim, L. & Paturel, G. 1983, A&A, 118, 4
Bottinelli, L., Gouguenheim, L., Paturel, G. & Teerikorpi, P. 1985a, ApJS, 59, 293
Bottinelli, L., Gouguenheim, L., Paturel, G. & de Vaucouleurs, G. 1984, A&AS, 56, 381
Bottinelli, L., Gouguenheim, L., Paturel, G. & de Vaucouleurs, G. 1985b, A&AS, 59, 43
Bottinelli, L., Gouguenheim, L., Paturel, G. & Teerikorpi, P. 1986, A&A 156, 157
Biretta, J., et al. 1996, Wide Field and Planetary Camera 2 Instrument Handbook, version 4.0 (Baltimore: STScI)
Capaccioli, M., Piotto, G. & Bresolin, F. 1992, AJ, 103, 1151
Cardelli, J.A., Clayton, G.C.,& Mathis, J.S. 1989, ApJ, 345, 245
de Vaucouleurs, G. 1975, in ‘Stars and Stellar System #9’, eds. A.Sandage, M.Sandage, J.Kristian, p. 557
de Vaucouleurs, G. 1978a, ApJ, 223, 351
de Vaucouleurs, G. 1978b, ApJ, 223, 730
de Vaucouleurs, G. 1978c, ApJ, 224, 14
de Vaucouleurs, G. 1978d, ApJ, 224, 710
de Vaucouleurs, G., de Vaucouleurs, A., Corwin, H. G., Buta, R. J., Paturel, G. & Fouque, P. 1991, Third Reference Catalog of Bright Galaxies (New York: Springer)
Ferrarese, L. et al. 1996, ApJ, 464, 568
Ferrarese, L. et al. 1998, in preparation
Freedman, W.L. 1988, ApJ, 326, 691
Freedman, W.L. & Madore, B.F. 1988, ApJL, 332, L63
Freedman, W.L., Wilson, C.D., Madore, B.F. 1991, ApJ, 372, 455

- Freedman, W.L. et al. 1992, ApJ, 396, 80
Freedman, W.L. et al. 1994a, ApJ 427, 628
Freedman, W.L. et al. 1994b, ApJL 435, L31
Freedman, W. L., et al. 1994c, Nature, 371, 757
Graham, J. et al. 1997, ApJ, 477, 535
Hill, R.J. et al. 1998, ApJ, in press
Hodge, P.W. & Wright, F.W. 1978, AJ, 83, 228
Hoessel, J.G. et al. 1990, AJ, 100, 1151
Hoessel, J.G., Saha, A., Krist, J., Danielson, G.E. 1994, AJ, 108, 645
Holtzman, J.A. et al. 1995a, PASP, 107, 156
Holtzman, J.A. et al. 1995b, PASP, 107, 1065
Hughes et al. 1998, ApJ, in press
Kelson, D. et al. 1996, ApJ, 463, 26
Kelson, D. et al. 1997, ApJ, 478, 430
Kennicutt, R. C., Freedman, W.L., & Mould, J.R. 1995, AJ, 110, 1476
Kennicutt, R. C. et al. 1998, ApJ, in press
Kochanek, C. S. 1998, ApJ, submitted
Lafler, J., Kinman T.D. 1965, ApJS, 11, 216
Madore, B.F. & Freedman, W.L. 1991, PASP, 103, 933
Madore, B.F. et al. 1998, in preparation
McAlary, C.W. et al. 1983, ApJ, 273, 539
Phelps R. et al. 1998, ApJ, in press
Pierce, M.J., et al. 1994, Nature, 371, 385
Rawson, D.M. et al. 1997, ApJ, 490, 517
Saha, A., Labhardt, L., Schwengeler, H., Macchetto, F. D., Panagia, N., Sandage, A. & Tammann, G. A. 1994, ApJ, 425, 14
Saha, A., Hoessel J.G. 1990, AJ 99, 97
Saha, A., Sandage, A., Labhardt, L., Schwengeler, H., Tammann, G. A., Panagia, N. & Macchetto, F. D. 1995, ApJ, 438, 8
Saha, A., Sandage, A., Labhardt, L., Tammann, G. A., Panagia, N. & Macchetto, F. D. 1996a, ApJ, 466, 55
Saha, A., Sandage, A., Labhardt, L., Tammann, G. A., Panagia, N. & Macchetto, F. D. 1996b, ApJS, 107, 693

- Saha, A., Sandage, A., Labhardt, L., Tammann, G. A., Macchetto, F. D. & Panagia, N. 1997,
ApJ, 486, 1
- Schechter, P.L., Mateo, M., Saha, A. 1993, PASP, 105, 1342
- Silbermann, N.A. et al. 1996, ApJ, 470, 1
- Silbermann, N.A. et al. 1998, ApJ, submitted
- Smith, H.A., Silbermann, N.A., Baird, S.R. & Graham, J.A. 1992, AJ, 104, 1430
- Stellingwerf, R.F. 1978, ApJ, 224, 953
- Stetson P.B. 1994, PASP, 106, 250
- Tanvir, N.R. et al. 1995, Nature, 377, 27
- Turner, A. et al. 1998, ApJ, submitted
- Welch, D.L. & Stetson, P.B. 1993, AJ, 105, 1813
- Welch, D.L., McLaren, R.A., Madore, B.F. & McAlary, C.W. 1987, ApJ, 321, 162
- Welch, D.L., Madore, B.F., McAlary, C.W. & McLaren, R.A. 1986, ApJ, 305, 583
- Willick, J.A. et al. 1997, ApJS, 109, 333
- Wilson, C.D. et al. 1996, AJ, 111, 1106
- Zaritsky, D., Kennicutt, R. C. & Huchra, J. P. 1994, ApJ, 420, 87
- Zepf, S.E. et al. 1997, BAAS, 29, 1208

Table 1. HST Observations of NGC 2541.

Date of Observation	JD ^a	Exposure Time	Filter
12/28/94	2449714.72809	1500 + 1000	F555W
	2449414.79916	1100 + 1400	F814W
10/30/95	2450020.58781	1100 + 1100	F555W
	2450020.64973	1300 + 1300	F814W
11/05/95	2450027.23003	1100 + 1100	F555W
	2450027.28363	1300 + 1300	F814W
11/13/95	2450035.00566	1100 + 1100	F555W
11/15/95	2450037.01763	1100 + 1100	F555W
11/17/95	2450038.96153	1100 + 1100	F555W
11/20/95	2450041.91476	900 + 900 + 260	F555W
	2450041.97876	1100 + 1100 + 260	F814W
11/22/95	2450044.32303	1100 + 1100	F555W
11/25/95	2450047.40519	1100 + 1100	F555W
11/29/95	2450051.22419	1100 + 1100	F555W
12/03/95	2450055.11055	1100 + 1100	F555W
12/08/95	2450060.33932	1100 + 1100	F555W
	2450060.40402	1300 + 1300	F814W
12/15/95	2450067.10285	1100 + 1100	F555W

^aThe Julian Date is given for the middle of the CR-split sequence.

Table 2. Photometric Coefficients

Chip	Filter	ZP _{DOP} ^a	AC _{DOP} ^{b,c}	ZP _{ALL} ^a	AC _{ALL,1} ^{b,d}	AC _{ALL,2} ^{b,e}	C2	C3
PC	F555W	23.878	-0.9061 ± 0.0086 (22)	24.031	0.009 ± 0.012 (21)	-0.023 ± 0.011 (23)	-0.52	0.27
WF2	F555W	23.969	-0.6858 ± 0.0046 (18)	24.042	0.007 ± 0.0085 (24)	-0.012 ± 0.0090 (23)	-0.52	0.27
WF3	F555W	23.956	-0.641 ± 0.011 (9)	24.051	0.040 ± 0.011 (21)	+0.021 ± 0.013 (19)	-0.52	0.27
WF4	F555W	23.954	-0.7341 ± 0.0086 (5)	24.027	0.023 ± 0.020 (13)	-0.009 ± 0.023 (10)	-0.52	0.27
PC	F814W	23.007	+1.0527 ± 0.0089 (72)	23.137	0.013 ± 0.012 (18)	+0.032 ± 0.012 (16)	-0.63	0.25
WF2	F814W	23.139	-0.7536 ± 0.0094 (85)	23.178	0.047 ± 0.0084 (23)	+0.022 ± 0.0083 (22)	-0.63	0.25
WF3	F814W	23.083	-0.765 ± 0.014 (23)	23.159	0.090 ± 0.010 (22)	+0.037 ± 0.010 (20)	-0.63	0.25
WF4	F814W	23.084	-0.786 ± 0.013 (12)	23.130	0.069 ± 0.014 (17)	0.038 ± 0.015 (15)	-0.63	0.25

^aErrors on both DoPHOT and ALLFRAME zero points are of the order 0.02 mag (Hill et al. 1998).

^bThe number of stars used to determine the aperture correction is shown in parenthesis.

^cDoPHOT aperture corrections calculated for the 10/30/95 CR-split combined reference epoch (see text for details).

^dALLFRAME aperture corrections calculated for the first CR-split exposure of the 10/30/95 epoch (see text for details).

^eAs for ^c but for the second CR-split exposure of the 10/30/95 epoch.

Table 3. Comparison of DoPHOT and ALLFRAME for Secondary Standard Stars

Chip	# of Stars	$\Delta(F555W)^*$	$\Delta(F814W)^*$
PC	24	+0.015 ± 0.042	-0.027 ± 0.079
WF2	29	+0.007 ± 0.061	+0.02 ± 0.10
WF3	32	-0.042 ± 0.042	-0.050 ± 0.050
WF4	29	0.013 ± 0.061	-0.023 ± 0.074

*The quoted magnitude differences are DoPHOT - ALLFRAME

Table 4. Comparison of DoPHOT and ALLFRAME for the Cepheids

Chip	# of Stars	$\Delta(F555W)^a$	$\Delta(F814W)^a$
PC	4	0.056 ± 0.016	0.057 ± 0.025
WF2	17	0.010 ± 0.034	0.006 ± 0.072
WF3	7	0.046 ± 0.063	0.026 ± 0.063
WF4	6	0.023 ± 0.044	0.040 ± 0.037

^aThe quoted magnitude differences are DoPHOT – ALLFRAME

Table 5. Astrometry for the NGC 2541 Cepheids

ID ^a	X ^b	Y ^b	RA(J2000) ^c	Dec(J2000) ^c	Chip
C1	778.40	383.03	8:14:39.3883	49:01:30.744	PC
C2	245.23	69.40	8:14:43.6650	49:02:09.536	WF3
C3	236.86	105.11	8:14:43.9341	49:02:07.069	WF3
C4	634.67	648.57	8:14:50.6798	49:02:14.827	WF3
C5	606.78	383.03	8:14:39.2542	49:02:50.263	WF2
C6	283.15	766.84	8:14:43.9961	49:03:07.804	WF2
C7	300.92	152.92	8:14:40.8157	49:02:15.454	WF2
C8	559.18	536.21	8:14:39.2727	49:01:42.799	PC
C9	526.92	602.44	8:14:43.7985	49:00:40.495	WF4
C10	178.55	725.74	8:14:44.7133	49:02:59.188	WF2
C11	229.14	126.18	8:14:44.0795	49:02:05.372	WF3
C12	764.46	560.16	8:14:38.7482	49:03:13.156	WF2
C13	639.39	344.56	8:14:38.7781	49:02:48.503	WF2
C14	299.21	70.01	8:14:43.9373	49:02:14.167	WF3
C15	640.66	491.09	8:14:39.4904	49:03:01.269	WF2
C16	350.56	773.73	8:14:43.4375	49:03:11.663	WF2
C17	375.52	170.34	8:14:44.6675	49:01:25.213	WF4
C18	353.98	340.57	8:14:46.5795	49:02:05.660	WF3
C19	157.76	103.42	8:14:43.1054	49:01:41.719	WF4
C20	260.79	79.30	8:14:40.8068	49:02:07.172	WF2
C21	622.43	605.45	8:14:44.6162	49:00:35.512	WF4
C22	422.29	259.51	8:14:44.6247	49:01:15.220	WF4
C23	146.71	392.39	8:14:43.3589	49:02:28.754	WF2
C24	480.66	445.47	8:14:39.8159	49:01:43.854	PC
C25	676.48	447.00	8:14:38.9581	49:02:59.175	WF2
C26	436.86	484.37	8:14:39.7602	49:01:46.464	PC
C27	647.39	454.90	8:14:39.2524	49:02:58.459	WF2
C28	277.12	687.76	8:14:43.6641	49:03:00.698	WF2
C29	771.82	435.99	8:14:38.0706	49:03:02.797	WF2
C30	101.78	65.83	8:14:42.1380	49:01:58.412	WF2
C31	146.16	536.68	8:14:47.2682	49:01:38.115	WF3
C32	307.34	64.38	8:14:44.6073	49:01:37.652	WF4
C33	161.59	298.56	8:14:42.7639	49:02:21.330	WF2
C34	315.08	416.30	8:14:41.9930	49:02:38.993	WF2

^aThe Variable Stars ID is the same in this and all subsequent tables.

^bThe X and Y coordinate are relative to the 10/30/95 epoch. For each 800×800 pixels chip, pixel [1,1] is located at the edge of the pyramid.

^cRA and Declination are calculated using the IRAF task STSDAS.HST_CALIB.WFP.C.METRIC, version 1.3.5 (July 1996)

Table 6. V Photometry for NGC 2541 Cepheids .

JD	$V \pm \sigma_V$					
2449700+	C1	C2	C3	C4	C5	C6
14.728	23.98 \pm 0.05	24.97 \pm 0.10	24.69 \pm 0.05	24.54 \pm 0.05	24.42 \pm 0.05	24.27 \pm 0.08
320.588	24.54 \pm 0.05	25.18 \pm 0.19	24.41 \pm 0.05	24.54 \pm 0.05	24.35 \pm 0.05	24.39 \pm 0.05
327.230	24.84 \pm 0.05	25.16 \pm 0.11	24.66 \pm 0.05	24.65 \pm 0.05	24.36 \pm 0.05	24.59 \pm 0.05
335.006	24.60 \pm 0.05	25.49 \pm 0.17	24.92 \pm 0.09	24.84 \pm 0.05	24.03 \pm 0.05	24.79 \pm 0.05
337.018	24.46 \pm 0.05	25.30 \pm 0.15	24.68 \pm 0.06	24.86 \pm 0.05	23.96 \pm 0.05	24.83 \pm 0.06
338.962	24.29 \pm 0.05	25.40 \pm 0.18	24.63 \pm 0.05	24.96 \pm 0.07	23.88 \pm 0.05	24.79 \pm 0.05
341.915	24.21 \pm 0.05	25.01 \pm 0.13	24.20 \pm 0.05	24.97 \pm 0.06	23.79 \pm 0.07	24.98 \pm 0.06
344.323	24.09 \pm 0.05	25.16 \pm 0.13	24.00 \pm 0.05	25.23 \pm 0.06	23.90 \pm 0.05	25.01 \pm 0.06
347.405	23.93 \pm 0.05	24.86 \pm 0.09	23.92 \pm 0.05	25.22 \pm 0.05	23.81 \pm 0.05	25.10 \pm 0.07
351.224	24.00 \pm 0.05	24.89 \pm 0.11	24.01 \pm 0.05	25.09 \pm 0.05	24.00 \pm 0.05	25.17 \pm 0.06
355.110	24.01 \pm 0.05	24.64 \pm 0.08	23.98 \pm 0.05	24.81 \pm 0.05	24.00 \pm 0.05	25.22 \pm 0.07
360.339	24.04 \pm 0.05	24.72 \pm 0.08	24.13 \pm 0.05	24.36 \pm 0.05	24.06 \pm 0.05	24.91 \pm 0.05
367.103	24.10 \pm 0.05	24.82 \pm 0.09	24.28 \pm 0.05	24.29 \pm 0.05	24.24 \pm 0.05	24.36 \pm 0.05
2449700+	C7	C8	C9	C10	C11	C12
14.728	25.02 \pm 0.06	25.23 \pm 0.10	25.59 \pm 0.09	25.28 \pm 0.05	26.39 \pm 0.14	25.19 \pm 0.07
320.588	24.87 \pm 0.06	24.95 \pm 0.13	24.59 \pm 0.06	25.27 \pm 0.06	26.72 \pm 0.24	25.21 \pm 0.08
327.230	24.46 \pm 0.05	25.24 \pm 0.07	24.93 \pm 0.08	25.22 \pm 0.06	26.77 \pm 0.26	25.92 \pm 0.14
335.006	24.76 \pm 0.06	24.85 \pm 0.07	25.21 \pm 0.06	24.58 \pm 0.05	26.10 \pm 0.13	25.91 \pm 0.13
337.018	24.77 \pm 0.05	24.80 \pm 0.07	25.24 \pm 0.06	24.56 \pm 0.05	25.92 \pm 0.08	26.16 \pm 0.14
338.962	24.84 \pm 0.05	24.63 \pm 0.06	25.36 \pm 0.06	24.69 \pm 0.05	26.00 \pm 0.10	26.01 \pm 0.14
341.915	24.88 \pm 0.05	24.85 \pm 0.06	25.49 \pm 0.09	24.96 \pm 0.07	25.91 \pm 0.11	25.50 \pm 0.10
344.323	24.96 \pm 0.09	24.69 \pm 0.06	25.21 \pm 0.06	24.99 \pm 0.05	26.26 \pm 0.12	24.95 \pm 0.06
347.405	25.01 \pm 0.06	24.88 \pm 0.07	24.45 \pm 0.05	25.18 \pm 0.05	26.44 \pm 0.16	24.85 \pm 0.06
351.224	25.26 \pm 0.09	24.97 \pm 0.06	24.42 \pm 0.05	25.18 \pm 0.06	26.38 \pm 0.14	25.34 \pm 0.08
355.110	25.24 \pm 0.07	25.02 \pm 0.06	24.61 \pm 0.05	25.45 \pm 0.06	26.44 \pm 0.20	25.46 \pm 0.10
360.339	25.42 \pm 0.09	25.19 \pm 0.08	24.84 \pm 0.06	25.23 \pm 0.06	26.41 \pm 0.19	25.74 \pm 0.10
367.103	24.85 \pm 0.09	25.23 \pm 0.07	25.02 \pm 0.05	24.41 \pm 0.05	26.15 \pm 0.14	26.22 \pm 0.14
2449700+	C13	C14	C15	C16	C17	C18
14.728	25.56 \pm 0.09	25.68 \pm 0.10	25.28 \pm 0.07	25.27 \pm 0.06	25.29 \pm 0.14	25.03 \pm 0.05
320.588	24.85 \pm 0.06	25.39 \pm 0.09	25.18 \pm 0.08	25.15 \pm 0.06	26.04 \pm 0.10	25.69 \pm 0.11
327.230	25.53 \pm 0.09	24.82 \pm 0.08	25.57 \pm 0.09	25.42 \pm 0.07	26.10 \pm 0.12	25.40 \pm 0.06
335.006	25.73 \pm 0.07	25.20 \pm 0.07	25.78 \pm 0.13	26.00 \pm 0.11	25.36 \pm 0.09	25.05 \pm 0.06
337.018	25.94 \pm 0.13	25.49 \pm 0.09	25.92 \pm 0.12	26.00 \pm 0.11	25.36 \pm 0.07	25.10 \pm 0.06
338.962	25.93 \pm 0.10	25.67 \pm 0.11	25.87 \pm 0.12	26.08 \pm 0.18	25.57 \pm 0.10	25.27 \pm 0.07
341.915	26.05 \pm 0.15	25.54 \pm 0.11	24.81 \pm 0.06	24.91 \pm 0.06	25.54 \pm 0.12	25.47 \pm 0.13
344.323	26.01 \pm 0.13	25.78 \pm 0.09	24.95 \pm 0.08	24.95 \pm 0.06	25.95 \pm 0.11	25.64 \pm 0.08
347.405	25.35 \pm 0.07	25.58 \pm 0.11	25.12 \pm 0.06	25.18 \pm 0.10	26.14 \pm 0.11	25.75 \pm 0.09
351.224	24.71 \pm 0.06	24.90 \pm 0.06	25.36 \pm 0.07	25.55 \pm 0.09	26.13 \pm 0.10	25.84 \pm 0.10
355.110	25.26 \pm 0.08	25.01 \pm 0.06	25.64 \pm 0.11	25.65 \pm 0.07	25.05 \pm 0.07	24.93 \pm 0.05
360.339	25.42 \pm 0.07	25.32 \pm 0.09	25.91 \pm 0.15	25.94 \pm 0.11	25.51 \pm 0.07	25.12 \pm 0.06
367.103	25.97 \pm 0.11	25.65 \pm 0.10	26.41 \pm 0.19	25.22 \pm 0.08	25.54 \pm 0.10	25.44 \pm 0.07
2449700+	C19	C20	C21	C22	C23	C24
14.728	25.17 \pm 0.06	26.14 \pm 0.11	25.47 \pm 0.06	25.40 \pm 0.06	25.53 \pm 0.09	25.29 \pm 0.05
320.588	25.92 \pm 0.12	26.60 \pm 0.19	25.34 \pm 0.08	26.16 \pm 0.12	25.63 \pm 0.09	25.60 \pm 0.08
327.230	26.01 \pm 0.10	25.55 \pm 0.09	25.54 \pm 0.08	26.54 \pm 0.15	26.08 \pm 0.11	25.86 \pm 0.10
335.006	25.31 \pm 0.08	25.93 \pm 0.10	26.24 \pm 0.12	25.69 \pm 0.07	25.23 \pm 0.06	25.08 \pm 0.05
337.018	25.44 \pm 0.08	26.05 \pm 0.13	26.25 \pm 0.14	25.81 \pm 0.13	25.41 \pm 0.08	25.42 \pm 0.08
338.962	25.70 \pm 0.10	26.15 \pm 0.13	26.10 \pm 0.11	25.64 \pm 0.09	25.52 \pm 0.09	25.55 \pm 0.06
341.915	25.84 \pm 0.11	26.51 \pm 0.17	25.23 \pm 0.06	26.11 \pm 0.14	25.78 \pm 0.13	25.63 \pm 0.10
344.323	25.98 \pm 0.11	26.24 \pm 0.16	25.17 \pm 0.06	26.34 \pm 0.13	26.07 \pm 0.13	25.84 \pm 0.09
347.405	25.98 \pm 0.11	25.23 \pm 0.06	25.31 \pm 0.06	26.10 \pm 0.09	25.91 \pm 0.11	26.00 \pm 0.09

Table 6—Continued

JD	$V \pm \sigma_V$					
351.224	26.50 ± 0.18	25.44 ± 0.07	25.61 ± 0.08	25.40 ± 0.07	25.10 ± 0.07	25.55 ± 0.07
355.110	25.08 ± 0.06	25.89 ± 0.09	26.01 ± 0.12	25.76 ± 0.08	25.33 ± 0.08	25.23 ± 0.06
360.339	25.42 ± 0.08	26.34 ± 0.16	26.01 ± 0.11	26.03 ± 0.10	25.84 ± 0.10	25.75 ± 0.08
367.103	26.00 ± 0.13	26.12 ± 0.12	25.23 ± 0.13	26.19 ± 0.12	26.04 ± 0.14	26.06 ± 0.11
2449700+	C25	C26	C27	C28	C29	C30
14.728	26.06 ± 0.13	25.76 ± 0.08	26.10 ± 0.13	25.55 ± 0.08	25.81 ± 0.10	26.57 ± 0.19
320.588	25.48 ± 0.11	26.32 ± 0.16	26.67 ± 0.27	26.08 ± 0.10	26.34 ± 0.15	...
327.230	25.86 ± 0.12	25.86 ± 0.09	26.16 ± 0.15	26.29 ± 0.16	26.30 ± 0.17	25.66 ± 0.12
335.006	25.83 ± 0.11	26.72 ± 0.19	26.42 ± 0.18	25.77 ± 0.12	26.22 ± 0.14	26.47 ± 0.19
337.018	25.25 ± 0.08	26.51 ± 0.15	26.75 ± 0.25	26.17 ± 0.15	25.79 ± 0.11	26.26 ± 0.16
338.962	25.28 ± 0.07	25.37 ± 0.07	25.77 ± 0.11	26.31 ± 0.13	25.91 ± 0.12	25.48 ± 0.10
341.915	25.63 ± 0.12	25.62 ± 0.10	25.63 ± 0.12	26.57 ± 0.19	26.11 ± 0.12	25.95 ± 0.12
344.323	...	25.91 ± 0.13	25.81 ± 0.12	26.38 ± 0.14	26.41 ± 0.16	26.03 ± 0.13
347.405	26.54 ± 0.22	26.06 ± 0.10	26.08 ± 0.14	25.50 ± 0.09	26.78 ± 0.29	26.29 ± 0.16
351.224	26.59 ± 0.20	26.45 ± 0.13	26.39 ± 0.19	25.63 ± 0.08	26.05 ± 0.13	26.25 ± 0.17
355.110	25.10 ± 0.06	26.44 ± 0.14	26.35 ± 0.17	26.51 ± 0.18	25.90 ± 0.11	25.59 ± 0.09
360.339	25.60 ± 0.08	25.66 ± 0.08	25.60 ± 0.10	26.10 ± 0.13	26.78 ± 0.26	25.73 ± 0.11
367.103	26.36 ± 0.18	26.65 ± 0.18	26.19 ± 0.14	25.62 ± 0.08	25.74 ± 0.09	26.58 ± 0.23
2449700+	C31	C32	C33	C34
14.728	26.53 ± 0.17	26.96 ± 0.23	25.81 ± 0.11	26.10 ± 0.12
320.588	27.04 ± 0.27	26.27 ± 0.15	26.48 ± 0.19	25.85 ± 0.12
327.230	26.36 ± 0.17	...	25.86 ± 0.11
335.006	...	26.38 ± 0.17	26.47 ± 0.16	25.96 ± 0.11
337.018	26.27 ± 0.14	26.33 ± 0.18	25.86 ± 0.13	26.09 ± 0.13
338.962	26.04 ± 0.15	26.61 ± 0.23	25.77 ± 0.15	26.32 ± 0.16
341.915	26.20 ± 0.15	26.86 ± 0.27	25.85 ± 0.17	26.83 ± 0.28
344.323	26.33 ± 0.16	26.84 ± 0.19	25.97 ± 0.17	26.35 ± 0.16
347.405	26.90 ± 0.21	26.06 ± 0.11	26.30 ± 0.15	25.78 ± 0.10
351.224	26.59 ± 0.18	26.31 ± 0.17	25.65 ± 0.12	26.48 ± 0.17
355.110	26.49 ± 0.15	27.12 ± 0.24	26.08 ± 0.13	26.35 ± 0.15
360.339	26.99 ± 0.23	26.50 ± 0.14	26.29 ± 0.12	25.35 ± 0.09
367.103	26.07 ± 0.12	26.61 ± 0.20	25.84 ± 0.13	26.56 ± 0.17

Table 7. I Photometry for NGC 2541 Cepheids

JD	$I \pm \sigma_I$					
2449700+	C1	C2	C3	C4	C5	C6
14.799	23.24 ± 0.05	23.24 ± 0.05	23.49 ± 0.05
320.650	23.40 ± 0.05	24.16 ± 0.10	23.33 ± 0.05	23.52 ± 0.05	23.41 ± 0.05	23.56 ± 0.05
327.284	23.63 ± 0.05	24.28 ± 0.11	23.52 ± 0.05	23.58 ± 0.05	23.37 ± 0.05	23.61 ± 0.05
341.979	23.44 ± 0.06	24.33 ± 0.13	23.36 ± 0.05	23.76 ± 0.05	23.10 ± 0.05	23.82 ± 0.05
360.404	23.11 ± 0.06	24.01 ± 0.10	23.19 ± 0.05	23.52 ± 0.05	23.00 ± 0.05	23.88 ± 0.05
2449700+	C7	C8	C9	C10	C11	C12
14.799	23.88 ± 0.05	24.20 ± 0.14	24.37 ± 0.07	24.23 ± 0.14	...	24.14 ± 0.07
320.650	23.81 ± 0.05	24.02 ± 0.13	23.69 ± 0.06	24.27 ± 0.06	25.11 ± 0.13	24.34 ± 0.09
327.284	23.62 ± 0.05	24.73 ± 0.22	23.94 ± 0.06	24.42 ± 0.06	24.95 ± 0.11	...
341.979	23.80 ± 0.05	23.87 ± 0.10	24.16 ± 0.08	23.79 ± 0.05	24.79 ± 0.10	24.59 ± 0.10
360.404	24.08 ± 0.05	23.86 ± 0.13	23.82 ± 0.05	24.24 ± 0.06	25.11 ± 0.13	24.64 ± 0.10
2449700+	C13	C14	C15	C16	C17	C18
14.799	24.35 ± 0.07	...	24.18 ± 0.06	24.36 ± 0.08	24.44 ± 0.09	...
320.650	24.07 ± 0.05	24.71 ± 0.08	24.28 ± 0.07	24.35 ± 0.06	24.90 ± 0.09	24.57 ± 0.07
327.284	24.28 ± 0.06	24.20 ± 0.07	24.45 ± 0.08	24.39 ± 0.06	24.92 ± 0.10	24.59 ± 0.09
341.979	24.67 ± 0.09	24.66 ± 0.10	24.13 ± 0.07	24.34 ± 0.08	24.96 ± 0.12	24.39 ± 0.08
360.404	24.43 ± 0.10	24.37 ± 0.07	24.66 ± 0.09	24.73 ± 0.12	24.46 ± 0.07	24.32 ± 0.07
2449700+	C19	C20	C21	C22	C23	C24
14.799	24.54 ± 0.07	25.12 ± 0.11	24.54 ± 0.07	24.91 ± 0.08	24.48 ± 0.07	24.70 ± 0.08
320.650	24.83 ± 0.14	25.26 ± 0.12	24.69 ± 0.06	25.05 ± 0.10	24.60 ± 0.08	24.58 ± 0.06
327.284	25.42 ± 0.15	24.69 ± 0.10	24.63 ± 0.06	25.65 ± 0.17	25.10 ± 0.11	25.06 ± 0.11
341.979	24.74 ± 0.11	25.26 ± 0.14	24.65 ± 0.08	25.35 ± 0.12	24.64 ± 0.10	24.85 ± 0.11
360.404	24.67 ± 0.08	25.03 ± 0.10	24.98 ± 0.08	25.05 ± 0.11	24.63 ± 0.09	24.68 ± 0.08
2449700+	C25	C26	C27	C28	C29	C30
14.799	25.66 ± 0.28	25.26 ± 0.14	24.79 ± 0.09	24.66 ± 0.12	24.94 ± 0.09	26.06 ± 0.30
320.650	24.67 ± 0.09	25.59 ± 0.15	25.02 ± 0.13	24.62 ± 0.09	25.45 ± 0.15	25.53 ± 0.14
327.284	25.48 ± 0.19	25.09 ± 0.12	24.72 ± 0.08	24.88 ± 0.09	25.00 ± 0.09	25.15 ± 0.13
341.979	24.76 ± 0.10	24.97 ± 0.13	24.68 ± 0.09	25.12 ± 0.14	25.18 ± 0.14	25.13 ± 0.12
360.404	24.94 ± 0.11	25.14 ± 0.10	24.84 ± 0.09	24.73 ± 0.11	25.59 ± 0.20	25.48 ± 0.14
2449700+	C31	C32	C33	C34		
14.799	25.24 ± 0.14	24.72 ± 0.09
320.650	26.03 ± 0.27	25.44 ± 0.16	25.78 ± 0.19	24.82 ± 0.12
327.284	25.48 ± 0.16	26.06 ± 0.26	25.15 ± 0.11	25.26 ± 0.13
341.979	25.68 ± 0.24	...	25.32 ± 0.21	25.14 ± 0.14
360.404	...	25.67 ± 0.16	25.59 ± 0.17	24.63 ± 0.08

Table 8. DoPHOT Mean Photometry of the NGC 2541 Cepheids

ID	P	F555W _{ph}	F555W _{av}	F814W _{ph} ^a	F814W _{av} ^a	V _{ph}	V _{av}	I _{ph}	I _{av}	χ^2
C1	> 65	24.26	24.21	23.31(0.00)	23.31(-0.04)	24.24	24.19	23.26	23.27	32.92
C2	> 55	25.01	25.02	24.20(0.03)	24.20(0.01)	24.99	25.00	24.15	24.16	5.96
C3	> 52	24.28	24.30	23.33(0.00)	23.33(-0.02)	24.27	24.28	23.28	23.29	36.74
C4	> 51	24.65	24.76	23.62(0.03)	23.67(0.08)	24.63	24.73	23.58	23.62	34.57
C5	> 50	24.08	24.04	23.17(0.01)	23.15(-0.06)	24.06	24.03	23.13	23.11	17.05
C6	> 43; < 60	24.75	24.76	23.74(0.01)	23.75(0.08)	24.74	24.74	23.70	23.70	27.10
C7	47.0	24.90	24.92	23.84(0.00)	23.85(0.02)	24.89	24.91	23.80	23.80	15.60
C8	39.0	24.95	24.95	24.03(-0.02)	24.03(-0.06)	24.93	24.93	23.99	23.98	9.24
C9	36.4	24.86	24.93	23.90(-0.08)	23.93(-0.04)	24.85	24.92	23.85	23.88	43.18
C10	33.8	24.94	24.95	23.99(-0.09)	24.05(-0.12)	24.93	24.94	23.94	24.01	40.33
C11	31.7	26.29	26.27	24.96(0.00)	24.92(-0.06)	26.28	26.26	24.92	24.87	4.69
C12	30.4	25.47	25.52	24.47(-0.01)	24.44(0.03)	25.45	25.50	24.43	24.39	29.96
C13	30.1	25.46	25.47	24.38(0.01)	24.38(0.04)	25.44	25.46	24.34	24.33	36.19
C14	27.5	25.28	25.34	24.49(0.02)	24.52(0.05)	25.26	25.32	24.45	24.48	17.56
C15	27.2	25.43	25.44	24.40(0.04)	24.40(0.08)	25.42	25.42	24.35	24.36	27.22
C16	25.7	25.46	25.42	24.52(0.06)	24.49(0.06)	25.44	25.39	24.48	24.45	26.27
C17	24.6	25.59	25.60	24.69(-0.05)	24.69(-0.02)	25.57	25.59	24.64	24.64	16.35
C18	24.5	25.32	25.33	24.44(-0.02)	24.42(-0.04)	25.31	25.31	24.40	24.38	20.74
C19	24.5	25.63	25.65	24.83(-0.01)	24.82(0.02)	25.61	25.63	24.79	24.77	24.74
C20	22.9	25.84	25.94	24.89(-0.10)	24.94(-0.11)	25.82	25.93	24.85	24.90	24.58
C21	21.8	25.62	25.59	24.74(0.01)	24.74(0.05)	25.61	25.57	24.70	24.70	21.98
C22	19.8	25.85	25.88	25.14(-0.02)	25.12(-0.05)	25.83	25.87	25.10	25.08	17.25
C23	19.7	25.55	25.61	24.57(-0.08)	24.60(-0.07)	25.54	25.60	24.53	24.55	15.33
C24	18.9	25.60	25.57	24.82(0.01)	24.74(-0.02)	25.58	25.55	24.78	24.70	20.72
C25	17.4	25.77	25.70	25.03(0.03)	25.03(-0.01)	25.75	25.68	24.99	24.99	26.81
C26	17.3	25.99	26.02	25.28(0.02)	25.30(0.11)	25.97	26.00	25.24	25.26	19.44
C27	17.0	26.01	26.09	24.76(-0.06)	24.87(0.06)	26.00	26.08	24.72	24.82	6.97
C28	16.5	25.93	25.98	24.70(-0.04)	24.74(-0.05)	25.90	25.97	24.66	24.70	13.29
C29	15.4	26.21	26.12	25.25(-0.03)	25.15(-0.05)	26.19	26.11	25.20	25.11	6.03
C30	15.2	25.97	26.01	25.41(-0.04)	25.47(0.05)	25.95	25.99	25.37	25.43	9.70
C31	14.3	26.50	26.44	25.73(-0.05)	25.69(-0.02)	26.47	26.43	25.69	25.65	3.77
C32	14.2	26.54	26.53	25.80(0.08)	25.77(0.07)	26.52	26.50	25.76	25.73	3.87
C33	13.6	25.99	25.99	25.38(-0.05)	25.37(-0.02)	25.97	25.97	25.35	25.34	3.75
C34	12.2	26.13	26.10	25.03(0.13)	24.98(0.09)	26.11	26.07	24.99	24.94	11.54

^aThe value of the magnitude correction applied to the F814W magnitudes, defined as in §4.4, is listed in parenthesis

Notes on the individual Cepheids. In what follows the term ‘isolated’ is used for stars for which no companions are identified within a three pixel radius. C1: Isolated; period too long to be determined; phase averaged magnitudes are calculated for P = 65.0 days. C2: crowded region; equal brightness companion 2.8 pixels away. Period is too long to be determined; phase averaged magnitudes are calculated for P = 59.0 days. C3: at the edge of a very crowded group, even if no other stars are identified within a three pixel radius. Period is too long to be determined; phase averaged magnitudes are calculated for P = 53.0 days. C4: isolated. Period is too long to be determined; phase averaged magnitudes are calculated for P = 61.0 days. C5: two magnitudes fainter companion 2.3 pixels away. Period is too long to be determined; phase averaged magnitudes are calculated for P = 51.5 days. C6: two fainter companions 2.8 and 2.0 pixels away. Phase averaged magnitudes are calculated for P = 50.7 days. C7: 2.3 magnitudes fainter companion 3.0 pixels away. C8: 0.5 magnitudes fainter companion 1.7 pixels away. C9: at the edge of a crowded group, even if no other stars are identified within a three pixel radius. C10: two companions (one of the same brightness and the other one magnitude fainter) 3.0 pixels away. C11: isolated. C12: two companions (0.8 and 1.4 mag fainter) within 2 pixels. C13: isolated. C14: one magnitude fainter companion 1.5 pixels away. C15: three companions at least 1 magnitude fainter 2.1 to 2.6 pixels away. C16: isolated. C17: 0.6 magnitudes fainter companion 1.6 pixels away. C18: isolated. C19: isolated. C20: two at least 1 magnitude fainter stars 2.4 and 2.8 pixels away. C21: isolated. C22: isolated. C23: two magnitudes fainter companion 2.8 pixels away. C24: isolated. C25: two at least 1 magnitude fainter companions within 3 pixels. C26: isolated. C27: 1.4 magnitudes fainter companion 2.8 pixels away. C28: two at least one magnitude fainter companions 2.3 pixels away. C29: isolated. C30: isolated. C31: isolated. C32: isolated. C33: isolated. C34: 1.4 magnitudes fainter companion 2.5 pixels away.

Table 9. ALLFRAME Mean Photometry of the NGC 2541 Cepheids

ID	P	F555W _{ph}	F555W _{av}	F814W _{ph} ^a	F814W _{av} ^a	V _{ph}	V _{av}	I _{ph}	I _{av}	σ
C1	>65	24.10	24.05	23.23(-0.02)	23.22(-0.05)	24.08	24.04	23.19	23.18	3.7
C2	>55	24.70	24.70	23.92(-0.01)	23.90(-0.01)	24.68	24.68	23.88	23.86	1.4
C3	>60	24.16	24.17	23.25(-0.02)	23.27(-0.05)	24.14	24.15	23.21	23.23	3.2
C4	>50	24.61	24.71	23.58(0.03)	23.61(0.08)	24.60	24.69	23.54	23.56	3.3
C5	>50	24.09	24.05	23.15(0.00)	23.14(-0.08)	24.07	24.04	23.11	23.10	2.3
C6	>45;<55	24.69	24.72	23.63(0.00)	23.60(0.05)	24.68	24.70	23.58	23.55	1.9
C7	43.6	24.77	24.77	23.73(-0.02)	23.77(-0.02)	24.76	24.76	23.69	23.72	1.4
C8	38.7	24.86	24.86	23.92(-0.04)	23.91(-0.09)	24.84	24.85	23.88	23.87	1.6
C9	36.3	24.76	24.83	23.88(-0.08)	23.90(-0.06)	24.74	24.81	23.84	23.86	4.3
C10	30.7	24.97	24.92	24.04(-0.05)	24.06(-0.10)	24.96	24.91	24.00	24.02	3.5
C11	31.7	26.19	26.16	24.97(-0.04)	24.95(-0.09)	26.17	26.15	24.93	24.91	1.3
C12	32.7	25.28	25.27	24.31(0.01)	24.26(0.04)	25.26	25.25	24.27	24.22	1.9
C13	28.9	25.39	25.43	24.40(0.04)	24.43(0.06)	25.37	25.40	24.36	24.39	3.0
C14	25.2	25.35	25.40	24.59(0.03)	24.64(0.01)	25.33	25.38	24.55	24.60	2.6
C15	29.6	25.40	25.41	24.39(0.05)	24.39(0.06)	25.38	25.38	24.35	24.35	2.0
C16	25.9	25.38	25.35	24.58(0.08)	24.55(0.07)	25.36	25.32	24.54	24.51	2.7
C17	24.2	25.62	25.63	24.64(0.00)	24.66(0.00)	25.60	25.61	24.60	24.62	2.4
C18	24.1	25.27	25.30	24.42(0.00)	24.44(0.01)	25.25	25.28	24.38	24.40	1.9
C19	22.7	25.65	25.62	24.76(0.01)	24.72(-0.01)	25.63	25.60	24.72	24.68	2.6
C20	20.6	25.84	25.91	24.99(-0.07)	24.98(-0.13)	25.82	25.89	24.95	24.94	2.0
C21	23.2	25.43	25.46	24.64(0.01)	24.66(0.03)	25.41	25.44	24.61	24.63	2.9
C22	18.8	25.88	25.88	25.11(-0.01)	24.98(-0.09)	25.86	25.86	25.08	24.94	2.0
C23	19.6	25.56	25.66	24.54(-0.12)	24.61(-0.10)	25.54	25.65	24.50	24.57	1.8
C24	18.7	25.51	25.50	24.74(-0.01)	24.72(-0.04)	25.49	25.48	24.71	24.69	2.4
C25	18.8	25.77	25.69	25.08(-0.03)	24.94(-0.02)	25.75	25.68	25.05	24.90	2.7
C26	17.0	25.88	25.93	25.09(0.02)	25.13(0.10)	25.86	25.90	25.05	25.09	3.4
C27	17.6	26.04	26.08	24.88(-0.03)	24.93(0.08)	26.03	26.06	24.83	24.89	1.7
C28	16.5	25.95	26.00	24.94(-0.04)	25.00(-0.04)	25.93	25.99	24.90	24.96	1.4
C29	15.3	26.28	26.17	25.26(-0.04)	25.15(-0.08)	26.27	26.16	25.22	25.11	1.3
C30	15.2	26.03	26.10	25.29(-0.06)	25.33(0.00)	26.01	26.08	25.26	25.29	1.6
C31	15.2	26.31	26.30	25.61(-0.23)	25.60(-0.20)	26.29	26.31	25.58	25.57	1.4
C32	14.7	26.48	26.51	25.58(-0.05)	25.61(-0.08)	26.46	26.50	25.54	25.57	1.5
C33	13.4	25.98	25.99	25.48(0.01)	25.50(-0.01)	25.96	25.97	25.46	25.48	1.3
C34	12.2	26.09	26.08	24.62(0.08)	24.67(0.05)	26.08	26.06	24.57	24.63	1.4

^aThe value of the magnitude correction applied to the F814W magnitudes, defined as in §4.4, is listed in parenthesis

Table 10. Error Budget in the Distance to NGC 2541

Source	Error (mag)	Notes
i) CEPHEID PL CALIBRATION		
(a) <i>LMC True Modulus</i> ¹	± 0.10	
(b) <i>V PL Zero Point</i> ²	± 0.05	
(c) <i>I PL Zero Point</i> ²	± 0.03	
(S1) PL Systematic Uncertainty	± 0.12	(a),(b) and (c) added in quadrature
ii) EXTINCTION CORRECTIONS		
(R1) Errors in the adopted value for R_V	± 0.01	See §6.1 for details
iii) NGC 2541 – LMC INTRINSIC DIFFERENCES		
(R2) Metallicity Differences	± 0.005	See §6.1 for details
(R3) R_V Differences	± 0.03	See §6.1 for details
iv) PHOTOMETRIC ERRORS		
(d) <i>HST V-Band Zero Point</i> ³	± 0.03	
(e) <i>HST I-Band Zero Point</i> ³	± 0.03	
(R4) Cepheid True Modulus	± 0.09	(d) and (e) added in quadrature
v) NGC 2541 PL FITTING		
(f) <i>PL Fit (V)</i>	± 0.03	
(g) <i>PL Fit (I)</i>	± 0.04	
(R5) Cepheid True Modulus ⁴	± 0.06	(f),(g) partially correlated, See Madore et al. 1998 for details
TOTAL UNCERTAINTY		
(R) Random Errors	± 0.11	R1,R2,R3,R4,R5 added in quadrature
(S) Systematic Errors	± 0.12	S1

¹ Adopted from Westerlund (1997)

² Derived from the observed scatter in the Madore & Freedman (1991) PL relation, with 32 contributing LMC Cepheids.

³ Contributing uncertainties from aperture corrections, the Holtzman et al. (1995) zero points, and the long-versus short uncertainty, combined in quadrature (see §6.1 for further details).

⁴ The partially correlated nature of the derived PL width uncertainties is taken into account by the (correlated) dereddening procedure, coupled with the largely ‘degenerate-with-reddening’ positioning of individual Cepheids within the instability strip.

Table 11. Previous Distance Determinations to NGC 2541 and the NGC 2841 Group

Method	Distance Modulus	Reference
Distance to NGC 2541		
Sosie Galaxies	29.50 ± 0.23	Bottinelli et al. 1985a
B-band Tully Fisher Relation	29.41 ± 0.18	Bottinelli et al. 1984
B-band Tully Fisher Relation	29.53 ± 0.26	Bottinelli et al. 1985b
B-band Tully Fisher Relation	29.82 ± 0.19	Bottinelli et al. 1986
IR Tully Fisher Relation	30.86 ± 0.30	Courteau, priv.comm.
Inverse IR Tully Fisher Relation	30.78 ± 0.30	Courteau, priv.comm.
Cepheids	30.47 ± 0.23	This paper
Other Distance to Group Members		
B-band Tully Fisher Relation ^a	30.54 ± 0.17	Bottinelli et al. 1986
B-band Tully Fisher Relation ^b	30.44 ± 0.91	Bottinelli et al. 1986
Variety of Secondary Distance Indicators ^c	29.53 ± 0.20	de Vaucouleurs 1975

^aDistance to NGC 2841

^bDistance to NGC 2500

^cDistance to the NGC 2841 group

Table A1. Astrometry for the Other NGC 2541 Variable Candidates

ID ^a	X ^b	Y ^b	RA(J2000) ^c	Dec(J2000) ^c	Chip
V1	440.73	200.34	8:14:39.8161	49:02:26.341	WF2
V2	536.65	712.08	8:14:41.4975	49:03:15.341	WF2
V3	583.55	629.59	8:14:38.8444	49:01:43.943	PC
V4	231.62	747.52	8:14:44.3542	49:03:03.641	WF2
V5	178.79	766.47	8:14:44.9080	49:03:02.705	WF2
V6	762.36	337.59	8:14:37.6688	49:02:53.834	WF2
V7	790.87	397.85	8:14:39.3009	49:01:30.591	PC
V8	452.80	359.74	8:14:40.4964	49:02:40.768	WF2
V9	398.41	110.01	8:14:39.7451	49:02:16.473	WF2
V10	382.84	662.37	8:14:42.6087	49:03:03.634	WF2
V11	231.13	170.62	8:14:41.5184	49:02:13.612	WF2
V12	659.71	456.15	8:14:39.1504	49:02:59.160	WF2
V13	214.22	342.18	8:14:45.8971	49:01:53.489	WF3
V14	86.07	593.60	8:14:44.8790	49:02:43.281	WF2
V15	81.27	344.74	8:14:45.2611	49:01:41.916	WF3
V16	246.08	70.71	8:14:40.8941	49:02:05.726	WF2
V17	60.57	352.96	8:14:43.9198	49:02:21.183	WF2
V18	168.19	431.14	8:14:41.5320	49:01:13.111	WF4
V19	433.59	387.67	8:14:40.8042	49:02:42.263	WF2
V20	169.32	774.10	8:14:45.0275	49:03:02.901	WF2
V21	170.09	777.79	8:14:45.0385	49:03:03.255	WF2
V22	489.67	249.68	8:14:39.6277	49:02:32.999	WF2
V23	621.48	472.14	8:14:49.0715	49:02:22.345	WF3

^aThe Variable Stars ID is the same in this and all subsequent tables.

^bThe X and Y coordinate are relative to the 10/30/95 epoch. For each 800×800 pixels chip, pixel [1,1] is located at the edge of the pyramid.

^cRA and Declination are calculated using the IRAF task STSDAS.HST_CALIB.WFPC.METRIC, version 1.3.5 (July 1996)

Table A2. V Photometry for Other NGC 2541 Variable Candidates

JD	$V \pm \sigma_V$					
2449700+						
	V1	V2	V3	V4	V5	V6
14.728	25.93 ± 0.10	25.17 ± 0.10	25.76 ± 0.08	25.39 ± 0.07	25.52 ± 0.08	24.45 ± 0.16
320.588	25.97 ± 0.10	25.23 ± 0.11	25.38 ± 0.06	25.15 ± 0.06	24.86 ± 0.06	25.19 ± 0.22
327.230	26.15 ± 0.14	25.17 ± 0.09	25.33 ± 0.08	25.13 ± 0.06	24.85 ± 0.06	25.36 ± 0.25
335.006	26.04 ± 0.10	25.24 ± 0.11	25.73 ± 0.08	25.17 ± 0.06	25.09 ± 0.06	24.39 ± 0.15
337.018	25.73 ± 0.09	25.24 ± 0.09	25.69 ± 0.07	25.07 ± 0.06	25.15 ± 0.06	24.49 ± 0.16
338.962	25.89 ± 0.11	25.03 ± 0.08	25.95 ± 0.11	25.22 ± 0.06	25.25 ± 0.08	24.43 ± 0.19
341.915	25.86 ± 0.12	24.84 ± 0.07	25.78 ± 0.10	25.25 ± 0.08	25.33 ± 0.09	24.44 ± 0.16
344.323	25.74 ± 0.10	24.93 ± 0.08	25.70 ± 0.12	25.40 ± 0.07	25.38 ± 0.07	24.59 ± 0.15
347.405	25.61 ± 0.09	24.88 ± 0.06	25.76 ± 0.13	25.48 ± 0.08	25.32 ± 0.09	24.74 ± 0.18
351.224	25.59 ± 0.10	24.97 ± 0.07	25.07 ± 0.05	25.43 ± 0.07	25.40 ± 0.07	24.86 ± 0.23
355.110	25.31 ± 0.09	25.03 ± 0.07	25.14 ± 0.06	25.43 ± 0.08	25.45 ± 0.09	24.91 ± 0.18
360.339	25.48 ± 0.08	25.05 ± 0.07	25.31 ± 0.07	25.40 ± 0.08	25.34 ± 0.09	25.16 ± 0.23
367.103	25.50 ± 0.08	25.18 ± 0.08	25.20 ± 0.05	25.32 ± 0.08	25.07 ± 0.07	25.48 ± 0.26
2449700+						
	V7	V8	V9	V10	V11	V12
14.728	25.00 ± 0.05	25.89 ± 0.09	26.00 ± 0.11	25.97 ± 0.12	26.21 ± 0.13	26.11 ± 0.16
320.588	-5.00 ± 0.00	25.74 ± 0.09	26.25 ± 0.15	26.11 ± 0.14	26.57 ± 0.17	26.21 ± 0.16
327.230	25.89 ± 0.17	25.95 ± 0.10	25.42 ± 0.09	25.56 ± 0.12	25.57 ± 0.07	26.23 ± 0.19
335.006	25.79 ± 0.11	25.66 ± 0.13	25.79 ± 0.10	25.79 ± 0.12	26.06 ± 0.13	25.75 ± 0.11
337.018	25.54 ± 0.08	25.84 ± 0.11	25.96 ± 0.15	26.44 ± 0.17	25.98 ± 0.14	25.91 ± 0.14
338.962	26.16 ± 0.14	25.63 ± 0.08	25.83 ± 0.11	26.19 ± 0.16	25.95 ± 0.12	26.38 ± 0.19
341.915	24.93 ± 0.05	25.16 ± 0.07	26.43 ± 0.24	26.38 ± 0.22	26.53 ± 0.21	26.28 ± 0.19
344.323	24.77 ± 0.05	25.49 ± 0.08	26.26 ± 0.14	26.44 ± 0.26	25.82 ± 0.09	26.39 ± 0.16
347.405	24.92 ± 0.07	25.56 ± 0.07	26.32 ± 0.24	25.88 ± 0.10	25.18 ± 0.05	26.24 ± 0.18
351.224	-5.00 ± 0.00	25.70 ± 0.09	25.48 ± 0.08	25.31 ± 0.15	25.48 ± 0.11	25.65 ± 0.09
355.110	-5.00 ± 0.00	25.85 ± 0.09	25.58 ± 0.09	25.85 ± 0.10	25.64 ± 0.10	25.96 ± 0.14
360.339	25.92 ± 0.10	26.03 ± 0.12	25.71 ± 0.10	26.13 ± 0.15	25.97 ± 0.11	26.43 ± 0.25
367.103	0.05 ± 0.00	26.11 ± 0.14	26.04 ± 0.10	26.25 ± 0.13	25.99 ± 0.11	25.51 ± 0.09
2449700+						
	V13	V14	V15	V16	V17	V18
14.728	25.83 ± 0.10	26.19 ± 0.14	26.58 ± 0.15	26.03 ± 0.12	25.81 ± 0.09	26.36 ± 0.13
320.588	25.88 ± 0.10	26.22 ± 0.17	26.31 ± 0.15	25.69 ± 0.11	26.80 ± 0.21	26.61 ± 0.16
327.230	26.48 ± 0.18	25.36 ± 0.08	26.04 ± 0.12	26.08 ± 0.14	25.77 ± 0.12	26.19 ± 0.15
335.006	26.51 ± 0.18	25.84 ± 0.11	26.83 ± 0.18	25.74 ± 0.11	26.69 ± 0.20	26.13 ± 0.13
337.018	26.56 ± 0.16	26.08 ± 0.14	26.44 ± 0.16	25.94 ± 0.11	26.73 ± 0.20	25.94 ± 0.09
338.962	25.93 ± 0.09	26.14 ± 0.16	26.16 ± 0.16	25.84 ± 0.10	26.38 ± 0.15	25.96 ± 0.09
341.915	25.93 ± 0.12	25.86 ± 0.11	25.80 ± 0.11	26.21 ± 0.17	25.91 ± 0.12	25.89 ± 0.11
344.323	26.08 ± 0.13	25.67 ± 0.14	25.92 ± 0.11	26.13 ± 0.12	26.03 ± 0.12	26.32 ± 0.16
347.405	26.54 ± 0.18	25.50 ± 0.11	26.20 ± 0.14	26.15 ± 0.14	26.48 ± 0.19	26.60 ± 0.19
351.224	26.34 ± 0.14	25.80 ± 0.12	26.82 ± 0.18	25.69 ± 0.10	26.97 ± 0.22	25.94 ± 0.09
355.110	26.26 ± 0.17	26.25 ± 0.14	26.33 ± 0.14	25.91 ± 0.11	26.35 ± 0.19	26.09 ± 0.11
360.339	25.99 ± 0.10	25.68 ± 0.09	26.09 ± 0.13	26.16 ± 0.14	26.08 ± 0.11	26.61 ± 0.19
367.103	26.62 ± 0.19	25.68 ± 0.11	26.40 ± 0.26	25.60 ± 0.09	26.31 ± 0.17	25.55 ± 0.07
2449700+						
	V19	V20	V21	V22	V23	
14.728	26.75 ± 0.19	26.69 ± 0.21	26.05 ± 0.11	26.10 ± 0.11	26.22 ± 0.13	...
320.588	26.24 ± 0.15	26.59 ± 0.18	25.69 ± 0.09	26.58 ± 0.15	26.00 ± 0.10	...
327.230	26.02 ± 0.12	26.21 ± 0.16	26.18 ± 0.15	26.17 ± 0.14	26.47 ± 0.15	...
335.006	26.44 ± 0.16	26.75 ± 0.20	25.79 ± 0.09	26.61 ± 0.19	26.10 ± 0.10	...
337.018	26.39 ± 0.19	26.92 ± 0.26	26.83 ± 0.23	26.53 ± 0.20
338.962	26.59 ± 0.25	26.31 ± 0.15	26.45 ± 0.17	26.22 ± 0.16	27.13 ± 0.25	...
341.915	25.87 ± 0.12	...	26.13 ± 0.13	25.99 ± 0.14	26.98 ± 0.24	...
344.323	26.02 ± 0.13	26.57 ± 0.17	25.65 ± 0.08	26.75 ± 0.22	26.34 ± 0.16	...
347.405	26.17 ± 0.12	26.31 ± 0.16	26.03 ± 0.13	26.40 ± 0.16	27.00 ± 0.22	...

Table A2—Continued

JD	$V \pm \sigma_V$					
351.224	26.44 ± 0.18	26.85 ± 0.19	26.34 ± 0.14	25.91 ± 0.13	26.50 ± 0.14	...
355.110	26.29 ± 0.17	26.24 ± 0.15	26.04 ± 0.11	25.90 ± 0.09	27.21 ± 0.24	...
360.339	26.09 ± 0.12	26.10 ± 0.12	26.32 ± 0.15	26.46 ± 0.16	26.60 ± 0.16	...
367.103	26.26 ± 0.16	26.01 ± 0.14	26.00 ± 0.14	26.26 ± 0.19	26.74 ± 0.19	...

Table A3. I Photometry for Other NGC 2541 Variable Candidates

JD	$I \pm \sigma_I$					
2449700+	V1	V2	V3	V4	V5	V6
14.799	23.80 ± 0.07	23.63 ± 0.06	24.58 ± 0.07	24.76 ± 0.09	24.29 ± 0.09	23.95 ± 0.16
320.650	23.68 ± 0.06	23.81 ± 0.06	24.11 ± 0.06	24.52 ± 0.06	24.06 ± 0.05	24.46 ± 0.22
327.284	23.80 ± 0.05	23.87 ± 0.06	24.27 ± 0.06	24.70 ± 0.08	23.97 ± 0.06	24.79 ± 0.25
341.979	23.48 ± 0.06	23.59 ± 0.05	24.48 ± 0.07	24.85 ± 0.11	24.22 ± 0.06	23.90 ± 0.16
360.404	23.41 ± 0.06	23.84 ± 0.07	24.07 ± 0.05	24.80 ± 0.09	24.33 ± 0.09	24.50 ± 0.23
2449700+	V7	V8	V9	V10	V11	V12
14.799	...	24.39 ± 0.07	24.42 ± 0.09	24.64 ± 0.08	24.97 ± 0.12	25.12 ± 0.14
320.650	...	24.64 ± 0.12	24.72 ± 0.09	24.88 ± 0.10	25.35 ± 0.13	25.15 ± 0.14
327.284	...	24.64 ± 0.06	24.35 ± 0.07	24.51 ± 0.07	24.67 ± 0.08	25.38 ± 0.15
341.979	...	24.43 ± 0.07	24.82 ± 0.12	25.00 ± 0.14	25.41 ± 0.13	25.38 ± 0.19
360.404	...	24.49 ± 0.06	24.45 ± 0.08	24.53 ± 0.09	24.77 ± 0.09	25.24 ± 0.14
2449700+	V13	V14	V15	V16	V17	V18
14.799	...	25.15 ± 0.13	...	25.49 ± 0.15	24.84 ± 0.10	25.38 ± 0.12
320.650	25.10 ± 0.13	25.34 ± 0.15	...	25.02 ± 0.12	25.65 ± 0.17	25.62 ± 0.16
327.284	25.17 ± 0.10	24.75 ± 0.10	25.02 ± 0.09	25.17 ± 0.17	25.15 ± 0.11	25.29 ± 0.12
341.979	24.94 ± 0.11	25.16 ± 0.11	25.12 ± 0.17	25.43 ± 0.19	25.06 ± 0.13	25.56 ± 0.12
360.404	25.04 ± 0.11	24.94 ± 0.10	25.35 ± 0.19	25.31 ± 0.16	25.14 ± 0.13	25.58 ± 0.14
2449700+	V19	V20	V21	V22	V23	...
14.799	25.30 ± 0.17	24.94 ± 0.11	25.15 ± 0.14	25.48 ± 0.19
320.650	25.34 ± 0.16	25.09 ± 0.12	25.06 ± 0.10	25.33 ± 0.14	25.64 ± 0.15	...
327.284	25.16 ± 0.15	25.11 ± 0.10	25.40 ± 0.13	25.84 ± 0.24	25.88 ± 0.20	...
341.979	25.21 ± 0.18	24.90 ± 0.11	25.40 ± 0.15	25.62 ± 0.25	25.95 ± 0.19	...
360.404	25.11 ± 0.11	24.99 ± 0.09	25.07 ± 0.10	25.87 ± 0.25	25.93 ± 0.22	...

Table A4. DoPHOT Mean Photometry of Other NGC 2541 Variables

ID	P	F555W _{ph}	F555W _{av}	F814W _{ph} ^a	F814W _{av} ^a	V _{ph}	V _{av}	I _{ph}	I _{av}	χ^2
V1	> 52	25.71	25.73	23.52(-0.03)	23.56(-0.06)	25.76	25.78	23.51	23.54	6.48
V2	> 45	25.09	25.07	23.76(0.03)	23.73(-0.01)	25.09	25.06	23.72	23.69	3.28
V3	> 40	25.42	25.49	24.24(-0.03)	24.28(-0.01)	25.41	25.48	24.20	24.24	19.48
V4	48.9	25.28	25.29	24.77(0.03)	24.74(0.02)	25.26	25.27	24.73	24.70	4.30
V5	48.3	25.16	25.21	24.17(0.01)	24.20(0.03)	25.14	25.19	24.12	24.16	10.36
V6
V7	33.1	25.28	25.32	57.51
V8	32.3	25.71	25.71	24.54(0.03)	24.52(0.01)	25.70	25.70	24.49	24.47	9.14
V9	27.9	25.85	25.88	24.53(-0.02)	24.53(-0.01)	25.84	25.88	24.48	24.49	8.73
V10	26.5	25.92	25.97	24.68(-0.04)	24.68(-0.02)	25.92	25.96	24.64	24.64	5.23
V11	23.2	25.75	25.85	24.79(-0.10)	24.87(-0.13)	25.73	25.84	24.74	24.82	24.88
V12	19.0	25.98	26.04	25.14(-0.12)	25.14(-0.11)	25.96	26.03	25.10	25.10	7.15
V13	18.0	26.25	26.19	25.18(0.08)	25.13(0.07)	26.24	26.17	25.14	25.09	5.71
V14	17.9	25.77	25.83	25.01(0.01)	25.06(0.01)	25.75	25.81	24.96	25.02	6.93
V15	17.7	26.24	26.26	25.24(0.15)	25.30(0.14)	26.22	26.23	25.20	25.26	5.24
V16	15.7	25.98	25.92	25.22(0.02)	25.22(-0.05)	25.96	25.90	25.18	25.18	3.41
V17	14.9	26.28	26.27	25.28(0.04)	25.27(0.13)	26.27	26.25	25.24	25.22	8.39
V18	14.3	26.16	26.12	25.37(-0.11)	25.39(-0.09)	26.14	26.12	25.32	25.35	10.38
V19	14.1	26.20	26.25	25.23(0.00)	25.27(0.05)	26.18	26.23	25.19	25.23	2.75
V20	12.9	26.46	26.42	25.04(0.04)	25.03(0.03)	26.45	26.42	24.99	24.99	3.42
V21	12.1	26.06	26.07	25.19(0.01)	25.22(0.01)	26.04	26.05	25.15	25.17	7.45
V22	11.7	26.26	26.27	25.60(-0.02)	25.62(0.01)	26.24	26.25	25.56	25.59	4.25
V23	7.5	26.66	26.54	25.93(0.07)	25.89(0.05)	26.62	26.52	25.89	25.85	8.41

^aThe value of the magnitude correction applied to the F814W magnitudes, defined as in §4.4, is listed in parenthesis

Notes on the individual variable stars. V1: isolated, symmetric light curve, period too long to be determined, phase average magnitudes are calculated for P=77 days. V2: very crowded region nearby, small amplitude. Phase average magnitudes are calculated for P=60.6 days. V3: at the edge of a very crowded group, several companions within five pixels. Bimodal V light curve. Phase average magnitudes are calculated for P=46.3 days. V4: fainter companion 3 pixels away. Small amplitude, symmetric light curve; phase average magnitudes are calculated for P=48.9 days.. V5: one magnitude fainter companion 2.4 pixels away; not variable from ALLFRAME photometry. V6: isolated, not found in DoPHOT photometry; magnitudes are derived from ALLFRAME photometry. V7: isolated, not found in the I photometry file. V8: three fainter companions 2.2 to 2.8 pixels away; not variable from ALLFRAME photometry. V9: two companions 2.8 pixels away, approx. 1 magnitude fainter; not in ALLFRAME photometry. V10: two magnitude fainter companion 2.1 pixels away; not variable from ALLFRAME photometry. V11: isolated; not in ALLFRAME photometry. V12: in a crowded region, even if no companions are identified within three pixels; not variable from ALLFRAME photometry. V13: isolated, V light curve has a flat minimum, possibly due to superposition to a brighter star. V14: 1.5 magnitudes fainter companion 2.9 pixels away, not in ALLFRAME photometry. V15: Fainter companion three pixels away. Symmetric light curve; not sufficient coverage of the light curve in F814W to derive a reliable I magnitude. V16: Fainter companion 1.5 pixels away. V light curve has flat minimum and small amplitude. V17: two fainter (0.6 and 1.4 magnitudes respectively) companions 2.3 and 2.9 pixels away; not in ALLFRAME photometry. V18: flat I light curve. V19: 0.9 magnitudes fainter companion 2.4 pixels away; not variable from ALLFRAME photometry. V20: crowded region, three companions between 3 and 5 pixels away. Not in ALLFRAME photometry, flat I light curve. V21: crowded region, three companions between 3 and 5 pixels away. Eclipsing variable? V22: crowded region, several companions within 5 pixels. Not in ALLFRAME photometry, I light curve does not phase with V light curve. V23: two fainter (.2 and 1.1 magnitudes) companions 2.5 and 2.2 pixels away; not in ALLFRAME photometry.

Table A5. ALLFRAME Mean Photometry of Other NGC 2541 Variables

ID	P	F555W _{ph}	F555W _{av}	F814W _{ph} ^a	F814W _{av} ^a	V _{ph}	V _{av}	I _{ph}	I _{av}	χ^2
V1	77.0	25.56	25.57	23.42(-0.07)	23.44(-0.13)	25.58	25.61	23.39	23.41	
V2	60.6	25.02	25.98	23.55(0.01)	23.53(-0.02)	25.01	24.97	23.51	23.48	
V3	46.3	25.27	25.32	24.12(-0.06)	24.14(-0.04)	25.25	25.31	24.07	24.10	
V4	50.0	25.23	25.24	24.78(0.00)	24.81(0.03)	25.21	25.22	24.76	24.78	
V5	
V6	40.3	24.75	24.70	24.00(0.00)	23.99(-0.05)	24.73	24.68	23.96	23.95	
V7	25.6	25.15	25.14	24.41(-0.06)	24.37(0.00)	25.13	25.12	24.37	24.34	
V8	
V9	
V10	
V11	
V12	
V13	18.0	26.24	26.17	25.03(0.05)	25.07(0.08)	26.22	26.15	24.99	25.03	
V14	
V15	17.7	26.22	26.24	25.36(0.01)	25.33(0.07)	26.20	26.22	25.33	25.29	
V16	15.9	24.69	24.70	23.87(-0.02)	23.90(-0.01)	24.67	24.68	23.84	23.86	
V17	
V18	14.3	26.18	26.14	25.39(-0.10)	25.38(-0.07)	26.16	26.13	25.35	25.35	
V19	
V20	
V21	12.4	25.91	25.94	25.04(-0.03)	25.05(-0.03)	25.89	25.93	25.00	25.01	
V22	
V23	

^aThe value of the magnitude correction applied to the F814W magnitudes, defined as in §4.4, is listed in parenthesis

Table A6a. Photometry for the PC Secondary Standards

X ^a	Y ^a	RA(J2000) ^b	Dec(J2000) ^b	F555W ^c	F814W ^c	V ^d	I ^d
93.72	148.16	8:14:41.8896	49:01:52.419	25.71 ± 0.03	24.09 ± 0.03	25.71	24.05
107.60	105.66	8:14:42.0266	49:01:50.920	25.63 ± 0.02	23.59 ± 0.02	25.65	23.55
174.50	79.58	8:14:41.9791	49:01:47.709	25.47 ± 0.02	23.78 ± 0.03	25.47	23.74
181.66	475.99	8:14:40.3791	49:01:56.350	26.35 ± 0.04	25.11 ± 0.05	26.34	25.07
272.00	469.11	8:14:40.1997	49:01:52.636	25.44 ± 0.02	25.12 ± 0.05	25.42	25.10
274.51	227.33	8:14:41.1637	49:01:47.088	25.64 ± 0.02	24.29 ± 0.03	25.63	24.24
278.64	394.70	8:14:40.4832	49:01:50.698	25.74 ± 0.02	25.49 ± 0.06	25.73	25.47
284.47	639.85	8:14:39.4870	49:01:55.976	25.22 ± 0.02	23.01 ± 0.02	25.26	22.99
410.12	426.81	8:14:40.0526	49:01:46.223	25.29 ± 0.02	24.60 ± 0.04	25.28	24.57
439.49	332.96	8:14:40.3622	49:01:42.946	26.69 ± 0.05	26.21 ± 0.26	26.68	26.18
450.43	175.37	8:14:40.9687	49:01:38.973	26.29 ± 0.04	25.86 ± 0.08	26.28	25.84
463.95	587.41	8:14:39.2853	49:01:47.714	25.20 ± 0.02	24.82 ± 0.04	25.19	24.79
485.50	754.73	8:14:38.5702	49:01:50.618	25.57 ± 0.03	24.02 ± 0.02	25.57	23.98
502.97	427.83	8:14:39.8357	49:01:42.575	25.64 ± 0.02	25.49 ± 0.07	25.63	25.48
528.58	76.95	8:14:41.1819	49:01:33.703	26.01 ± 0.03	25.83 ± 0.14	26.00	25.82
539.43	492.97	8:14:39.4909	49:01:42.604	25.54 ± 0.02	25.37 ± 0.07	25.53	25.35
549.40	744.21	8:14:38.4669	49:01:47.865	24.98 ± 0.02	23.40 ± 0.02	24.98	23.36
594.72	262.68	8:14:40.2884	49:01:35.241	25.88 ± 0.03	24.26 ± 0.03	25.88	24.22
609.81	637.40	8:14:38.7538	49:01:43.085	25.13 ± 0.02	24.92 ± 0.04	25.13	24.90
615.42	702.39	8:14:38.4833	49:01:44.327	25.55 ± 0.02	25.71 ± 0.08	25.56	25.72
715.48	129.18	8:14:40.5458	49:01:27.547	24.89 ± 0.02	24.86 ± 0.05	24.89	24.86
723.56	332.43	8:14:39.7150	49:01:31.750	25.67 ± 0.02	25.52 ± 0.08	25.66	25.51
762.40	480.53	8:14:39.0348	49:01:33.559	25.01 ± 0.02	24.79 ± 0.04	25.00	24.77
778.91	655.28	8:14:38.3039	49:01:36.856	25.85 ± 0.03	25.89 ± 0.12	25.85	25.90

^aThe X and Y coordinate are relative to the 10/30/95 epoch. For each 800×800 pixels chip, pixel [1,1] is located at the edge of the WFPC2 pyramid.

^bRA and Dec are calculated using the IRAF task STSDAS.HIST_CALIB.WFPC.METRIC, version 1.3.5 (July 1996).

^cF555W and F814W instrumental magnitudes are intensity averaged over the 13 epochs

^dV and I magnitudes are calculated from the instrumental F555W and F814W magnitudes as described in §3

Table A6b. Photometry for the WF2 Secondary Standards

X ^a	Y ^a	RA(J2000) ^b	Dec(J2000) ^b	F555W ^c	F814W ^c	V ^d	I ^d
63.06	270.53	8:14:43.4904	49:02:14.168	24.22 ± 0.01	24.16 ± 0.03	24.22	24.16
70.41	749.62	8:14:45.7706	49:02:55.991	24.54 ± 0.01	24.14 ± 0.03	24.52	24.11
74.74	784.64	8:14:45.9009	49:02:59.208	25.51 ± 0.02	25.39 ± 0.07	25.51	25.38
84.72	478.62	8:14:44.3277	49:02:33.246	25.26 ± 0.02	23.75 ± 0.03	25.26	23.71
92.47	146.89	8:14:42.6205	49:02:04.916	25.28 ± 0.02	25.20 ± 0.06	25.28	25.19
109.09	252.53	8:14:42.9976	49:02:14.819	25.74 ± 0.03	25.65 ± 0.07	25.74	25.65
120.57	139.48	8:14:42.3372	49:02:05.620	25.02 ± 0.02	24.53 ± 0.04	25.00	24.50
121.19	298.54	8:14:43.1191	49:02:19.382	25.44 ± 0.02	24.55 ± 0.04	25.43	24.51
137.44	668.47	8:14:44.7948	49:02:52.249	25.23 ± 0.02	25.03 ± 0.05	25.22	25.02
140.15	399.40	8:14:43.4512	49:02:29.045	23.42 ± 0.01	23.09 ± 0.02	23.41	23.07
174.25	510.80	8:14:43.7008	49:02:40.371	25.18 ± 0.02	25.14 ± 0.05	25.18	25.13
189.75	497.35	8:14:43.4983	49:02:39.954	25.26 ± 0.02	25.08 ± 0.05	25.25	25.06
247.19	114.67	8:14:41.1008	49:02:09.560	25.18 ± 0.02	25.04 ± 0.05	25.17	25.03
248.64	78.69	8:14:40.9108	49:02:06.534	25.69 ± 0.03	24.17 ± 0.02	25.68	24.12
248.77	766.62	8:14:44.2965	49:03:06.117	25.53 ± 0.03	23.78 ± 0.03	25.53	23.74
280.82	627.28	8:14:43.3355	49:02:55.648	25.11 ± 0.02	24.96 ± 0.05	25.11	24.95
354.57	550.27	8:14:42.3062	49:02:52.554	24.73 ± 0.02	24.10 ± 0.03	24.71	24.07
355.46	538.66	8:14:42.2411	49:02:51.589	24.81 ± 0.02	24.83 ± 0.05	24.81	24.83
409.65	57.17	8:14:39.3873	49:02:12.466	25.82 ± 0.03	25.77 ± 0.09	25.81	25.76
450.51	157.46	8:14:39.5190	49:02:23.104	25.49 ± 0.02	25.36 ± 0.06	25.49	25.35
458.49	256.92	8:14:39.9383	49:02:32.112	24.87 ± 0.02	25.04 ± 0.04	24.88	25.06
487.66	563.51	8:14:41.1964	49:03:00.156	25.19 ± 0.02	24.79 ± 0.05	25.18	24.77
557.55	581.89	8:14:40.6709	49:03:05.123	25.24 ± 0.02	25.10 ± 0.06	25.24	25.09
567.64	632.88	8:14:40.8340	49:03:10.012	24.96 ± 0.02	24.60 ± 0.03	24.95	24.58
584.62	410.63	8:14:39.5855	49:02:51.586	22.93 ± 0.01	21.10 ± 0.01	22.93	21.06
599.65	294.05	8:14:38.8782	49:02:42.194	25.00 ± 0.02	25.09 ± 0.05	25.01	25.09
605.55	290.18	8:14:38.8074	49:02:42.145	24.73 ± 0.02	24.76 ± 0.04	24.73	24.76
607.14	261.29	8:14:38.6514	49:02:39.715	25.48 ± 0.02	25.23 ± 0.06	25.47	25.22
621.52	313.34	8:14:38.7811	49:02:44.929	25.09 ± 0.02	24.86 ± 0.04	25.08	24.84

^{a,b,c,d} Notes as in Table A6a

Table A6c. Photometry for the WF3 Secondary Standards

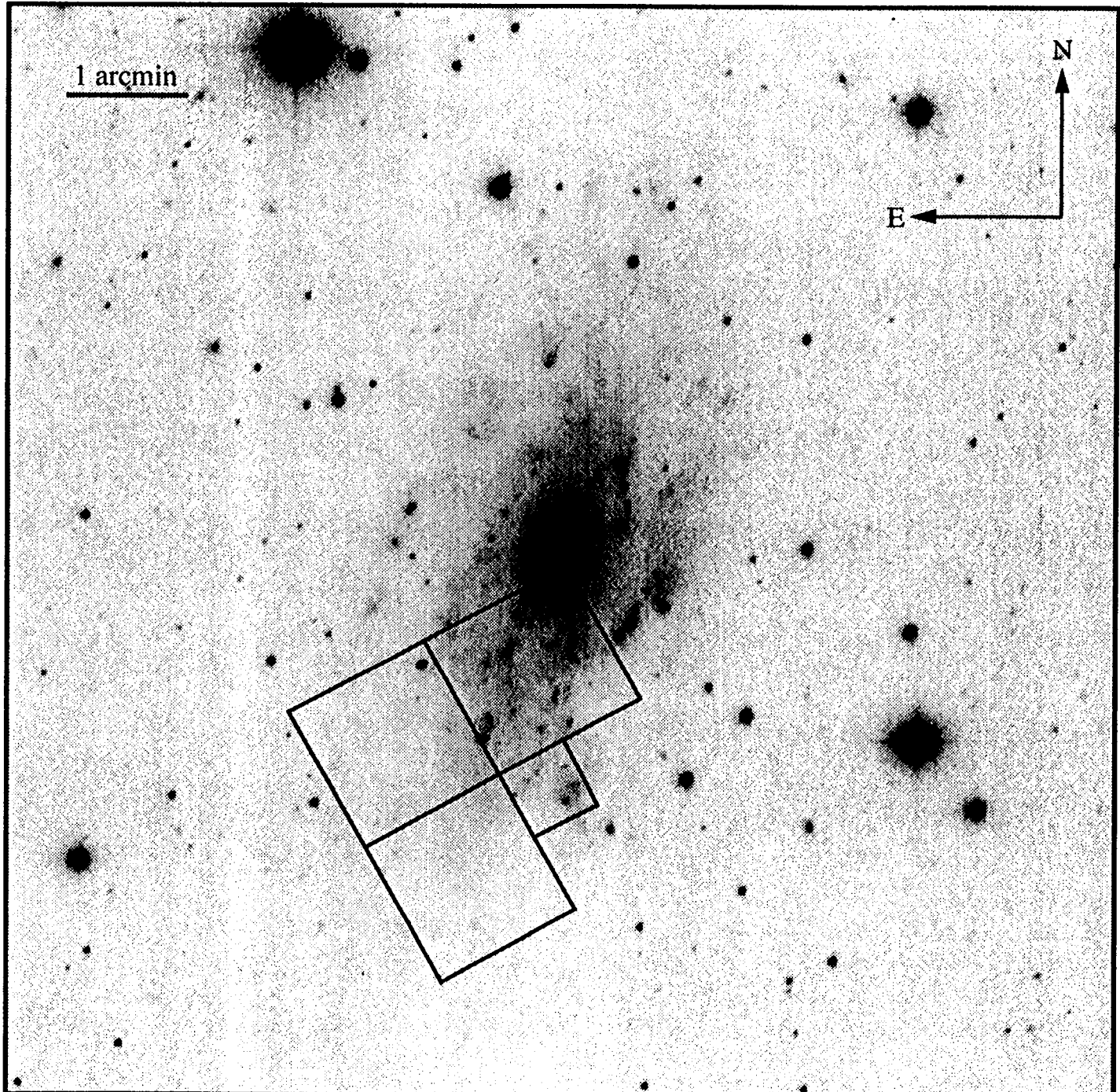
X ^a	Y ^a	RA(J2000) ^b	Dec(J2000) ^b	F555W ^c	F814W ^c	V ^d	I ^d
61.89	508.53	8:14:46.6027	49:01:32.262	25.60 ± 0.03	24.23 ± 0.03	25.59	24.19
77.23	369.25	8:14:45.4561	49:01:40.369	25.65 ± 0.03	25.32 ± 0.06	25.64	25.30
116.81	680.74	8:14:48.3842	49:01:28.633	25.18 ± 0.02	25.28 ± 0.06	25.18	25.29
123.62	281.23	8:14:44.9134	49:01:48.669	25.65 ± 0.03	23.97 ± 0.02	25.65	23.93
139.25	95.32	8:14:43.3690	49:01:59.135	25.70 ± 0.03	25.90 ± 0.11	25.71	25.91
162.15	188.38	8:14:44.2914	49:01:56.544	24.82 ± 0.02	24.22 ± 0.03	24.80	24.19
180.54	632.60	8:14:48.2808	49:01:36.413	25.98 ± 0.03	25.48 ± 0.06	25.96	25.45
209.09	360.71	8:14:46.0345	49:01:52.138	25.26 ± 0.02	25.20 ± 0.06	25.26	25.19
222.31	93.31	8:14:43.7597	49:02:06.390	23.26 ± 0.01	23.01 ± 0.03	23.25	23.00
246.48	115.09	8:14:44.0686	49:02:07.411	24.49 ± 0.02	22.04 ± 0.01	24.54	22.03
279.43	102.34	8:14:44.1206	49:02:10.881	25.13 ± 0.02	24.93 ± 0.05	25.12	24.91
307.57	564.42	8:14:48.3168	49:01:50.675	24.21 ± 0.01	22.18 ± 0.01	24.24	22.14
414.19	710.44	8:14:50.1268	49:01:52.774	23.92 ± 0.01	22.10 ± 0.01	23.92	22.06
425.46	688.52	8:14:49.9917	49:01:54.813	25.62 ± 0.02	25.58 ± 0.07	25.61	25.58
433.48	705.46	8:14:50.1793	49:01:54.682	24.76 ± 0.02	23.09 ± 0.02	24.76	23.05
436.23	77.69	8:14:44.6861	49:02:25.626	24.97 ± 0.02	24.94 ± 0.05	24.97	24.93
447.86	751.14	8:14:50.6483	49:01:53.704	25.38 ± 0.02	23.94 ± 0.02	25.38	23.89
467.57	76.80	8:14:44.8349	49:02:28.373	25.55 ± 0.02	25.24 ± 0.06	25.54	25.22
471.26	611.66	8:14:49.5478	49:02:02.524	25.81 ± 0.03	25.83 ± 0.08	25.81	25.84
490.36	725.33	8:14:50.6347	49:01:58.627	25.31 ± 0.02	25.30 ± 0.05	25.31	25.30
490.52	678.03	8:14:50.2236	49:02:00.946	25.45 ± 0.02	25.32 ± 0.06	25.45	25.31
494.98	720.64	8:14:50.6169	49:01:59.254	25.84 ± 0.03	24.45 ± 0.03	25.83	24.40
498.46	244.11	8:14:46.4538	49:02:22.893	25.75 ± 0.03	25.67 ± 0.07	25.74	25.66
540.88	623.54	8:14:49.9977	49:02:07.961	26.01 ± 0.03	24.57 ± 0.03	26.00	24.53
554.65	548.80	8:14:49.4118	49:02:12.814	25.32 ± 0.02	24.91 ± 0.04	25.31	24.88
568.60	479.24	8:14:48.8709	49:02:17.432	25.65 ± 0.03	25.64 ± 0.07	25.65	25.64
616.28	418.59	8:14:48.5755	49:02:24.523	25.70 ± 0.03	24.15 ± 0.03	25.70	24.10
619.28	455.07	8:14:48.9107	49:02:22.993	25.24 ± 0.02	25.26 ± 0.06	25.25	25.26
637.72	716.68	8:14:51.2866	49:02:11.756	24.84 ± 0.01	25.01 ± 0.04	24.85	25.02
640.36	760.61	8:14:51.6797	49:02:09.838	24.94 ± 0.02	24.29 ± 0.03	24.92	24.26
685.61	129.80	8:14:46.3884	49:02:44.542	25.92 ± 0.03	25.41 ± 0.08	25.91	25.38
710.44	106.44	8:14:46.3086	49:02:47.784	25.50 ± 0.02	25.45 ± 0.07	25.50	25.44

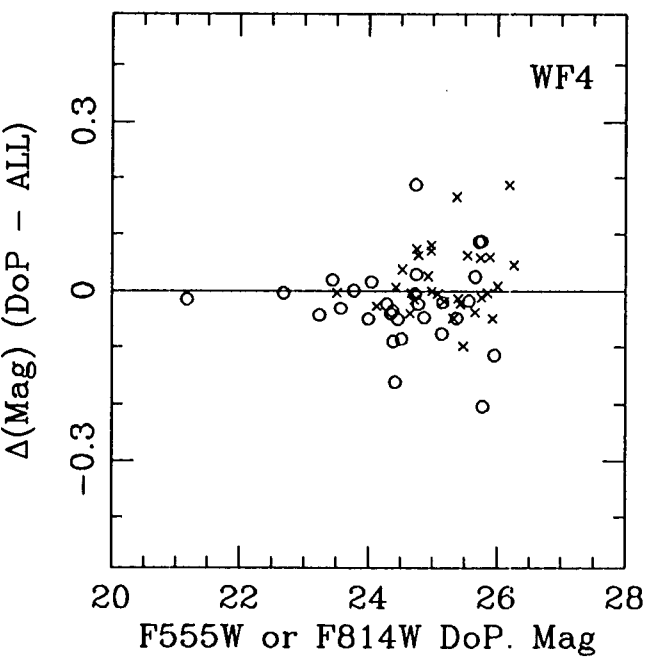
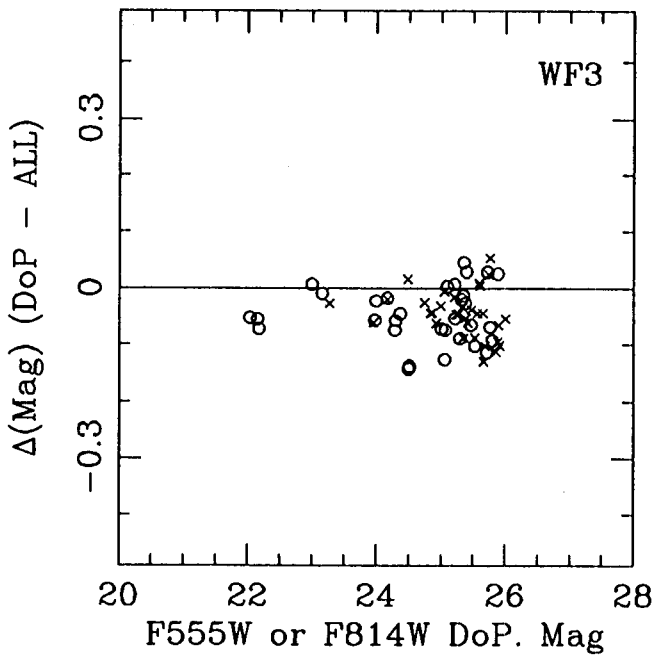
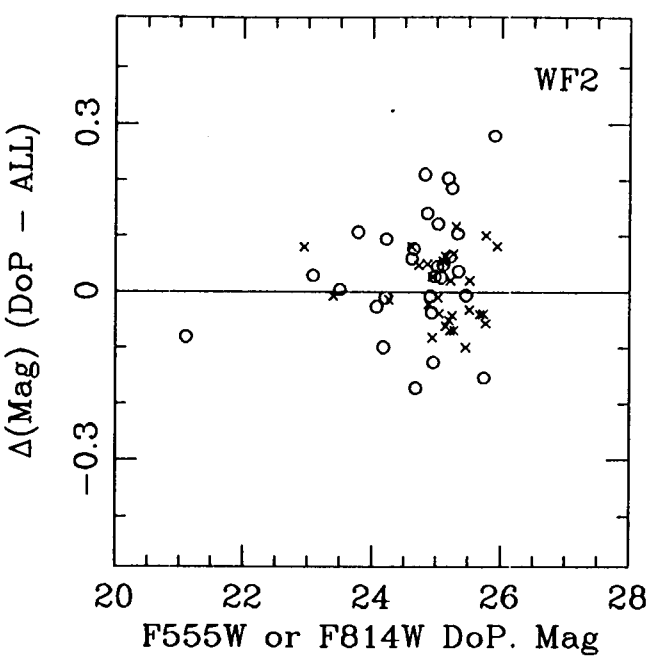
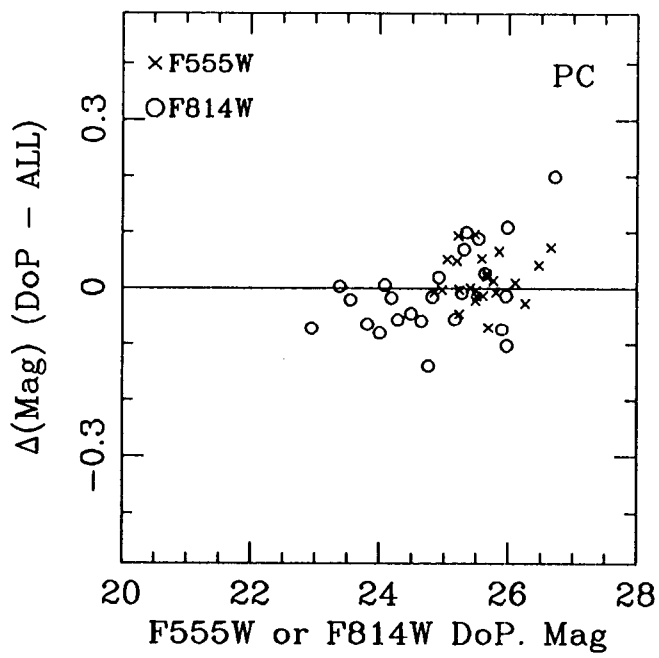
^{a,b,c,d}Notes as in Table A6a

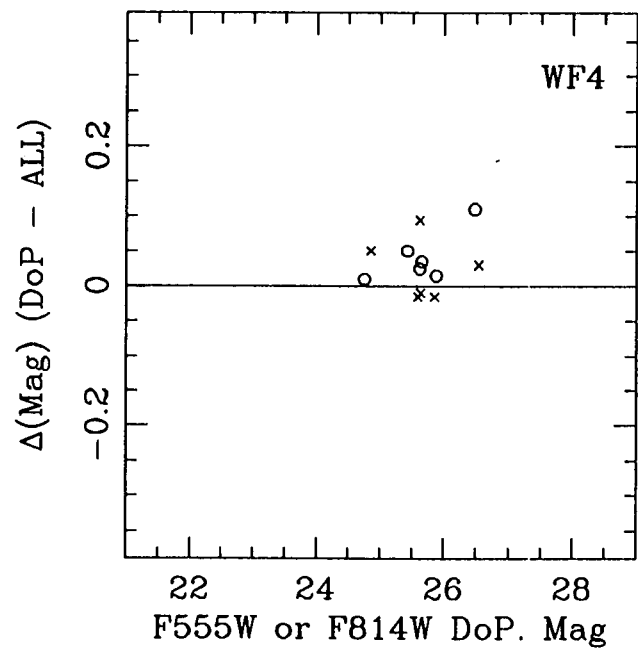
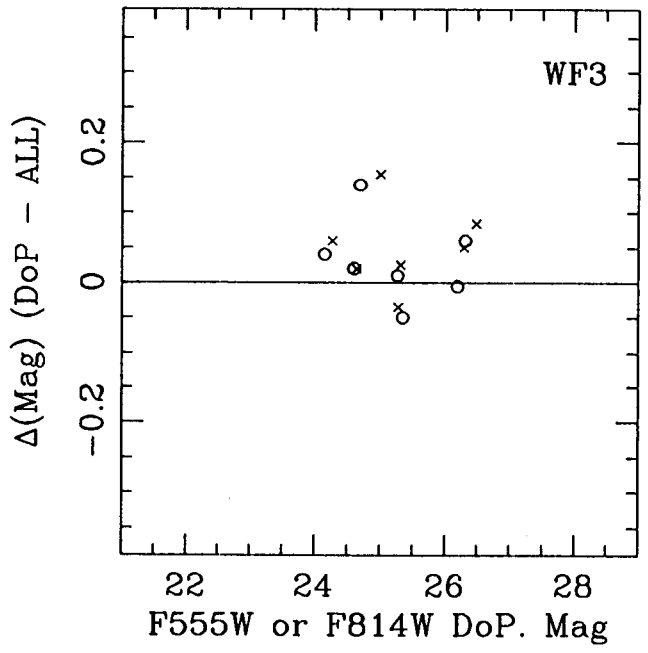
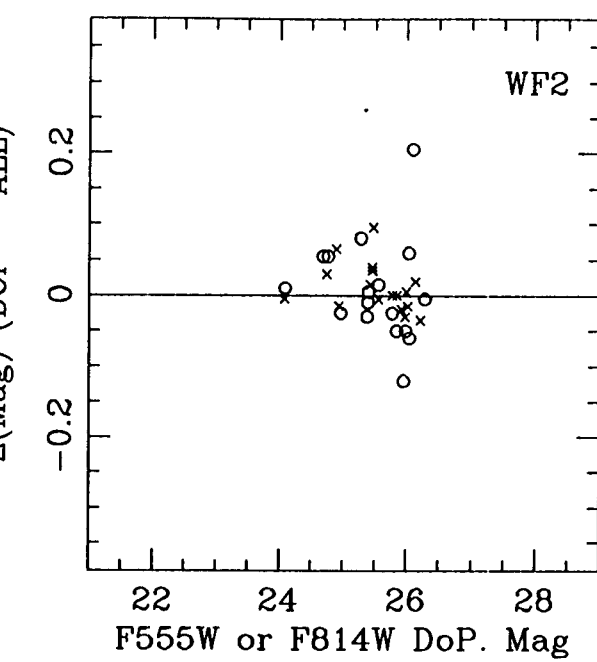
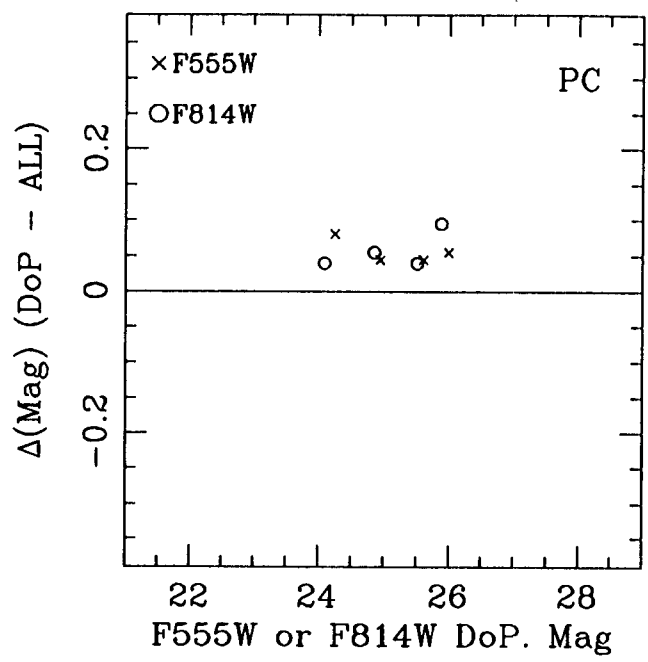
Table A6d. Photometry for the WF4 Secondary Standards

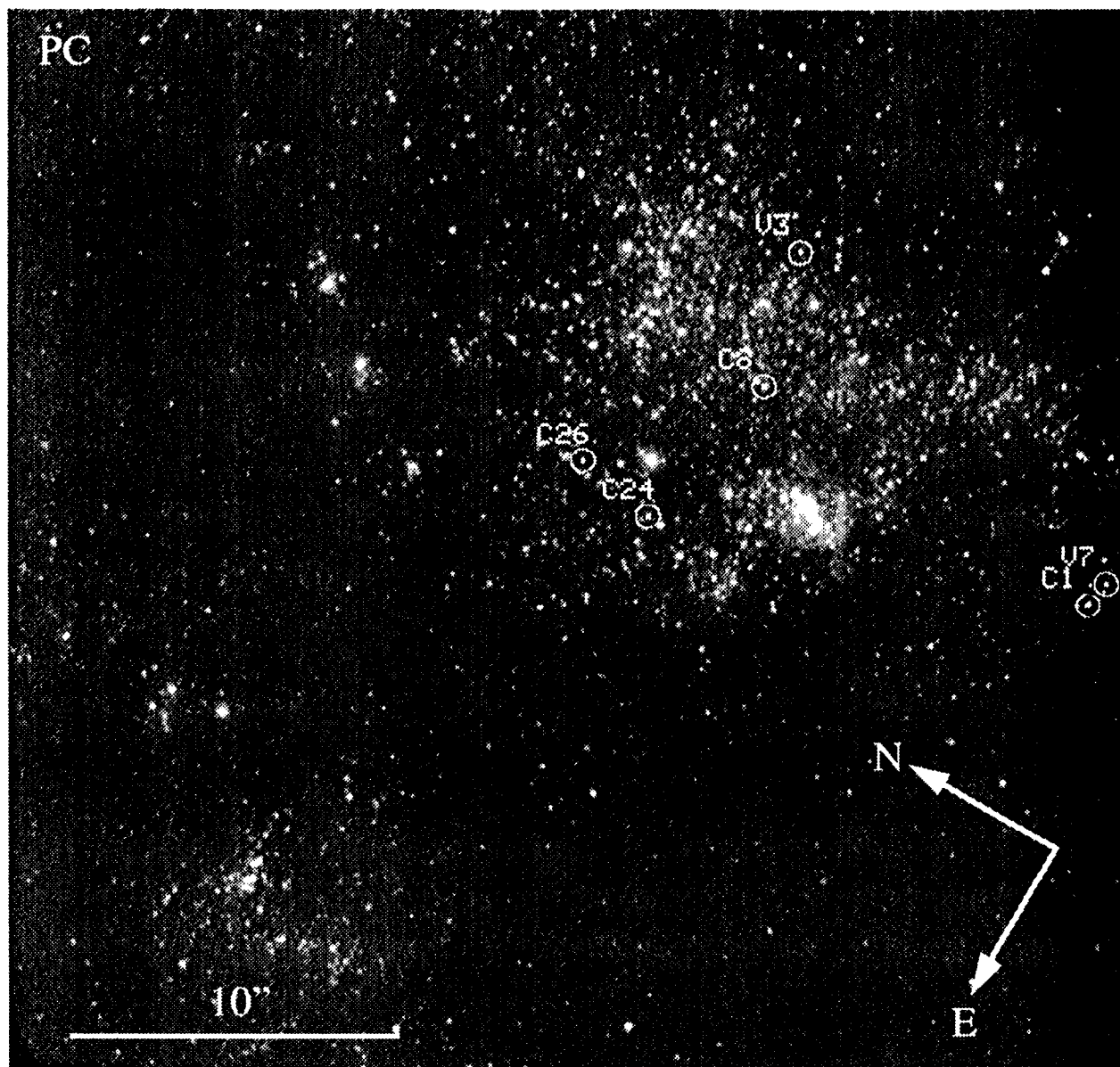
X ^a	Y ^a	RA(J2000) ^b	Dec(J2000) ^b	F555W ^c	F814W ^c	V ^d	I ^d
84.10	389.18	8:14:41.0137	49:01:20.889	25.81 ± 0.03	25.52 ± 0.07	25.80	25.50
86.01	590.40	8:14:40.0163	49:01:03.495	25.76 ± 0.03	25.70 ± 0.08	25.76	25.69
105.91	486.49	8:14:40.7109	49:01:11.439	25.15 ± 0.02	23.57 ± 0.02	25.14	23.53
151.28	168.81	8:14:42.7170	49:01:36.467	24.59 ± 0.01	24.05 ± 0.03	24.58	24.02
201.37	488.42	8:14:41.5311	49:01:06.527	24.97 ± 0.02	24.80 ± 0.03	24.96	24.79
265.35	522.09	8:14:41.9188	49:01:00.437	25.43 ± 0.02	25.39 ± 0.05	25.43	25.38
298.38	604.80	8:14:41.7894	49:00:51.675	25.20 ± 0.02	23.41 ± 0.02	25.20	23.37
331.40	559.56	8:14:42.3063	49:00:53.915	25.99 ± 0.03	25.68 ± 0.08	25.98	25.66
376.42	212.30	8:14:44.4628	49:01:21.568	23.43 ± 0.01	21.16 ± 0.01	23.46	21.14
376.92	336.78	8:14:43.8353	49:01:10.835	25.79 ± 0.03	25.77 ± 0.08	25.79	25.77
394.02	234.25	8:14:44.5055	49:01:18.804	24.99 ± 0.02	25.03 ± 0.05	24.99	25.03
435.40	383.21	8:14:44.1113	49:01:03.912	25.99 ± 0.03	25.46 ± 0.08	25.97	25.43
483.26	263.20	8:14:45.1390	49:01:11.855	24.64 ± 0.01	24.48 ± 0.03	24.63	24.47
524.12	617.98	8:14:43.6953	49:00:39.303	24.49 ± 0.01	24.52 ± 0.03	24.49	24.52
534.90	491.20	8:14:44.4328	49:00:49.648	24.16 ± 0.01	24.24 ± 0.03	24.16	24.24
600.83	476.76	8:14:45.0816	49:00:47.612	24.37 ± 0.01	22.67 ± 0.01	24.37	22.63
604.54	333.50	8:14:45.8408	49:00:59.748	26.09 ± 0.03	23.92 ± 0.02	26.12	23.89
623.85	364.25	8:14:45.8531	49:00:56.141	25.61 ± 0.02	24.18 ± 0.02	25.60	24.13
629.49	649.46	8:14:44.4544	49:00:31.408	25.22 ± 0.02	24.92 ± 0.04	25.21	24.91
642.32	153.43	8:14:47.0767	49:01:13.327	25.43 ± 0.02	25.11 ± 0.05	25.42	25.09
670.62	215.83	8:14:47.0086	49:01:06.564	25.00 ± 0.02	24.49 ± 0.03	24.98	24.46
675.74	721.70	8:14:44.4902	49:00:23.004	25.93 ± 0.03	25.78 ± 0.08	25.92	25.77
713.34	144.41	8:14:47.7353	49:01:10.551	25.79 ± 0.03	25.68 ± 0.08	25.79	25.67
717.34	457.58	8:14:46.1916	49:00:43.490	24.90 ± 0.02	23.27 ± 0.02	24.90	23.23
728.40	437.18	8:14:46.3908	49:00:44.693	24.61 ± 0.01	23.74 ± 0.02	24.59	23.70
730.48	588.67	8:14:45.6397	49:00:31.633	24.80 ± 0.01	24.73 ± 0.04	24.80	24.73
733.43	447.63	8:14:46.3813	49:00:43.549	24.73 ± 0.01	24.58 ± 0.04	24.72	24.57
735.67	278.51	8:14:47.2556	49:00:57.949	24.71 ± 0.01	24.73 ± 0.04	24.71	24.74
761.48	491.30	8:14:46.4023	49:00:38.429	25.75 ± 0.03	24.40 ± 0.03	25.74	24.35

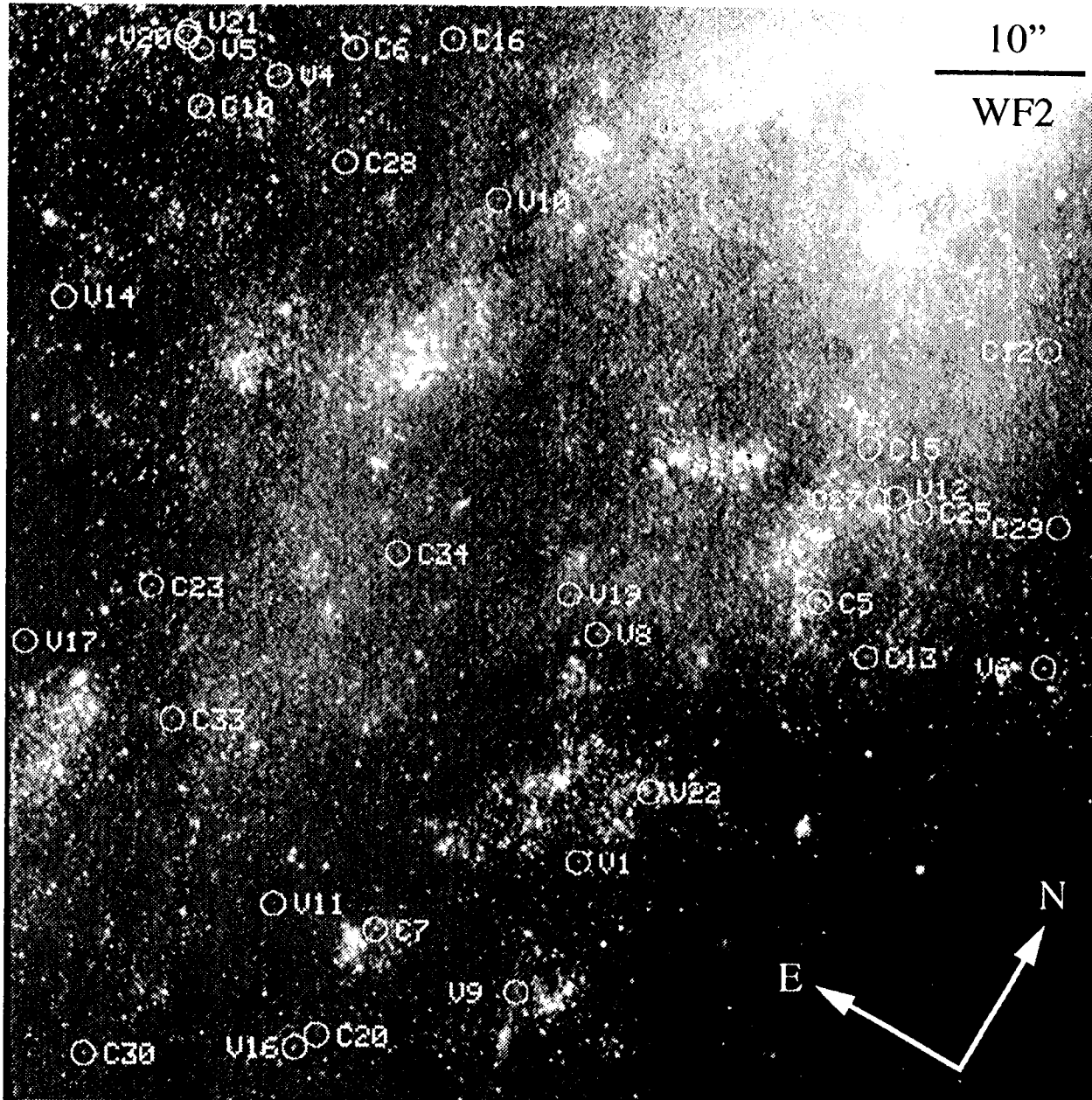
^{a,b,c,d}Notes as in Table A6a

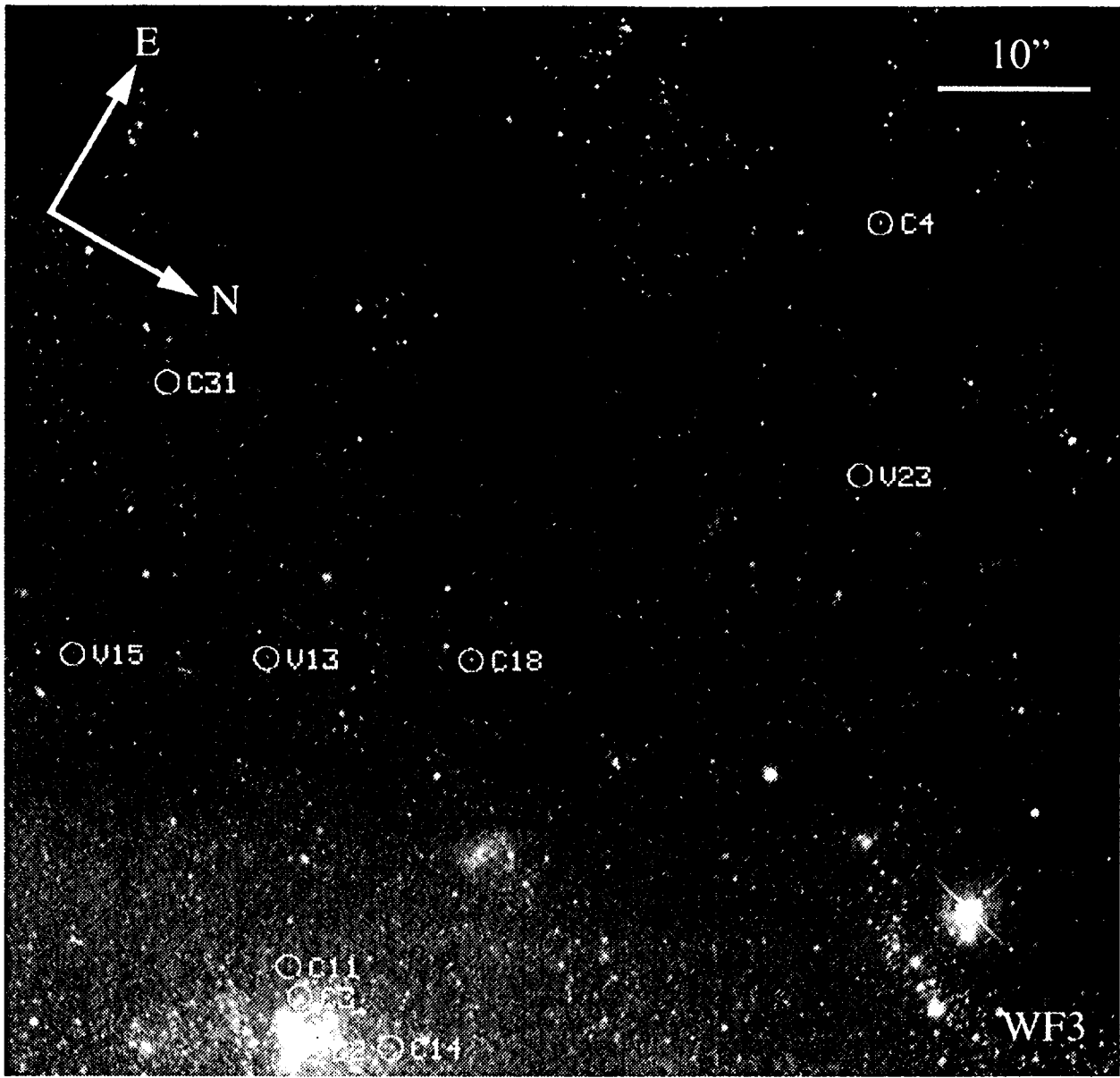


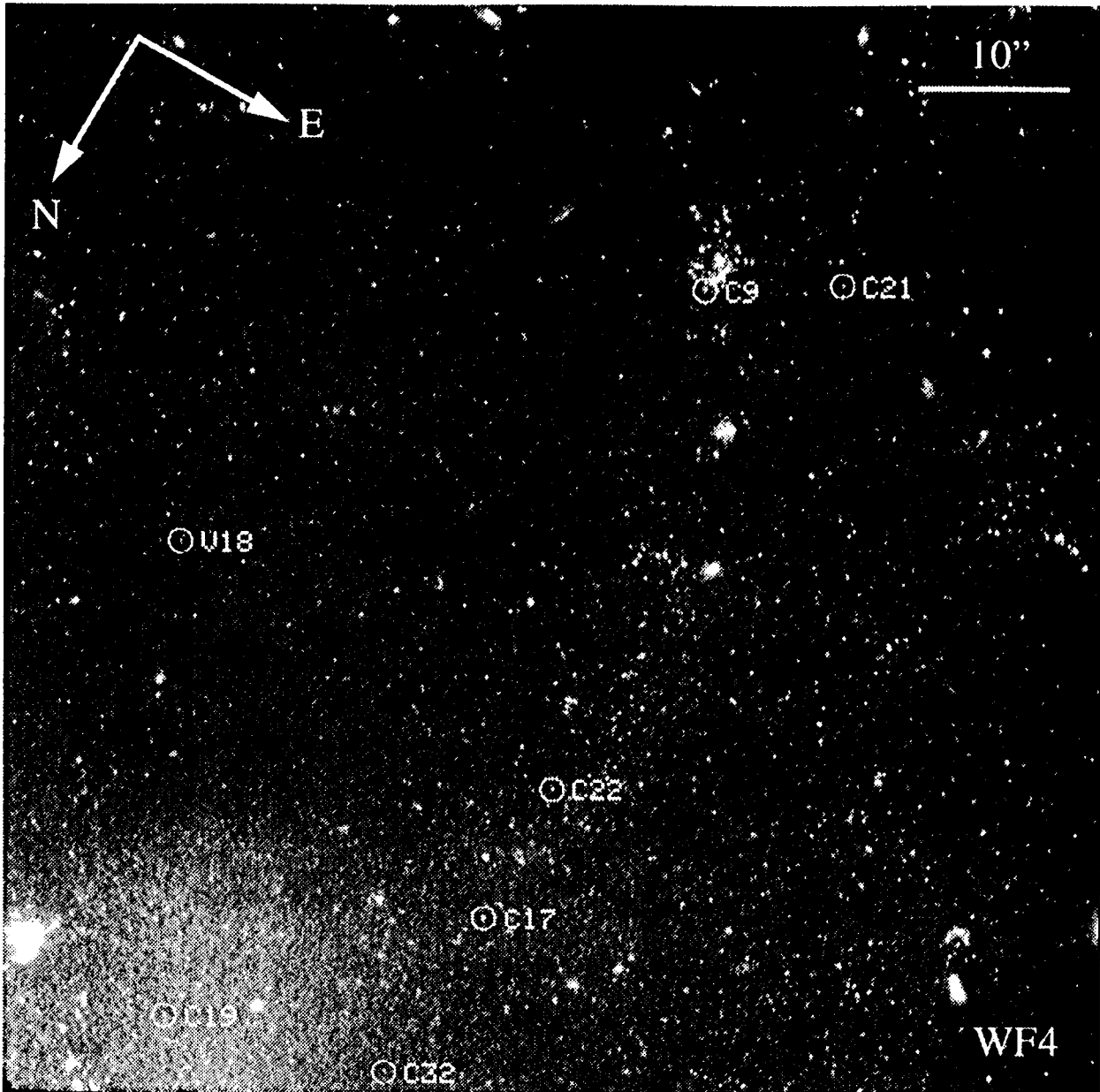




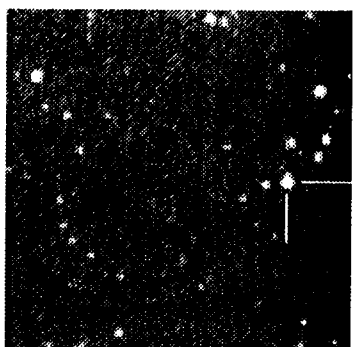




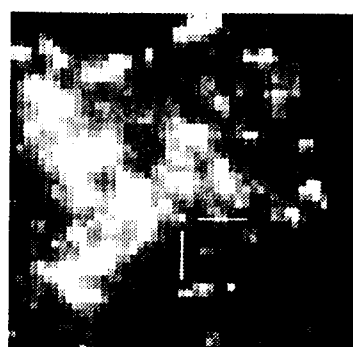




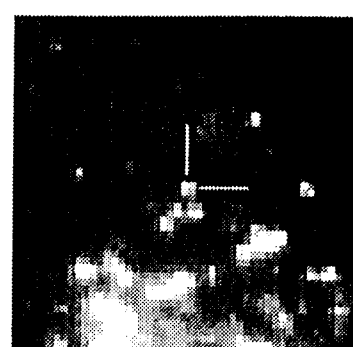
C1



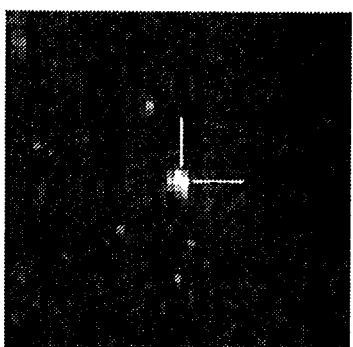
C2



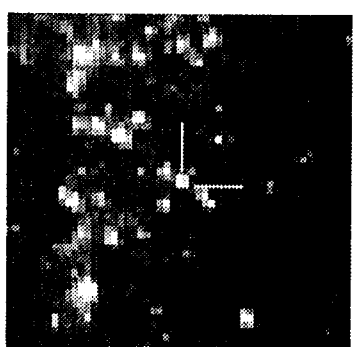
C3



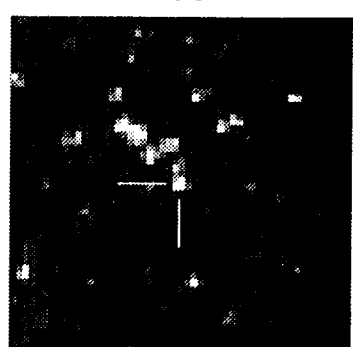
C4



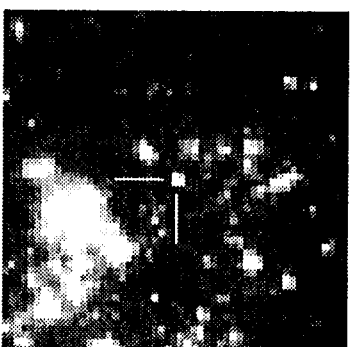
C5



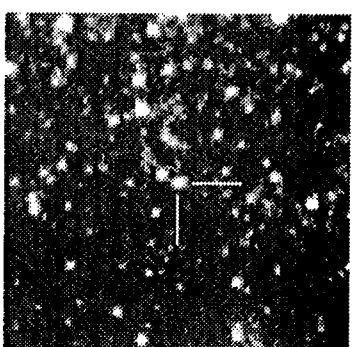
C6



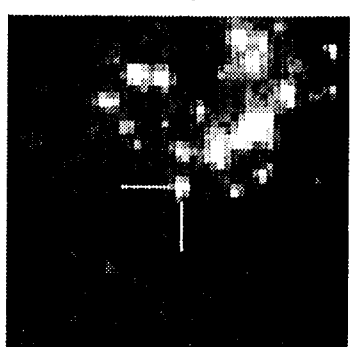
C7



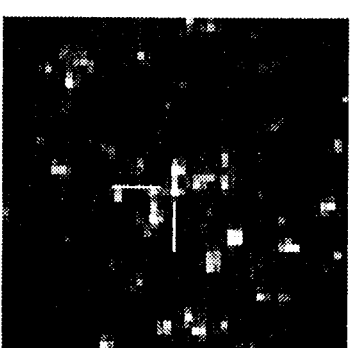
C8



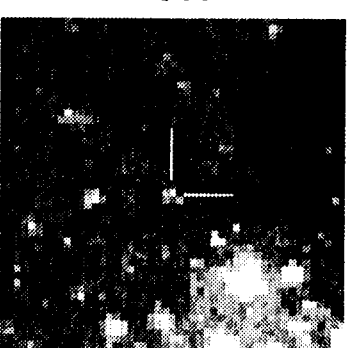
C9



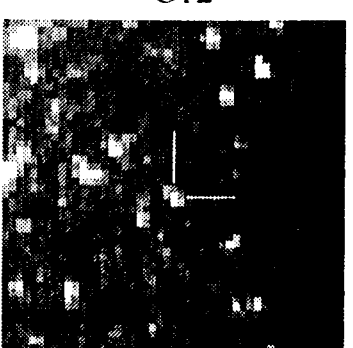
C10



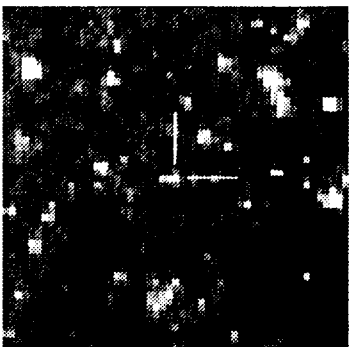
C11



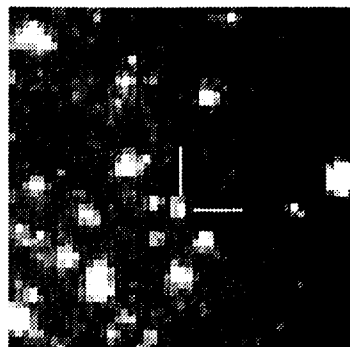
C12



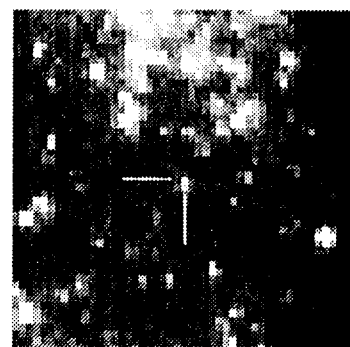
C13



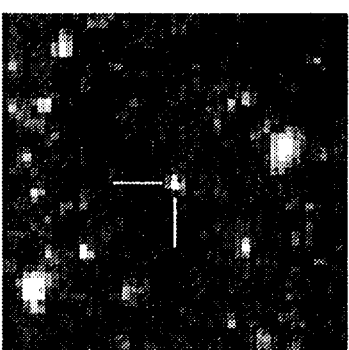
C14



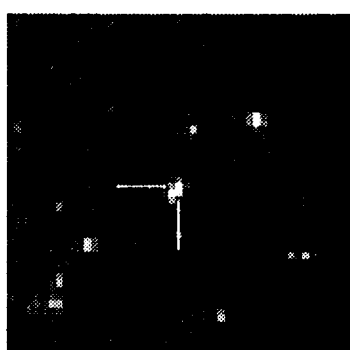
C15



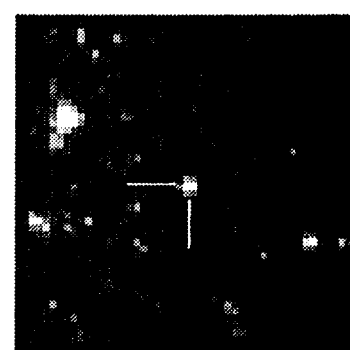
C16



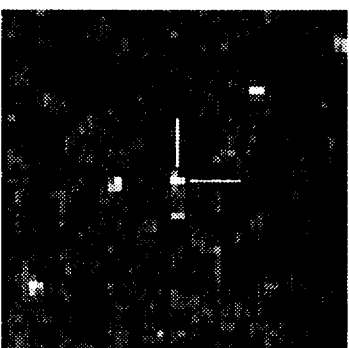
C17



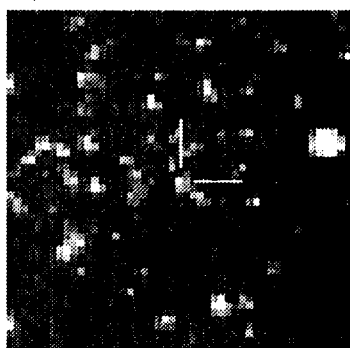
C18



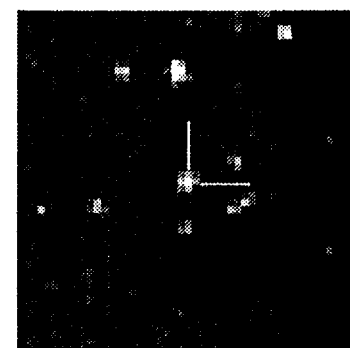
C19



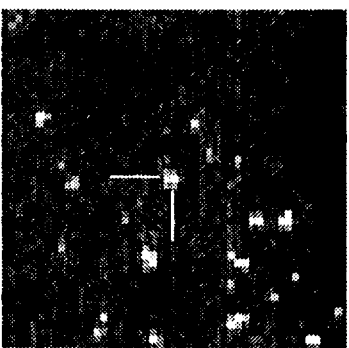
C20



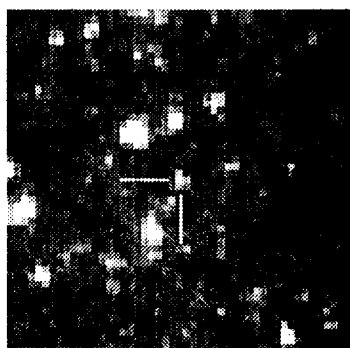
C21



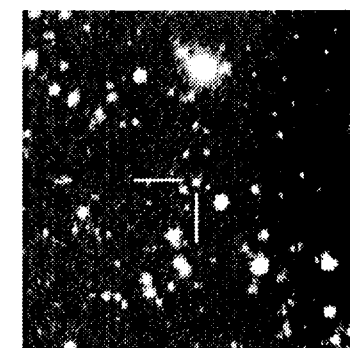
C22



C23



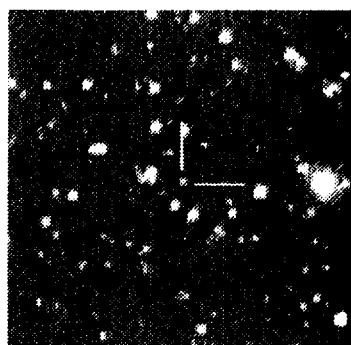
C24



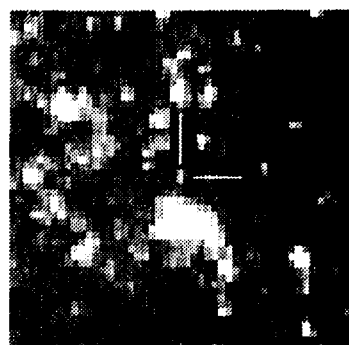
C25



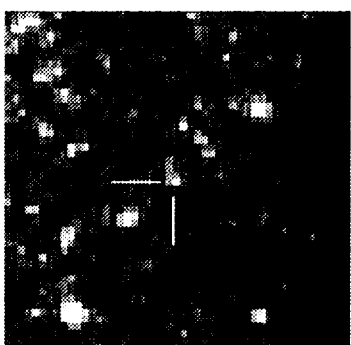
C26



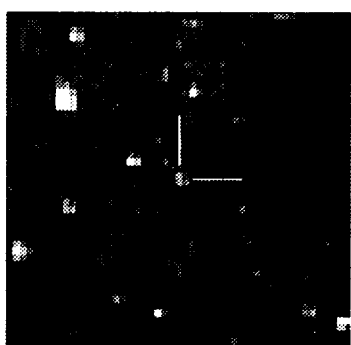
C27



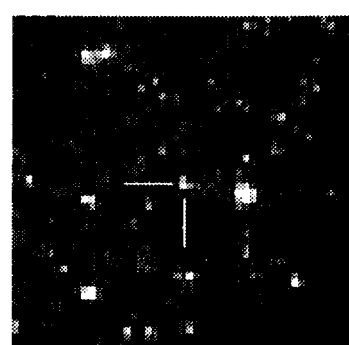
C28



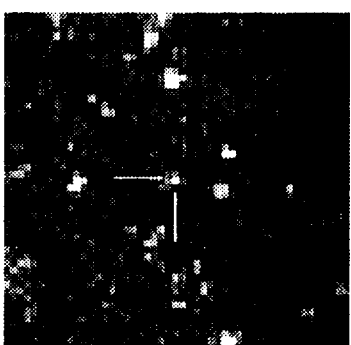
C29



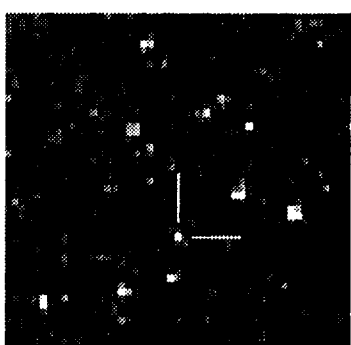
C30



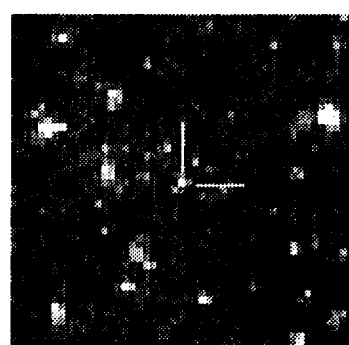
C31



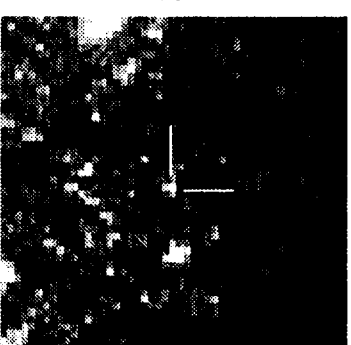
C32

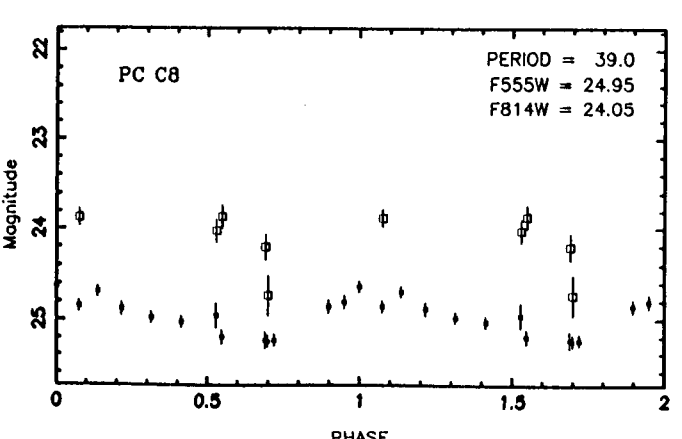
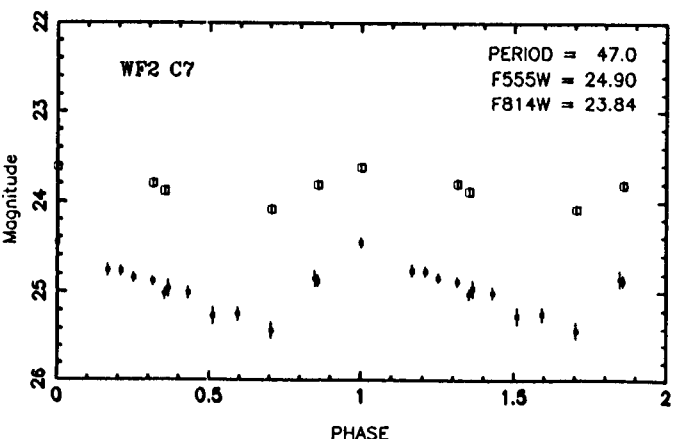
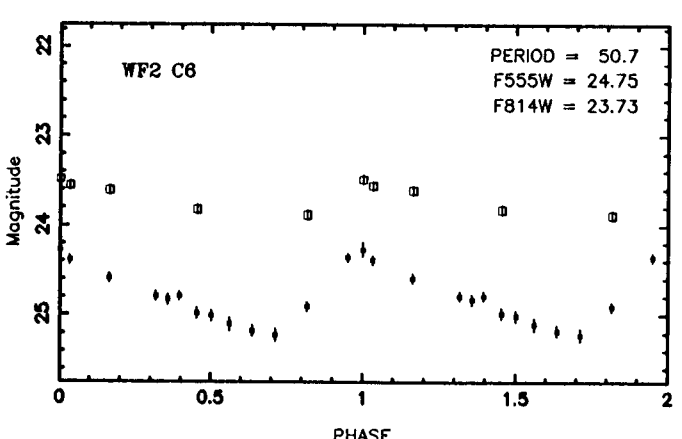
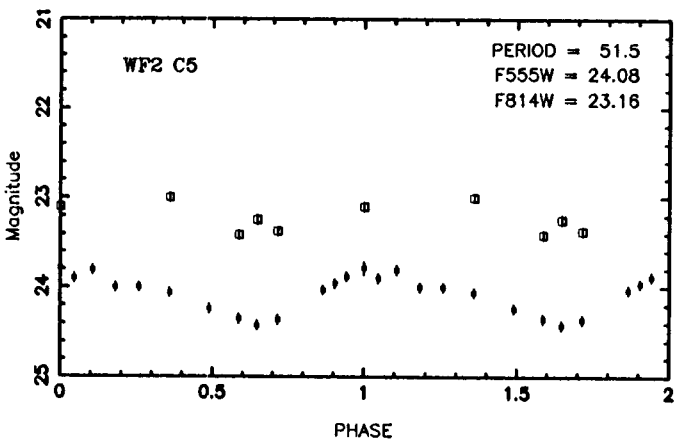
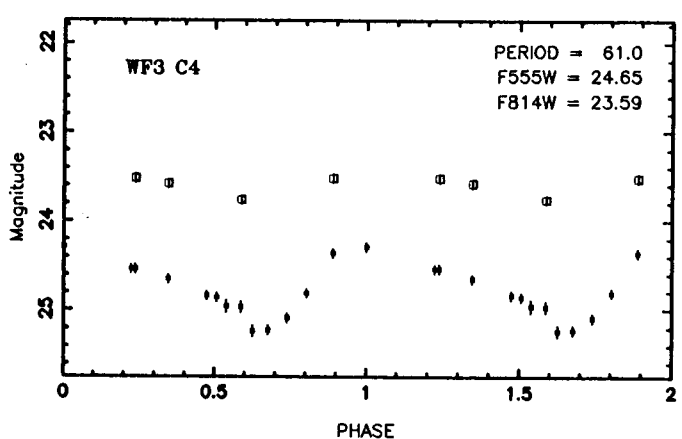
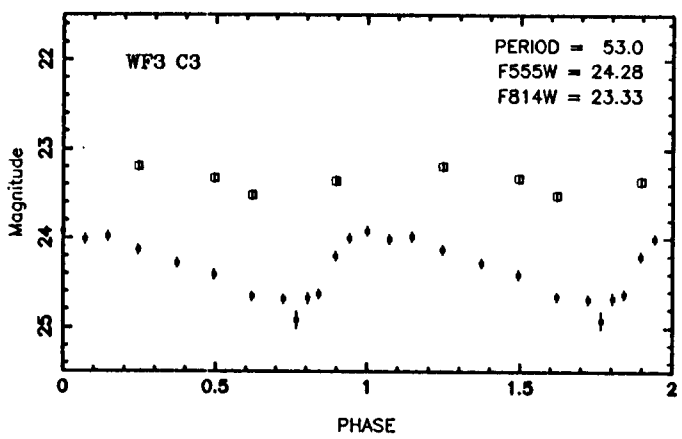
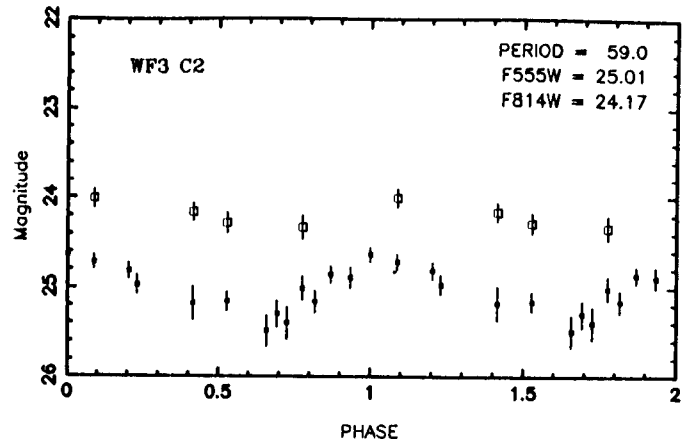
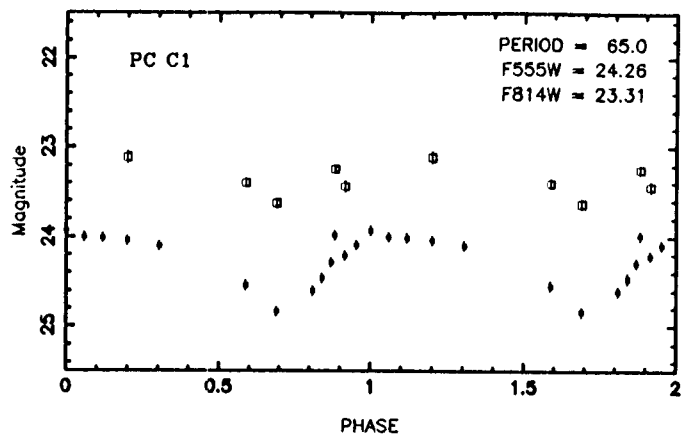


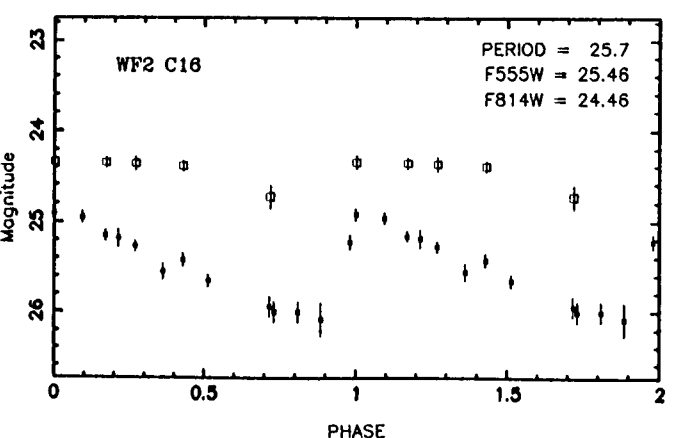
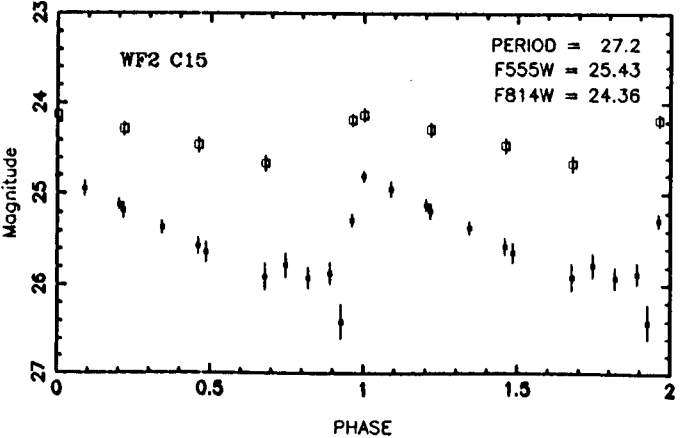
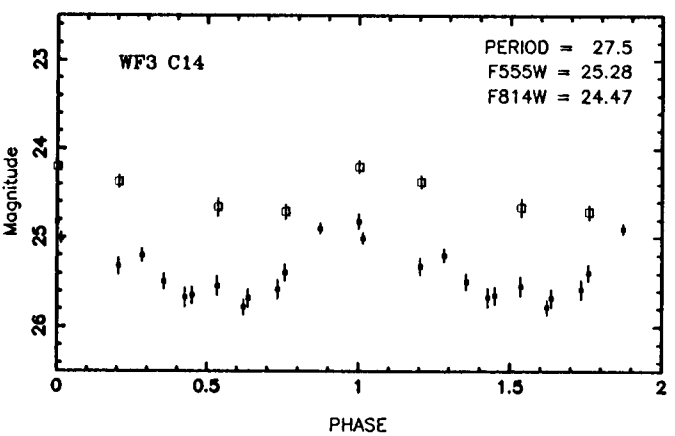
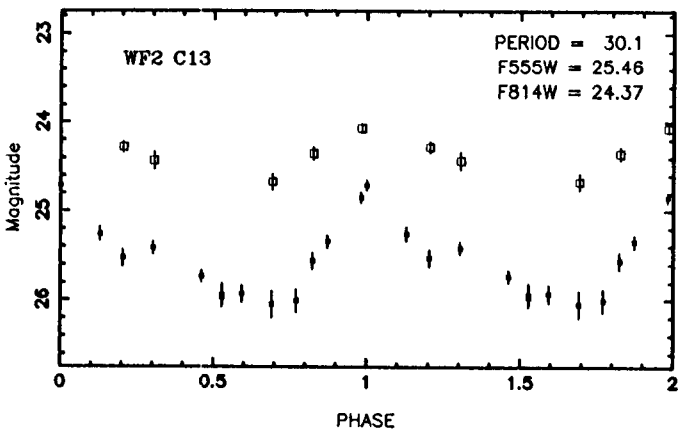
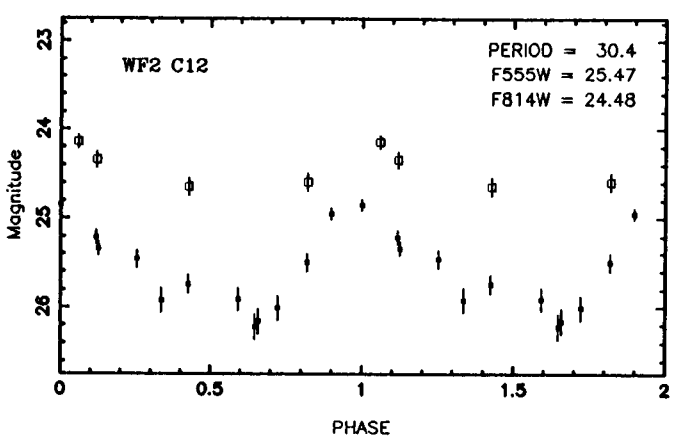
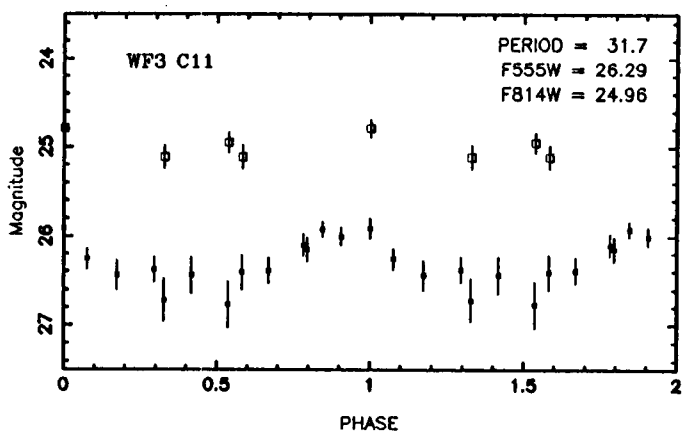
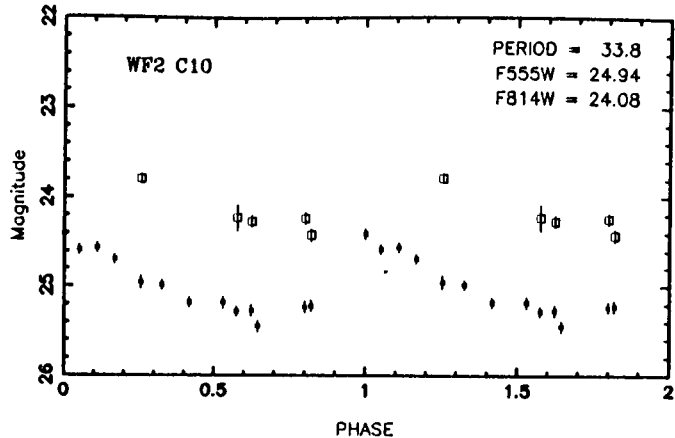
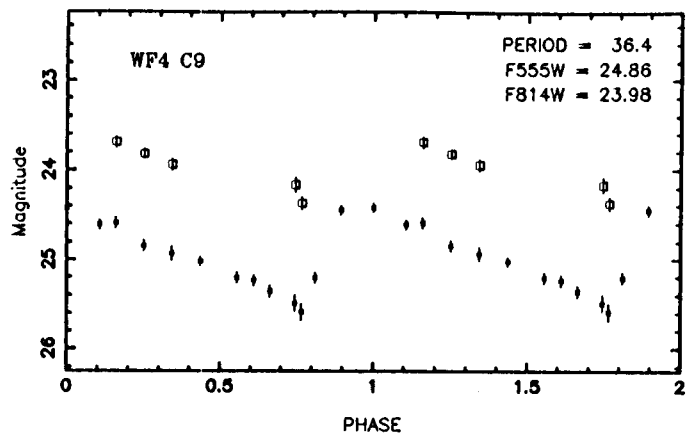
C33

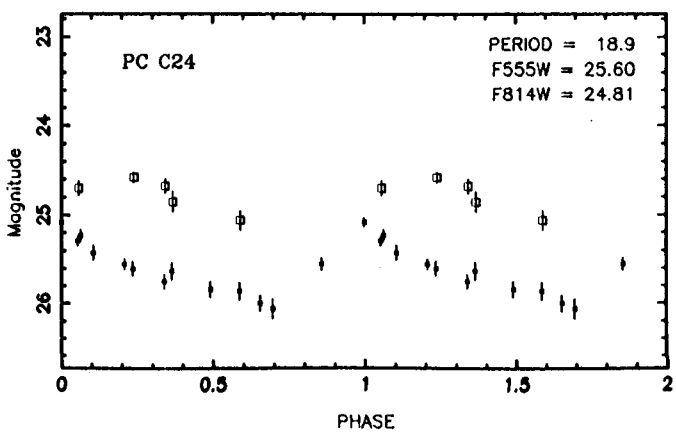
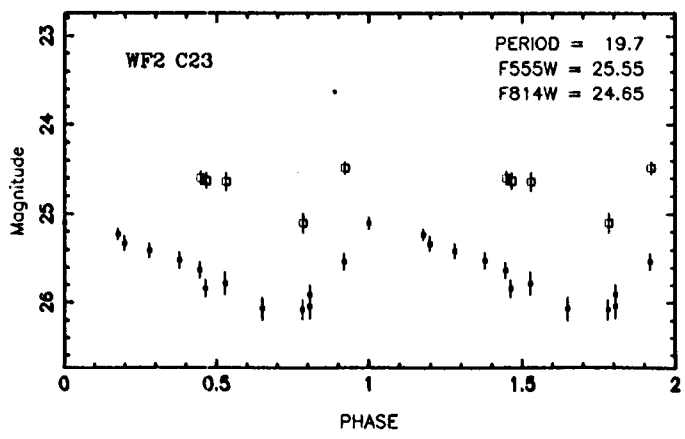
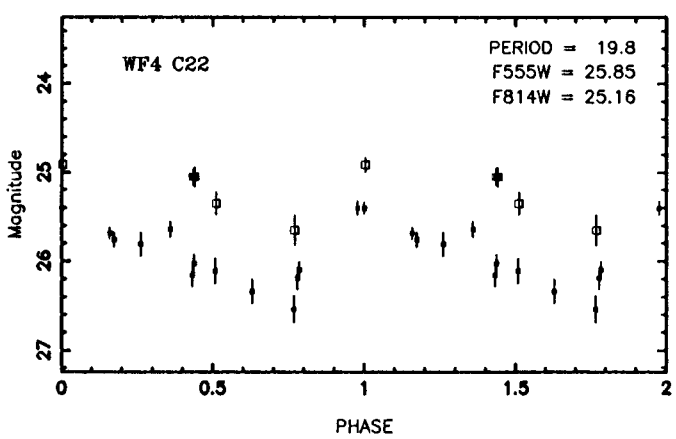
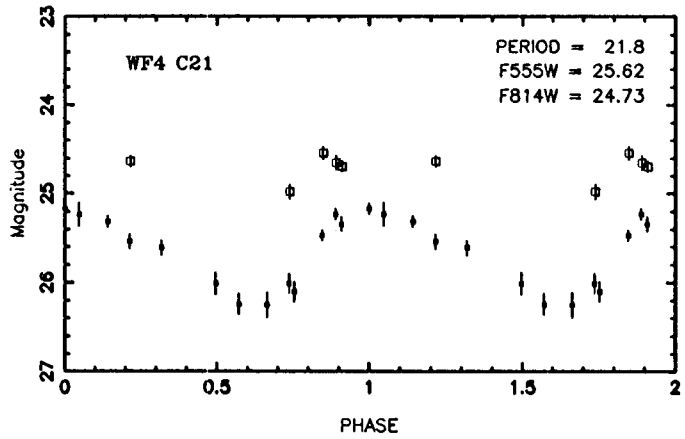
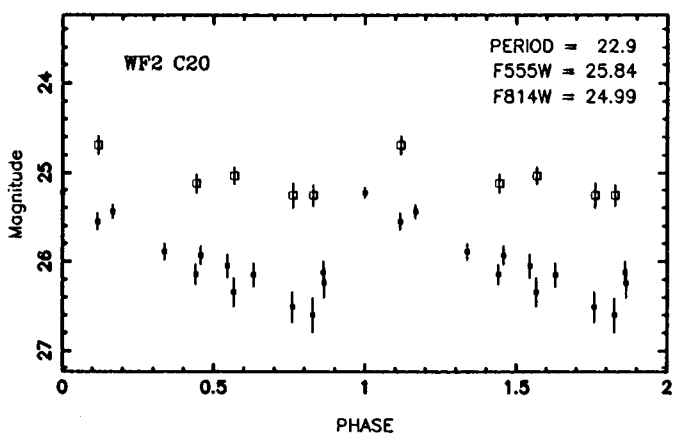
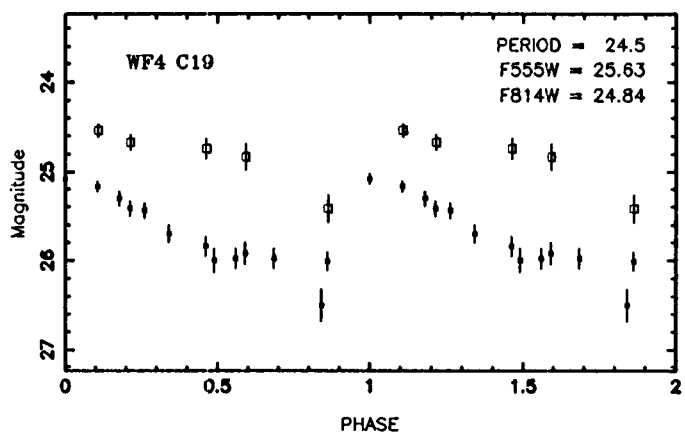
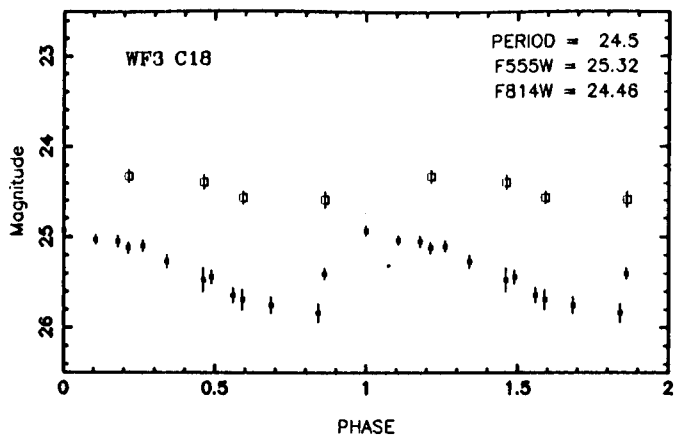
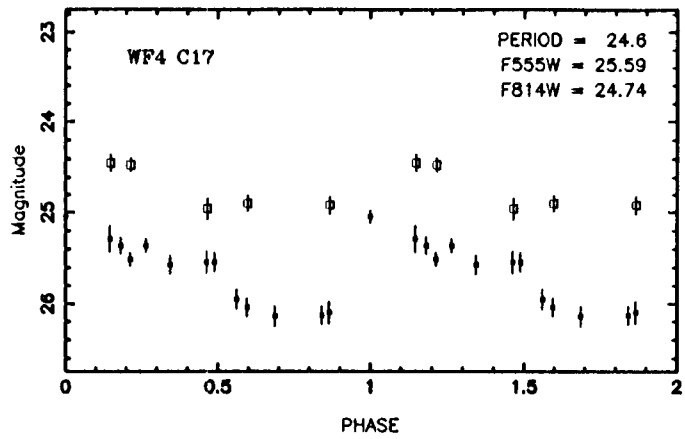


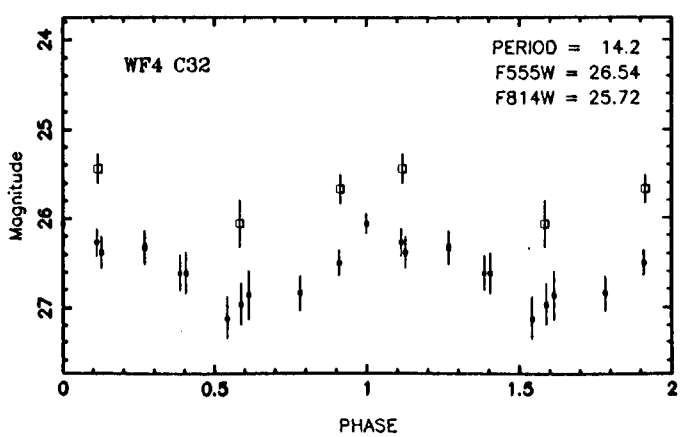
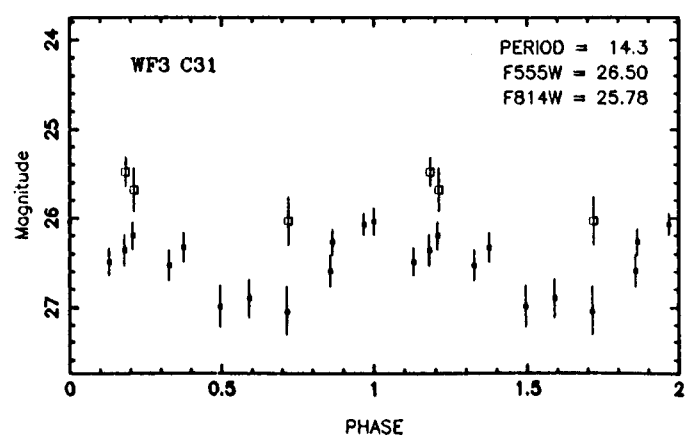
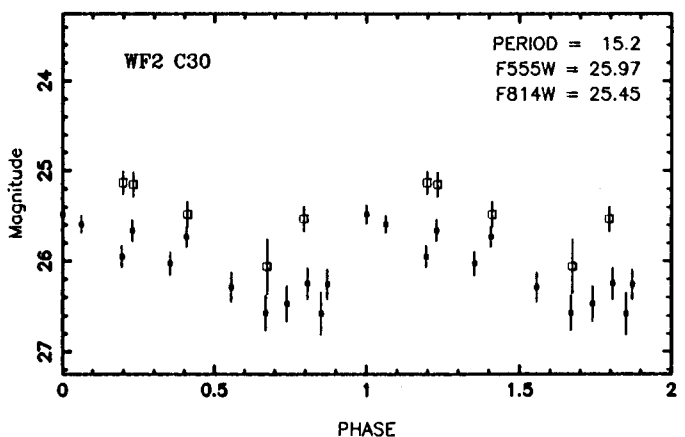
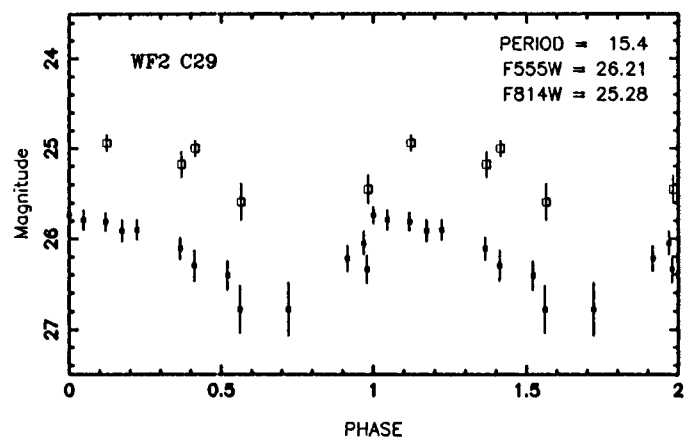
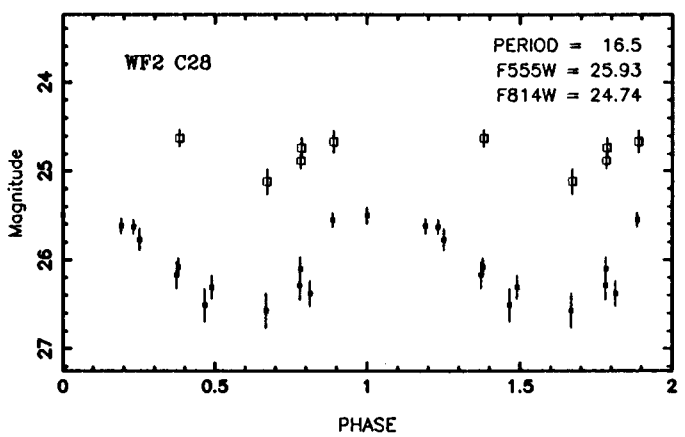
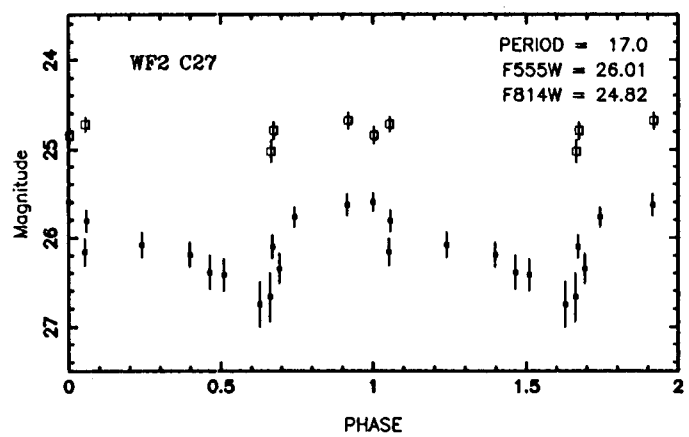
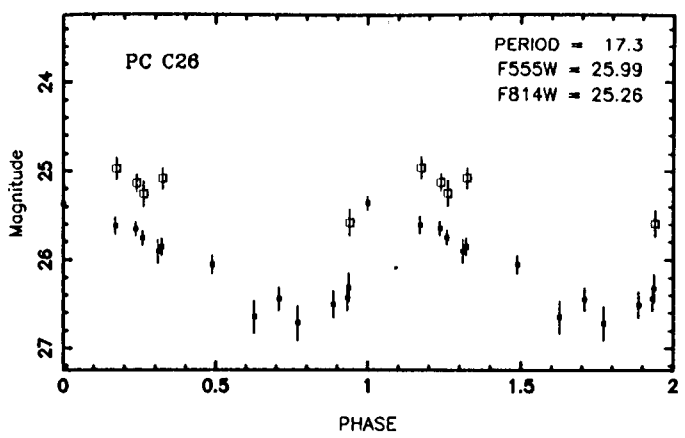
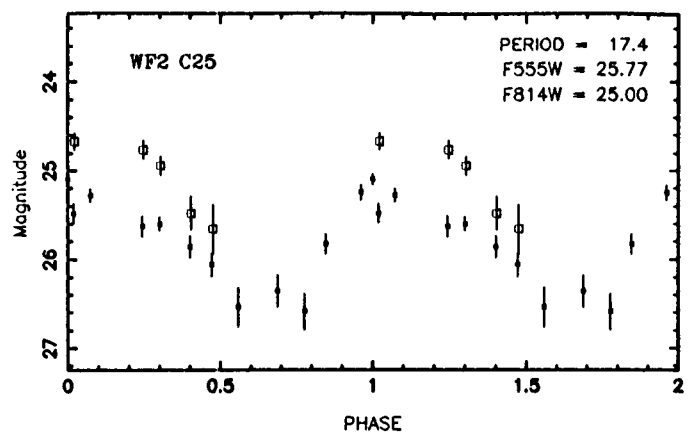
C34

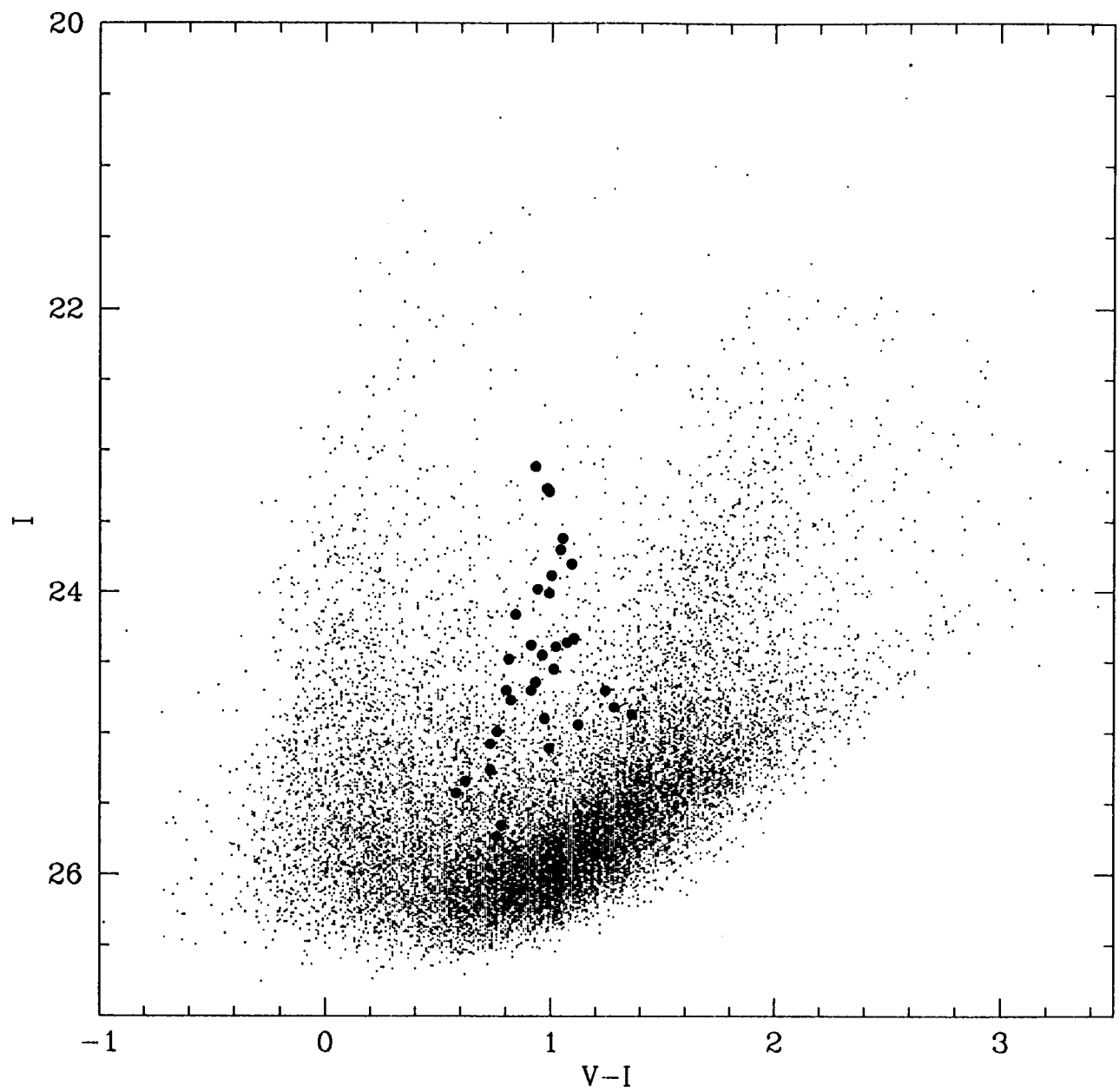


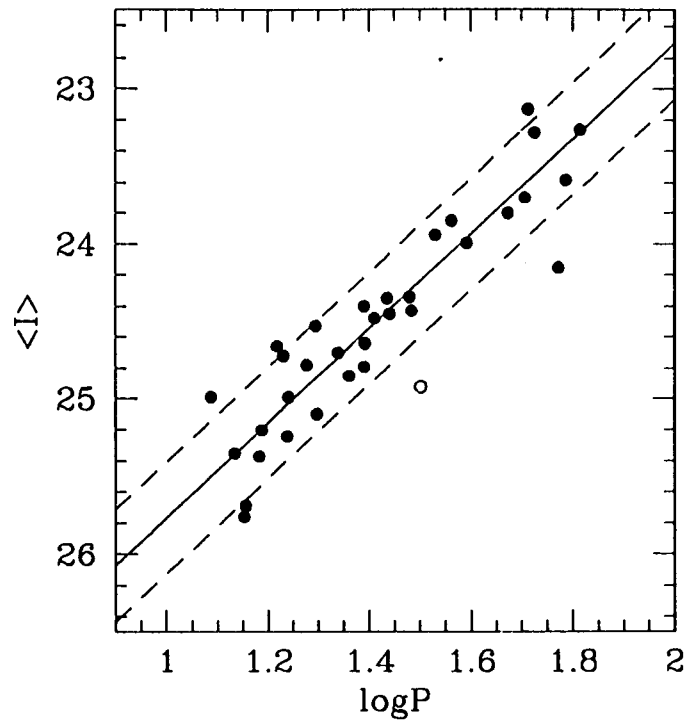
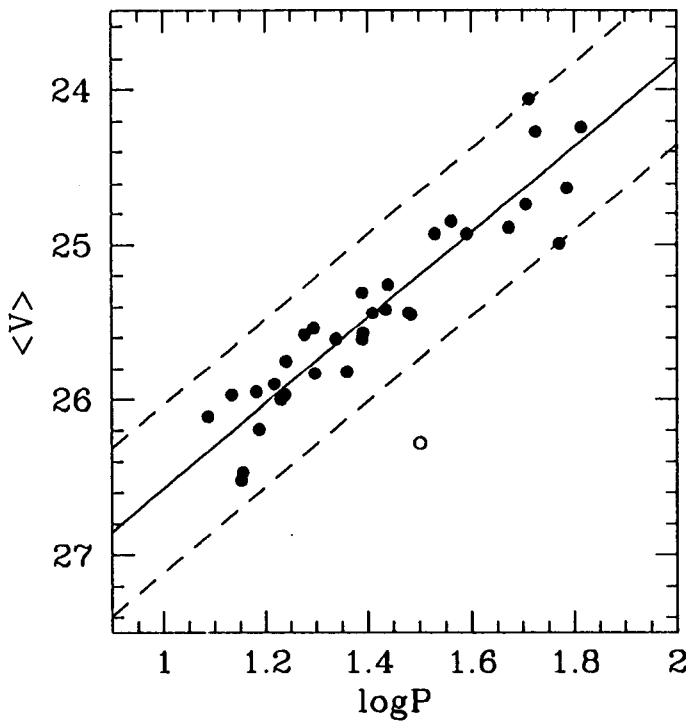




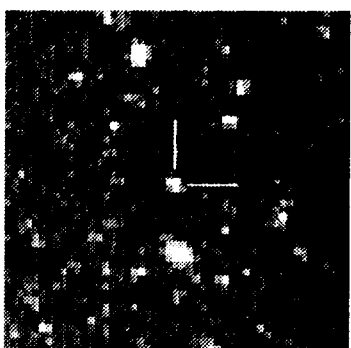




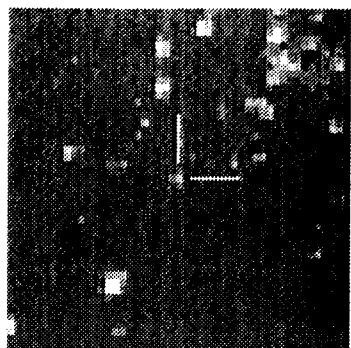




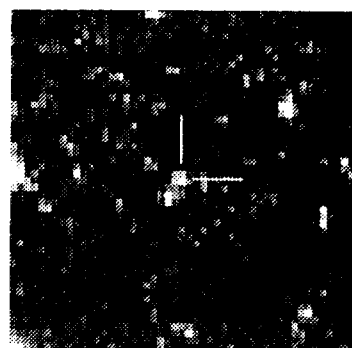
V13



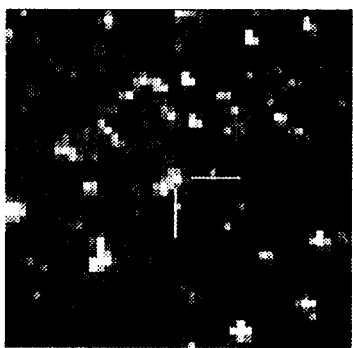
V14



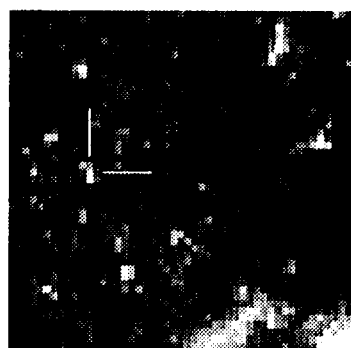
V15



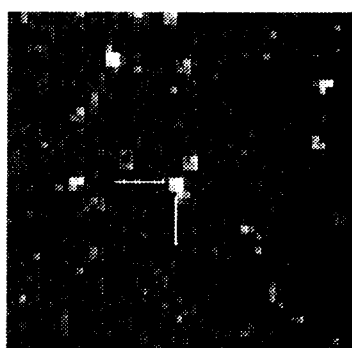
V16



V17



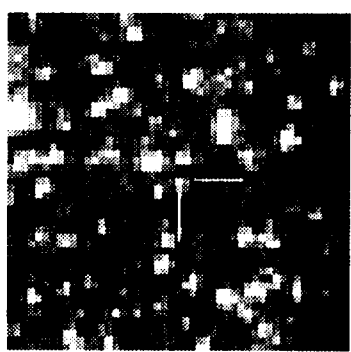
V18



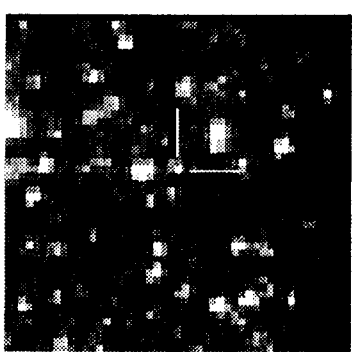
V19



V20



V21



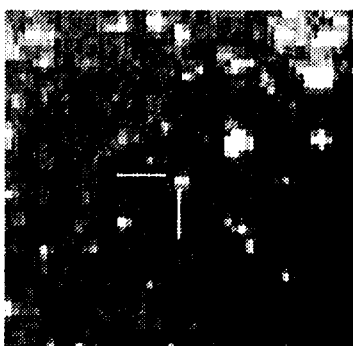
V22



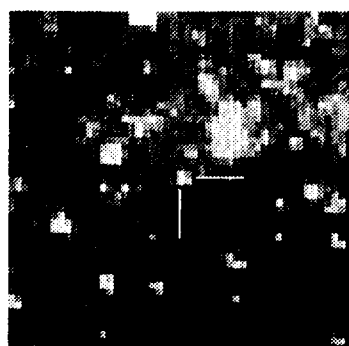
V23



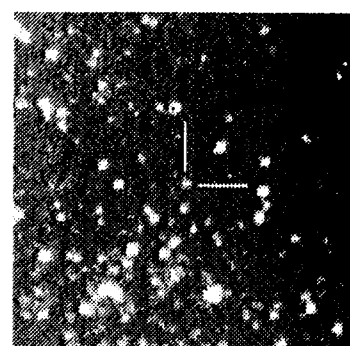
V1



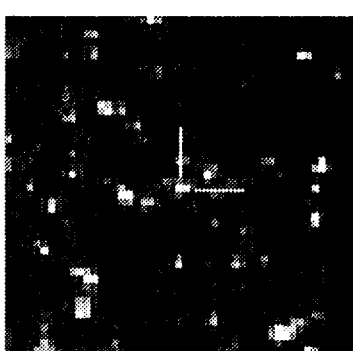
V2



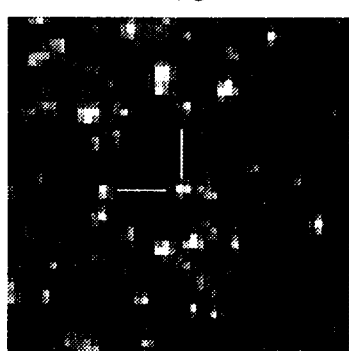
V3



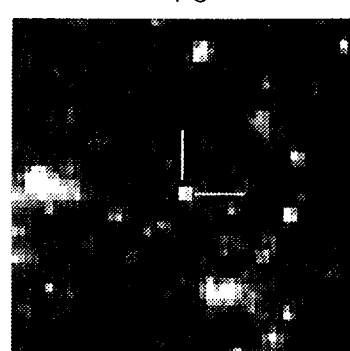
V4



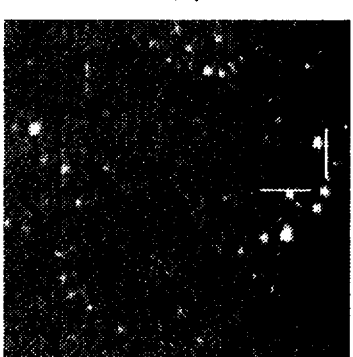
V5



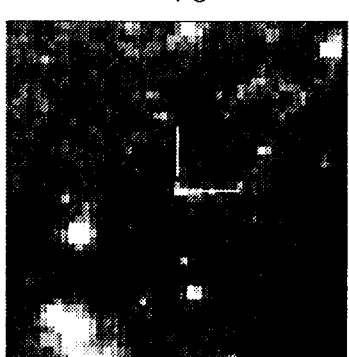
V6



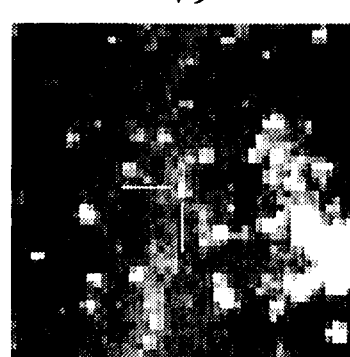
V7



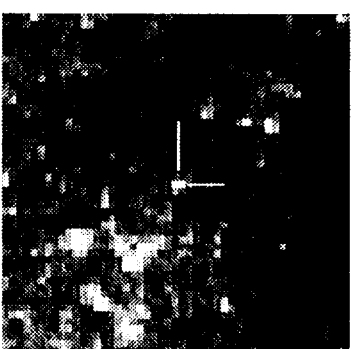
V8



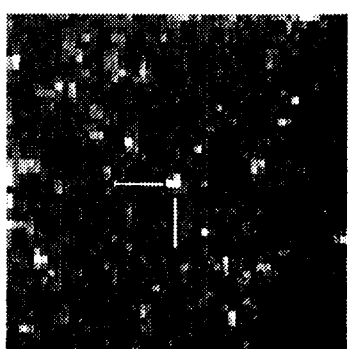
V9



V10



V11



V12

